

NASA/TM—2001-210892



Finite Element Analysis of Active and Sensory Thermopiezoelectric Composite Materials

Ho-Jun Lee
Glenn Research Center, Cleveland, Ohio

National Aeronautics and
Space Administration

Glenn Research Center

May 2001

Available from

NASA Center for Aerospace Information
7121 Standard Drive
Hanover, MD 21076

National Technical Information Service
5285 Port Royal Road
Springfield, VA 22100

Available electronically at <http://gltrs.grc.nasa.gov/GLTRS>

CONTENTS

LIST OF ILLUSTRATIONS	v
LIST OF TABLES	vii
CHAPTER 1. INTRODUCTION	1
1.1 Overview of Smart Structures	1
1.2 Piezoelectric Materials	1
1.3 Objectives of This Research	2
CHAPTER 2. ANALYTICAL MODELING OF PIEZOELECTRIC MATERIALS	3
2.1 Introduction	3
2.2 Induced Strain Models	3
2.2.1 Actuator Models	4
2.2.2 Actuator and Sensor Models	6
2.3 Coupled Electromechanical Models	7
2.3.1 Analytical Models	7
2.3.2 Finite Element Models	7
2.4 Coupled Thermoelectromechanical Models	9
2.4.1 Analytical Models	9
2.4.2 Finite Element Models	10
2.5 Limitations of Existing Analytical Models	11
CHAPTER 3. THEORETICAL DEVELOPMENT	13
3.1 Current Formulation Assumptions	13
3.2 Governing Material Equations	13
3.2.1 Strain and Electric Field in Cartesian Coordinates	14
3.2.2 Strain and Electric Field in Curvilinear Coordinates	14
3.3 Thermopiezoelectric Constitutive Equations	17
3.3.1 Piezoelectric Beam	18
3.3.2 Piezoelectric Plate and Shell	18
CHAPTER 4. LAMINATE MECHANICS	21
4.1 Layerwise Laminate Theory	21
4.1.1 Beam Laminate Theory	21
4.1.2 Plate Laminate Theory	22
4.1.3 Shell Laminate Theory	23
4.2 Generalized Laminate Matrices	24
4.2.1 Beam Laminate Matrices	24
4.2.2 Plate Laminate Matrices	27
4.2.3 Shell Laminate Matrices	29

CHAPTER 5. FINITE ELEMENT FORMULATION	33
5.1 Beam Element	34
5.2 Plate Element	36
5.3 Shell Element	38
CHAPTER 6. CASE STUDIES AND DISCUSSION OF RESULTS	47
6.1 Comparisons with Room Temperature Experimental Results	47
6.1.1 Piezoelectric Bimorph Beam	47
6.1.2 Composite Plate with Piezoelectric Patches	47
6.2 Comparisons with Analytical Results for Temperature Effects	54
6.2.1 Piezoelectric Bimorph Beam	54
6.2.2 Composite Plate with Piezoelectric Patches	54
6.3 Comparisons with a Commercial Finite Element Analysis Program	60
6.3.1 Sensory Mode	60
6.3.2 Active Mode	60
6.4 Additional Numerical Studies	66
6.4.1 Pyroelectric Effects	66
6.4.2 Temperature Dependent Material Properties	70
6.4.3 Selective Shape Control of Bending and Twisting	78
6.4.4 Thermal Stresses	83
6.4.5 Influence of Curvature on Active and Sensory Response	89
CHAPTER 7. CONCLUSIONS AND SUGGESTIONS FOR FUTURE WORK	101
7.1 Suggested Plan of Future Experimental Studies	101
REFERENCES	111

ILLUSTRATIONS

1.	Curvilinear piezoelectric laminate and coordinate system	15
2.	Piezoelectric bimorph beam (Lee and Moon, 1989)	48
3.	Comparisons of deflections of a PVDF bimorph beam	49
4.	Cantilevered composite plate with discrete piezoelectric patches (Crawley and Lazarus, 1991)	50
5.	Comparisons of deflections of a $[0/\pm 45]_s$ graphite/epoxy plate	52
6.	Comparisons of deflections of a $[30/0_2]_s$ graphite/epoxy plate	53
7.	Piezoelectric bimorph beam (Sunar and Rao, 1997)	55
8.	Comparisons of thermal effects on the deflections of a PVDF bimorph beam	56
9.	Simply supported composite plate with discrete piezoelectric patches (Ha et al., 1992)	57
10.	Comparisons of applied active voltage effects on the centerline deflection of a $[0/\pm 45]_s$ graphite/epoxy plate	59
11.	Clamped composite plate with a piezoelectric layer	61
12.	Comparison of centerline deflections of a clamped $[0_8/p]$ plate	63
13.	Comparison of sensory electric potentials of a clamped $[0_8/p]$ plate	64
14.	Comparison of applied active voltage effects on the centerline deflection of a clamped $[0_8/p]$ plate	65
15.	Pyroelectric effects on the centerline deflections of a clamped $[0_8/p]$ plate	68
16.	Pyroelectric effects on the sensory electric potentials of a clamped $[0_8/p]$ plate	69
17.	Temperature dependence of AS4-3501-6 properties	71
18.	Temperature dependence of PZT-5A properties d_{31} and ϵ_{33}	72
19.	Temperature dependence of PZT-5A properties α_{11} , and p_3	73
20.	Influence of temperature dependence on deflections at the center of a $[0/\pm 45]_s$ carbon/epoxy plate for different applied thermal gradients	75
21.	Influence of temperature dependence on sensory voltages at the center of a $[0/\pm 45]_s$ carbon/epoxy plate for different applied thermal gradients	76
22.	Influence of temperature dependence on applied voltages to minimize the center deflection of a $[0/\pm 45]_s$ carbon/epoxy plate for different applied thermal gradients	77
23.	Initial bending and twisting deformation of a $[45_3/-45_3]$ plate	79
24.	Selective shape control of the bending deformation of a $[45_3/-45_3]$ plate	80
25.	Selective shape control of the twisting deformation of a $[45_3/-45_3]$ plate	81
26.	Shape control of bending and twisting deformations of a $[45_3/-45_3]$ plate	82
27.	Cantilevered $[0_8/p]$ beam	84
28.	Comparison of normal stresses at the middle of a $[0_8/p]$ beam	86
29.	Comparison of normal stresses at the free end of a $[0_8/p]$ beam	87
30.	Comparison of shear stresses at the free end of a $[0_8/p]$ beam	88
31.	Geometry of a $[0_9/p]$ circular cylinder with an attached piezoelectric layer	90
32.	Different types of applied thermal loads	91

33.	Influence of pyroelectric effects on the displacements of a $[0_p/p]$ circular cylinder under a uniform thermal load	92
34.	Influence of pyroelectric effects on the sensory electric potential of a $[0_p/p]$ circular cylinder under a uniform thermal load	93
35.	Influence of pyroelectric effects on the displacements of a $[0_p/p]$ circular cylinder under a cosine thermal load	94
36.	Influence of pyroelectric effects on the sensory electric potential of a $[0_p/p]$ circular cylinder under a cosine thermal load	95
37.	Influence of pyroelectric effects on the displacements of a $[0_p/p]$ circular cylinder under a double cosine thermal load	96
38.	Influence of pyroelectric effects on the sensory electric potential of a $[0_p/p]$ circular cylinder under a double cosine thermal load	97
39.	Displacements of a $[0_p/p]$ circular cylinder under a uniform thermal load	98
40.	Displacements of a $[0_p/p]$ circular cylinder under a cosine thermal load	99
41.	Displacements of a $[0_p/p]$ circular cylinder under a double cosine thermal load	100
42.	Dynamic experimental setup	103
43.	High temperature test configuration of a cantilevered beam with one piezoelectric patch	104
44.	High temperature test configuration of a cantilevered beam with two piezoelectric patches	106
45.	Test configuration of a flat plate with attached piezoelectric patches.	108
46.	Test configuration of a curved plate with attached piezoelectric patches	109

TABLES

1.	Material properties of PVDF piezoelectric polymer (Lee and Moon, 1989)	49
2.	Material properties of piezoceramic (G-1195) and Graphite/Epoxy (AS4/3501) (Crawley and Lazarus, 1991)	51
3.	Material properties of PVDF piezoelectric polymer (Sunar and Rao, 1997)	56
4.	Material properties of piezoceramic (G-1195) and Graphite/Epoxy (AS4/3501) (Ha et al., 1992)	58
5.	Material properties of piezoceramic and Carbon/Epoxy	62
6.	Material properties of piezoceramic and Carbon/Epoxy	67
7.	Material properties of piezoceramic (PZT-5A) and carbon/epoxy (AS4/3501-6) composite	74
8.	Material properties of piezoelectric and Graphite/Epoxy	85
9.	Series of tests for a cantilevered beam with one piezoelectric patch	105
10.	Series of tests for a cantilevered beam with two piezoelectric patches	107

CHAPTER 1 INTRODUCTION

Smart composite structures offer the capability to combine the low density, superior mechanical and thermal properties of composite materials along with the inherent capabilities of smart materials to sense and adapt to their environments. Thus, the use of smart structures (also referred to as intelligent or adaptive structures) offers the potential to significantly improve the performance of aerospace structural components. However, before these materials can be implemented into actual structures, the coupled mechanical, electrical, and thermal behavior of smart materials must be fully characterized. This has led to extensive research since the 1980's to assess both the sensory and active responses of smart materials.

1.1 Overview of Smart Structures

Smart structures are distinguished from conventional structures by the presence of integrated actuator and sensor elements. In a typical smart structure application, the sensors are used to monitor the mechanical response of the structure through changes in the displacements, strains, or accelerations. Once an adverse or undesirable structural response is detected in the sensors, a controller generates the required input to the actuators. The actuators respond to this input and produce a corresponding change in the mechanical response of the structure to a more benign or acceptable state. The capability of smart structures to sense and adapt to their environment leads to a wide range of potential applications including: vibration suppression of aircraft structures; noise control of helicopter rotors; health monitoring of bridges; shape control of large space trusses; aeroelastic control of aircraft lifting components; and seismic control of buildings. Crawley (1993) and Loewy (1997) provide detailed overviews of the current state of smart structures research for aerospace applications.

A variety of different materials can be utilized as either sensor or actuator elements in smart structure applications. Depending on the specific material used, the sensor and actuator elements are controlled through either electric, magnetic, thermal, or light energy. Some of the common actuator and sensor materials include: piezoelectric materials, shape memory alloys, fiber optics, electrostrictive materials, magnetostrictive materials, and electro-rheological fluids. Of the different materials available for use in smart structures, only piezoelectric materials have the unique capability to be used effectively as both actuator and sensor elements. Other advantages of piezoelectric materials which help account for their widespread popularity include: simple integration into the structure; a readily obtainable commercial supply of piezopolymers and piezoceramics; and familiarity in using these materials gained from previous applications in transducers.

1.2 Piezoelectric Materials

Historically, piezoelectric materials have been utilized mainly as active structural elements in transducers for application in strain gages, accelerometers, and sonar. Recently, the focus of research has shifted away from the transducer applications toward the development of smart structure applications which combine the active and sensory behavior of piezoelectric materials.

The basic characteristics of piezoelectric materials which allow for their use as sensors and actuators are the direct piezoelectric effect, converse piezoelectric effect, and the pyroelectric effect. In the direct piezoelectric effect, the application of a mechanical load on the piezoelectric material induces an electrical response. Through measurement of this electrical response, the mechanical state of deformation in the structure can be determined and monitored, leading to the sensory application. In contrast, the converse piezoelectric effect transforms an electrical input in the piezoelectric material into a corresponding mechanical strain. This leads to the active applications of piezoelectric materials, in which the state of deformation of the structure can be controlled or altered by applying the appropriate electrical input. The third characteristic behavior is the pyroelectric effect, in which the piezoelectric material responds to changes in temperature by producing an electrical response, which will influence both the direct and converse piezoelectric effects in changing temperature environments.

1.3 Objectives of This Research

The renewed interest in the application of piezoelectric materials in smart structures has led to extensive efforts to fully characterize the sensory and active behavior of these materials. Due to the complex coupled mechanical, electrical, and thermal behavior of piezoelectric materials, new analytical formulations and mechanics are required to accurately analyze the response of smart structures which contain piezoelectric elements. Thus, the purpose of this research is to develop comprehensive mechanics for accurately predicting the sensory and active behavior of composite laminates which contain piezoelectric elements. Special emphasis is placed on capturing the coupled response at the material level through the thermopiezoelectric constitutive equations and to introduce the displacements, electric potentials, and temperature as state variables in the analysis. This unified representation of the coupled response leads to the inherent capability to model both the sensory and active responses of piezoelectric composite laminates.

The mechanics incorporate a layerwise laminate theory for more accurate analysis of displacements, strains, stresses, electric fields, and thermal fields, especially for thick laminates and laminates which contain strong inhomogeneities through-the-thickness. Thermal effects which arise from coefficient of thermal expansion mismatch, pyroelectric effects of the piezoelectric materials, and temperature dependent material properties are explicitly accounted for in the formulation. Corresponding finite element formulations are developed for piezoelectric beam, plate, and shell elements to provide a more generalized capability for the static and dynamic analysis of piezoelectric composite structures under arbitrary thermoelectromechanical loads and boundary conditions. The accuracy of the current formulation is verified by comparison with published experimental data and results from other analytical models. Additional numerical studies are also conducted to demonstrate additional capabilities of the formulation to represent the sensory and active behaviors. A future plan of experimental studies is also provided to characterize the high temperature dynamic response of piezoelectric composite materials.

CHAPTER 2 ANALYTICAL MODELING OF PIEZOELECTRIC MATERIALS

2.1 Introduction

The initial use of piezoelectric materials dates back to 1880, when the Curie brothers first discovered the direct piezoelectric effect. Until recently, the use of piezoelectric materials has been limited to a variety of transducer applications. The widespread use of piezoelectric materials as distributed actuators began only in the 1980's, when advances in design and manufacturing technologies made these applications feasible. The experimental work of Bailey and Hubbard (1985) is usually cited as the first application of piezoelectric materials as actuators for vibration control. Using a piezoelectric polymer film as the active element on a cantilevered beam, they were able to demonstrate active damping of the first vibrational mode. This new actuator application has led to renewed interest in the development of piezoelectric materials for advanced aerospace structures.

As research into characterizing the active and sensory behavior of piezoelectric materials progressed, a variety of different analytical models were developed. These models can be classified into three broad categories as induced strain models, coupled electromechanical models, and coupled thermoelectromechanical models. The induced strain models use approximate theories to incorporate the piezoelectric effects and are generally limited to predicting only the active response of piezoelectric materials since the electric potential is neglected as a state variable in the formulation. The coupled electromechanical models provide a more consistent representation of both the sensory and active responses of piezoelectric materials by incorporating both the displacements and electric potential as state variables in the formulation. Typically, these models are implemented as finite element codes to provide a more general analysis tool and a wide variety of different beam, plate, shell, and solid elements have been developed. A natural extension of the coupled electromechanical models is to also incorporate thermal effects. These coupled thermoelectromechanical models include temperature as an additional state variable to account for thermal effects in addition to the piezoelectric effects. A more limited number of finite element codes have been developed with this capability.

2.2 Induced Strain Models

The induced strain models can be separated into two categories: (1) actuator models and (2) actuator and sensor models. The actuator models are concerned only with analyzing the active behavior of piezoelectric materials. They typically approximate the strain generated in the piezoelectric material by an applied electric voltage using statically equivalent forces and moments. The combined actuator and sensor models were developed to include predictions of the sensory response of piezoelectric materials. Although these models introduce the piezoelectric constitutive equations into their formulation, the electric potential is usually not included as a state variable, the conservation of electric flux is not considered in the equations of motion, and the sensory voltages are back calculated using the charge equation.

2.2.1 Actuator Models

Crawley and de Luis (1987) developed an induced strain actuator model for beams. They formulated static and dynamic analytical models based on the governing equations for beams with attached and embedded piezoelectric actuators to model extension and bending. Experiments were performed on both isotropic and composite cantilevered beams with attached and embedded piezoelectric actuators to validate their models. The study found that segmented actuators are always more effective than continuous actuators since the output of each actuator can be individually controlled. They also showed that embedded actuators in composites degrade the ultimate tensile strength, but have no effect on the elastic modulus. Baz and Poh (1988) investigated methods to optimize the location of piezoelectric actuators on beams to minimize the vibration amplitudes. Numerical studies demonstrated the potential to control vibrations in large flexible structures using a small number of bonded piezoelectric actuators. Im and Atluri (1989) presented a more complete beam model which accounted for transverse and axial deformations in addition to extension and bending. Governing equations were formulated for a beam with bonded piezoelectric actuators for applications in dynamic motion control of large scale flexible space structures.

Tzou and Gadre (1989) formulated an induced strain piezoelectric shell theory. A dynamic model was derived from Love's shell theory for application to multi-layered thin shells with active distributed actuators. A case study was validated with experimental results for the vibration suppression of a cantilevered beam with a piezopolymer actuator film. Crawley and Anderson (1990) developed a Bernoulli-Euler model to more accurately model actuation induced extension and bending in one-dimensional beams than the model of Crawley and de Luis (1987). The model neglected shear effects and was shown to be best suited for the analysis of thin beams and actuators. Clark et al. (1991) also extended the model of Crawley and de Luis (1987) to study the response of multiple piezoelectric actuators on beam excitations. Based on Euler beam theory, their model was validated with experimental results for the vibration response of a simply supported isotropic beam. The model was found to be best suited for performing initial studies to determine the optimal location of actuators for exciting specific vibration modes.

Crawley and Lazarus (1991) developed induced strain actuation models for plates. Equations of strain actuation were derived for both isotropic and anisotropic plates. Exact solutions were found for simple geometries and boundary conditions, while approximate solutions were used to solve more complex problems. The models were verified with experimental results. Static analysis of a cantilevered composite plate with attached piezoceramic actuators were conducted to show the potential for shape control of structures. Dimitriadis et al. (1991) extended the one-dimensional induced strain beam model of Crawley and de Luis (1987) to two-dimensional plates with bonded piezoelectric actuators. Dynamic analyses were performed on simply supported plates to demonstrate the use of actuators to excite selective modes and the influence of actuator geometry on the modal response. Robbins and Reddy (1991) developed a piezoelectric layerwise laminate theory which was implemented into a beam element. Numerical comparisons were conducted using four different displacement theories (two equivalent single layer theories and two layerwise laminate theories) to demonstrate the increased accuracy in displacement and stress predictions obtained from using the layerwise theories.

Wang and Rogers (1991) formulated an induced strain piezoelectric plate theory. The formulation was based on classical laminated plate theory and used Heaviside functions to represent the distributed piezoelectric actuators. The model was verified with the analytical work of Dimitriadis et al. (1991) and additional case studies were performed to demonstrate the capability of actuators to induce bending and extension in laminated plates. Clark et al. (1993) experimentally

validated the induced strain plate model developed by Dimitriadis et al. (1991). Results from the free vibration analysis demonstrated capabilities to excite selective vibration modes of a simply supported plate using bonded actuators, as well as the significance of actuator location and excitation frequency on the structural response. Pai et al. (1993) accounted for geometric nonlinearities (large rotations and displacements) in piezoelectric composite plates. The developed partial differential equations characterize the dynamic response of composite plates through elastic and geometric couplings between the extension, bending, and twisting motions.

Mitchell and Reddy (1995b) formulated a power series solution for axisymmetric composite cylinders with either attached or embedded piezoelectric laminae. The solution was verified with finite element analysis. Numerical studies were performed to damp vibrations in truss-type structures using both an embedded cylindrical truss actuator element and an attached actuator patch. Lin et al. (1996) presented an induced actuation plate finite element based on first order shear deformation theory. Numerical studies were verified with analytical solutions and demonstrated capabilities to control the deflection of composite plates using piezoelectric actuators. Park and Chopra (1996) formulated one-dimensional models to predict the extension, bending, and torsion behavior of beams under piezoelectric actuation. Comparisons with experimental data showed good correlation only for applications in which actuators have low orientation angles (less than 45°) with respect to the beam neutral axis.

Sonti and Jones (1996) developed differential equations of motion for a composite cylindrical shell with surface bonded piezoelectric elements. Approximate analytical solutions were obtained for the equivalent forces exerted by the actuator and shell. Chandrashekhara and Varadarajan (1997) implemented a finite element model for laminated composite beams with integrated piezoelectric actuators derived from a higher order shear deformation theory. Numerical studies investigated the effect of stacking sequence and boundary conditions on the actuator voltages and demonstrated the capability to achieve adaptive shape control of beam structures. Charette et al. (1997) formulated analytical models based on a variational approach to study plates with piezoelectric actuators. The model was specialized for a simply supported plate and used to determine the effects of piezoelectric actuator on the dynamic behavior of the plate. Results of the study were verified with experiments and showed only slight changes in the mode shapes of the plate.

Chattopadhyay and Seeley (1997) implemented a third-order laminate theory into a finite element formulation to investigate piezoelectric actuators. Numerical results were verified with published experimental data. Additional comparisons were conducted to demonstrate the limitations of classical laminate theory in analyzing through-the-thickness stress and strain variations. Librescu et al. (1997) presented a model for composite beams with piezoelectric actuators that included structural tailoring and boundary-moment control. Numerical results demonstrated the potential to improve the dynamic responses of thin-walled cantilevered structures. Bhattacharya et al. (1998) developed a finite element formulation based on first order shear deformation theory for beams and plates. An eight noded isoparametric piezoelectric element was developed to perform free vibration analysis of laminated composite beams and plates. Numerical studies assessed the impact of stacking sequence, boundary conditions, and applied electric potentials on the free vibration response.

Oguamanam et al. (1998) formulated a piezoelectric composite beam finite element using von Karman nonlinear strain-displacement relations. Numerical studies demonstrated the influence of stress stiffening effects on the natural frequency of slender beams. Tong et al. (1998) developed a two dimensional thin plate finite element to investigate shape control applications. Numerical

studies were performed to determine the optimum applied voltage, actuator layout, and actuator number for shape control of composite plates with distributed piezoelectric actuators. Chattopadhyay et al. (1999) implemented a third-order laminate theory into a finite element formulation to investigate the dynamic response of delaminated smart composite plates. Numerical studies were conducted on piezoelectric composite plates with single and multiple delaminations to demonstrate changes in the dynamic response. Hong and Chopra (1999) developed an induced strain plate finite element for composite plates based on classical laminate theory. The model was verified with experimental results and demonstrated the capability to achieve shape control using piezoelectric actuators.

2.2.2 Actuator and Sensor Models

Lee and Moon (1989) studied the control and sensing of bending and torsional deformations produced by an applied electric field using piezopolymer bimorphs. The experimental results validated the analytical model and demonstrated the use of piezopolymers as actuators. Lee (1990) developed a model that incorporated the piezoelectric constitutive relations. The model was based on classical laminated plate theory and was able to predict both the active and sensory behavior of piezoelectric materials. Lee et al. (1991) investigated the use of sensor actuator pairs for active damping control. Experimental studies were conducted on the active damping control of the first mode of a cantilevered plate using a sensor and actuator pair to validate the piezoelectric plate theory.

Chandrashekhara and Agarwal (1993) developed a laminated piezoelectric plate element based on a first-order shear deformation theory applicable to both thin and moderately thick laminates. Numerical results were verified with previously published results for a cantilevered plate with attached piezoceramic actuators subjected to a static electric field. Hwang and Park (1993) developed a piezoelectric plate element based on classical laminate theory and Hamilton's principle. The piezoelectric constitutive relations were used to formulate a four noded, two-dimensional quadrilateral plate element for both sensory and active applications. Case studies were performed to investigate the static response of a piezoelectric bimorph beam and the vibration control of a cantilevered plate with attached piezoelectric sensors and actuators. Koconis et al. (1994a, 1994b) developed separate analytical models to investigate the sensory and active behavior of piezoelectric composite beams, plates, and shells. One model is used to predict the change in shape when a specified electric voltage is applied to the actuator, while the second model is used to determine the electric voltages necessary to achieve a desired shape. Both models were formulated using a two-dimensional, linear, shallow shell theory which includes transverse shear effects and validated with other numerical, analytical, and experimental results.

Sung et al. (1996) derived sensor and actuator equations for a cylindrical piezoelectric composite shell. Based on classical laminate theory, these equations formed the basis of a sensor and actuator design methodology to control flexural and torsional vibrations in cylindrical shells. This methodology was used to design an experimental rig to demonstrate capabilities of the modal sensor and actuator to monitor and control the different vibration modes. Lam et al. (1997) developed a finite element model based on classical laminated plate theory for the active vibration control of composite plates with distributed piezoelectric actuators and sensors. Numerical studies were conducted on a cantilevered composite plate to demonstrate capabilities for static and dynamic analysis. Plettner and Abramovich (1997) implemented a consistent methodology based on Kirchoff-

Love thin shell theory to model the static and dynamic response of anisotropic laminated piezoelectric shells. The formulation replaced the induced piezoelectric strain with an equivalent mechanical load. The model was verified with experimental and finite element results for a rectangular isotropic plate.

Peng et al. (1998) implemented a beam finite element using a third order laminate theory for active vibration control of piezoelectric composite beams. Numerical studies were conducted to assess shape control applications and to investigate the effect of sensor and actuator locations on the response of the beam. Liu et al. (1999) formulated a plate finite element based on classical laminated plate theory for modeling the static and dynamic response of composite plates containing piezoelectric actuators and sensors. Numerical studies were conducted to verify the model with results from previously developed models and to study the influence of stacking sequence and sensor/actuator position on the response of composite plates.

2.3 Coupled Electromechanical Models

Attempts to develop a more comprehensive representation of piezoelectric material behavior led to the development of more consistent models that captured the coupled response between the mechanical and electrical behavior. In these coupled models, the charge equation is incorporated into the equations of motion and the electric potential is introduced as an additional degree of freedom in the analysis. These models are generally also implemented as finite element programs to provide a more flexible and general purpose analytical tool.

2.3.1 Analytical Models

Mitchell and Reddy (1995a) formulated a refined hybrid theory for laminated piezoelectric composite plates. The displacement fields are modeled using third order shear deformation theory while electric potentials are represented using a layerwise laminate theory. An analytical solution was developed for simply supported boundary conditions and numerical results demonstrated the limitations of the induced strain methods in modeling thick laminates. Heyliger and Saravanos (1995) developed exact solutions to predict the vibration characteristics of simply supported laminated piezoelectric plates. Numerical studies were conducted to determine the influence of different laminations and aspect ratios on the natural frequencies and mode shapes. Batra and Liang (1997) developed three-dimensional elasticity solutions for the simply supported rectangular laminated plate with embedded piezoelectric layers. Numerical studies examined the steady state vibration of both thin and thick plates containing one actuator layer and one sensor layer.

2.3.2 Finite Element Models

The groundwork for much of the current research into finite element formulations was initiated by Allik and Hughes (1970) with the development of a three-dimensional tetrahedron element. Derived at a time when piezoelectric materials were used mainly as crystals in transducer applications, the finite element formulation incorporated the piezoelectric constitutive relations and

demonstrated the potential advantages of utilizing the finite element method. Naillon et al. (1983) formulated a finite element model to study the resonance phenomena of single piezoelectric structures typically used in ultrasonic transducers. Numerical studies were performed on the resonance characteristics of two-dimensional parallelepiped bars to assess potential applications in the design of ultrasonic probes. Lerch (1990) formulated two and three dimensional finite elements for performing vibrational analysis of piezoelectric sensors and actuators. The models were verified with experimental data. The natural frequencies and mode shapes of various piezoelectric structures were determined and used to optimize applications as transducers.

Tzou and Tseng (1990) developed a thin piezoelectric solid element. Derived from Hamilton's principle and the piezoelectric constitutive relations, the element is specifically formulated for thin plate and shell structures with distributed piezoelectric sensors and actuators. Numerical studies were performed on the vibration response of a cantilevered plate with both an active and sensory layer of polymeric piezoelectric material. Lammering (1991) developed a piezoelectric shell element. Based on the Reissner-Mindlin shell theory and incorporating the piezoelectric constitutive equations, a shell element was formulated for thin shell structures with attached piezoelectric layers. Case studies were conducted on a cantilevered beam with an attached piezoelectric polymer layer. Ha et al. (1992) formulated a three-dimensional brick element. Using a variational principle and the piezoelectric constitutive relations, they developed an eight-noded solid element. Results from static and dynamic case studies were verified with experimental results for composite plates with attached piezoceramic actuator and sensor patches.

Heyliger et. al. (1994) implemented a layerwise laminate theory into a finite element formulation for plates. Two separate layerwise models were developed which incorporated the coupled equations of piezoelectricity to account for both the active and sensory behavior of laminated plates with piezoelectric layers. Numerical results for a simply supported composite plate with attached polymer piezoelectric layers were verified with exact solutions. Ray et al. (1994) developed a two-dimensional quadrilateral element using a higher order laminated plate theory. An eight-noded quadratic isoparametric quadrilateral element was formulated. Results from the static analysis of a simply supported cross-ply laminated plate bonded with a piezoelectric polymer were verified using previously reported exact solutions. Shieh (1994) developed a multiaxially active and sensory laminated piezoelectric beam element. Based on adjusted elementary beam assumptions to account for warping effects, the element can simultaneously model axial extension, biaxial bending, and torsional twisting of the beam. Numerical studies were performed on a space antenna frame to demonstrate capabilities for three-dimensional multiaxial vibration control.

Saravanos and Heyliger (1995) developed a layerwise finite element formulation for beams. Two separate theories were used to perform static and free vibration analysis of composite beams. Numerical results were verified with previously published analytical studies and demonstrated the increased accuracy of stress-strain predictions with the layerwise theory. Shen (1995) developed a finite element formulation for beams containing piezoelectric actuators and sensors. Based on Timoshenko beam theory, the methodology captured the coupling between the longitudinal and bending motions. The theory was validated with previously published analytical results for a piezoelectric polymer bimorph beam and experimental results for a cantilevered beam with attached piezoelectric sensors and actuators. Suleman and Venkayya (1995) formulated a plate element for analyzing composite plates with layered piezoelectric actuators and sensors. Based on classical laminate theory, a four-noded bilinear Mindlin plate element was developed. Previously published

experimental and analytical results for a cantilevered piezoelectric bimorph beam and a cantilevered composite plate with distributed piezoelectric actuators were used to validate the formulation.

Donthireddy and Chandrashekhara (1996) also formulated a layerwise theory for beams. Results from the static response of a cantilevered composite beam with attached piezoelectric actuators was validated with previous analytical results. Additional parametric studies were conducted to study the influence of boundary conditions and ply orientation on the shape control of beams. Heyliger et al. (1996) implemented a layerwise laminate theory into a finite element formulation for shells. Results were verified with exact solutions for the static and free vibration response of a simply supported plate. Additional studies were performed on the active and sensory response of a cylindrical shell. Kim et al. (1996) developed a transition element to connect three-dimensional solid elements to flat shell elements. The reported approach used solid elements to provide detailed models of the piezoelectric material, while flat shell elements were used to provide a more flexible model for the substrate structure, and transition elements were used to connect the two regions. The model was verified experimentally for a cantilevered plate.

Samanta et al. (1996) extended the eight-noded quadrilateral element developed by Ray et al. (1994) for dynamic analysis. Based on a higher order shear deformable displacement theory, the model was developed for active vibration control of laminated plates with integrated piezoelectric layers. Numerical results were performed on a simply supported cross-ply plate with attached piezopolymer layers to demonstrate the potential to achieve significant reductions in vibration amplitude. Kim et al. (1997) provided additional details of the theoretical development of the transition element reported by Kim et al. (1996). Numerical studies were conducted to demonstrate convergence characteristics and to show the increased computational efficiency of this approach. Saravanos (1997) presented a shell element for curvilinear piezoelectric laminates which combined a first order shear deformation theory for the displacements along with a layerwise theory for the electric potential. The quadratic element was intended for static and dynamic analysis of thin to moderately thick shell structures. Numerical studies quantified the effects of curvature on the active and sensory response of piezoelectric shells.

2.4 Coupled Thermoelctromechanical Models

All of the previously described models neglect the implication of thermal effects on both the active and sensory response of piezoelectric structures. Although Mindlin (1974) derived the two-dimensional thermopiezoelectric equations for plates over twenty years ago, only limited research has been performed into this area. The development of models for thermopiezoelectric materials can be separated into two categories: (1) analytical models and (2) finite element models. The analytic models extend existing piezoelectric laminate theories to account for thermal effects and obtain solutions for specific problems. The finite element models provide a more general purpose tool to efficiently analyze complex problems.

2.4.1 Analytical Models

Tauchert (1992) developed a thermopiezoelectric laminate plate theory. His theory extended classical laminate theory to account for thin laminated plates with thermopiezoelectric layers. Specific solutions were developed for both free and simply supported composite plates with attached piezoelectric polymer layers. Numerical results demonstrated the capability to reduce thermal deformations through application of active electric voltages. Tzou and Howard (1994) formulated

a thermopiezoelectric thin shell theory for applications to active structures. The generic shell theory was derived using Kirchoff-Love shell theory and Hamilton's principle. Using a simplification procedure based on the Lamé parameters and radii of curvatures, specific solutions were obtained for a cylindrical piezoelectric ring, a piezoelectric ring, and a piezoelectric beam. Tang and Xu (1995) developed dynamic solutions for a simply supported anisotropic piezothermoelastic composite plate. The coupling between the elastic field and the electric and thermal fields were neglected to simplify the analysis. Numerical results demonstrated a significant reduction in deflection of a plate by the addition of a piezoelectric layer with a harmonic electric field.

Tzou and Bao (1995) extended the thermopiezoelectric thin shell theory developed by Tzou and Howard (1994) for applications to anisotropic shell laminates with distributed sensors and actuators. The governing equations were simplified and applied to a thin piezothermoelastic laminated shell made of a piezoelectric polymer. Applications demonstrated the coupling between the elastic, electric, and thermal fields and the importance of all three fields on the overall behavior of the shell. Stam and Carmen (1996) presented axisymmetric thermoelectromechanical solutions for concentric piezoelectric cylinders. The analytical approach was used to model the quasistatic response of a linear piezoelectric motor. Results of the study demonstrated the capability to extrapolate the nonlinear dependence of the piezoelectric coefficients with electric fields to lower temperatures using the constitutive equations. Friswell et al. (1997) developed a linear model to investigate active damping of thermally induced vibrations. Numerical studies were conducted on a simply supported aluminum beam with a piezoelectric sensor/actuator pair to demonstrate the influence of pyroelectric effects on vibration control.

2.4.2 Finite Element Models

Rao and Sunar (1993) developed a finite element formulation with applications for integrated sensing and control of thermopiezoelectric materials. Numerical studies were performed on a piezoelectric bimorph beam and an isotropic beam with attached piezoelectric polymer layers. The results demonstrated the significance of thermal effects on the performance of distributed control systems. Jonnalagadda et al. (1994) implemented a nine-noded Lagrangian plate element using a first-order shear deformation theory. Numerical studies were performed on a simply supported composite plate with an attached piezoelectric active layer and demonstrated the importance of a higher order laminate theory to accurately predict shear deformations in thick laminates. Tzou and Ye (1994) extended the previously developed solid element of Tzou and Tseng (1990) to account for thermal effects. The resulting three-dimensional thin hexahedron element represented the displacements, electric potential, and temperature as state variables. Numerical studies were performed on a cantilevered isotropic beam with attached piezoelectric layers to demonstrate the influence of thermal effects on sensing and control.

Chandrashekhara and Tenneti (1995) developed a nine-noded finite element for active thermal control of composite plates with piezoelectric actuators and sensors. The approach incorporated an induced strain approach to approximate the piezoelectric and thermal strains. Numerical studies demonstrated the capability to suppress thermally induced deformations through the application of electrical voltages in piezoelectric patches. Shen and Weng (1995) implemented a three-dimensional brick finite element to investigate composite plates with piezoelectric layers. Numerical studies demonstrated the significant coupling between the strain and electric fields and the capability to achieve thermal shape control of a simply supported piezoelectric composite plate.

Sunar and Rao (1997) formulated finite element equations for the design of thermopiezoelectric sensors and actuators. Numerical studies were conducted on cantilevered beams with piezoelectric actuators to show the significance of temperature effects on distributed control.

2.5 Limitations of Existing Analytical Models

The previously described analytical models contain three limitations that restrict the general application of these models. The first limitation is found in the induced strain models and arises from the use of approximate forces to represent the piezoelectric strains. This approximate representation fails to capture the coupled mechanical and electrical response and limits these models for use in predicting only the actuator behavior of piezoelectric materials. The induced strain limitations are overcome in the coupled electromechanical and thermoelectromechanical models through the use of a more consistent representation of the coupling which occurs between the electrical and mechanical responses. However, both the coupled electromechanical and thermoelectromechanical models are restricted by a second limitation arising from the predominant use of single layer laminate theories to predict the laminate response. In general, the single layer theories only provide good predictions for thin laminates and are inaccurate for both thick laminates and laminates which contain strong inhomogeneities through-the-thickness. The third limitation is found in both the induced strain and coupled electromechanical models, and arises due to neglecting thermal effects, even though these effects can be significant in changing temperature environments. Even in the coupled thermoelectromechanical models which account for thermal effects, many of the analytical formulations fail to account for all the mechanisms which produce thermal effects in piezoelectric materials: induction of thermal strains due to thermal expansion mismatch, pyroelectric effects, and temperature dependent material properties. Currently, no analytical model addresses all three of these limitations.

Thus, in this research, each of these three limitations are addressed to provide an enhanced analysis capability for modeling arbitrary structures which contain piezoelectric materials. A consistent representation of the coupled mechanical, electrical, and thermal response of piezoelectric materials is implemented to overcome the induced strain limitations and provides an inherent capability to model both the sensory and active behaviors of piezoelectric materials. A layerwise laminate theory is implemented to address the single layer laminate theory limitations and leads to more accurate analysis of thick laminates and laminates with contain strong inhomogeneities through-the-thickness. Thermal effects arising from thermal expansion mismatch, pyroelectric effects, and temperature dependent material properties are explicitly accounted for in the formulation. The development of this enhanced formulation has been reported for a linear beam element (Lee and Saravanos, 1996), a bi-linear plate element (Lee and Saravanos, 1997, 1998) and a quadratic curvilinear shell element (Lee and Saravanos, 2000).

CHAPTER 3 THEORETICAL DEVELOPMENT

This section outlines the foundations and steps for developing the analytical formulation for piezoelectric composite materials. This development is based on the theory of linear piezoelectricity which have been previously reported in detail by Cady (1964), Tiersten (1969), Nye (1972), and Parton and Kudryavstev (1988).

3.1 Current Formulation Assumptions

The current formulation is based on the linear theory of piezoelectricity in which the equations of linear elasticity are coupled to the charge equations of electrostatics through the piezoelectric constants. Due to the assumption of a linear theory, both mechanical and electric body forces and couples are neglected in the derivation. The current model also assumes infinitesimal deformations and strains, and, thus, no distinction is made between the initial and final positions. The current formulation also neglects the two way thermopiezoelectric coupling and focuses only on the one way heat conduction analysis. This assumption essentially provides that temperature changes due to changes in strains and electric fields are small compared to the magnitude of the thermal load. Thus, temperature changes only produce mechanical and electrical forcing on the piezoelectric material.

3.2 Governing Material Equations

The mechanical response of the piezoelectric material is represented by the equation of motion,

$$\sigma_{ij,j} + f_i = \rho \ddot{u}_i \quad (1)$$

while the electrical response is described by the electrostatic equation for the conservation of electric flux,

$$D_{i,i} = 0 \quad (2)$$

where σ_{ij} are the stresses, f_i are the body forces per unit volume, ρ is the density, u_i are the displacements, and D_i are electrical fluxes. In addition, i, j ranges from 1 to 3, superscript dots represent time derivatives, and subscript commas represent differentiation. Through use of the divergence theorem and neglecting body forces, Equations (1) and (2) can be expressed in an equivalent variational form as

$$\int_V (\rho \ddot{u}_i \delta u_i + \sigma_{ij} \delta S_{ij} - D_i \delta E_i) dV = \int_{\Gamma_t} t_i \delta u_i d\Gamma + \int_{\Gamma_p} q \delta \phi d\Gamma \quad (3)$$

where S_{ij} represent the strains, E_i are the electric fields, t_i are the surface tractions applied on the

surface Γ , q is the electrical charge applied on the surface Γ_p of the piezoelectric material, ϕ is the electric potential, and V represents the whole volume including both composite and piezoelectric materials.

3.1.1. Strains and Electric Field in Cartesian Coordinates

Two additional relationships for the strain and electric field are required in the equivalent variational form (Equation 3). In a Cartesian coordinate system, the small deformation strain-displacement relations are

$$S_{ij} = \frac{1}{2} (u_{i,j} + u_{j,i}) \quad (4)$$

while the electric field vector is related to the electric potential by

$$E_i = - \phi_{,i} \quad (5)$$

3.1.2. Strains and Electric Field in Curvilinear Coordinates

The curvilinear coordinate system employed in the formulation is shown in Figure 1. Each ply of the laminate remains parallel to a reference curvilinear surface A_o and an orthogonal curvilinear coordinate system $\bar{O}_{\xi\eta\zeta}$ is defined, such that the axes ξ and η lie on the curvilinear reference surface A_o , while the axis ζ remains straight and perpendicular to the layers of the laminate. A global Cartesian coordinate system O_{xyz} is used to define A_o , hence, a point $r = (x,y,z)$ on the curvilinear laminate is,

$$r(\xi, \eta, \zeta) = r_o(\xi, \eta) + \zeta \hat{\zeta} \quad (6)$$

where, $r_o = (x_o, y_o, z_o)$ are the Cartesian coordinates of the reference surface A_o and $\hat{\zeta}$ indicates the unit vector perpendicular to the reference surface.

The strain and electric field in this curvilinear coordinate system take the following form (Fung, 1965)

$$S_{ij} = \frac{1}{2\sqrt{g_{ii}g_{jj}}} [(u_{i,j} + u_{j,i}) - u_k(\Gamma^{kj}_i + \Gamma^{ki}_j)] \quad (7)$$

$$E_i = - \frac{\phi_{,i}}{\sqrt{g_{ii}}} \quad (8)$$

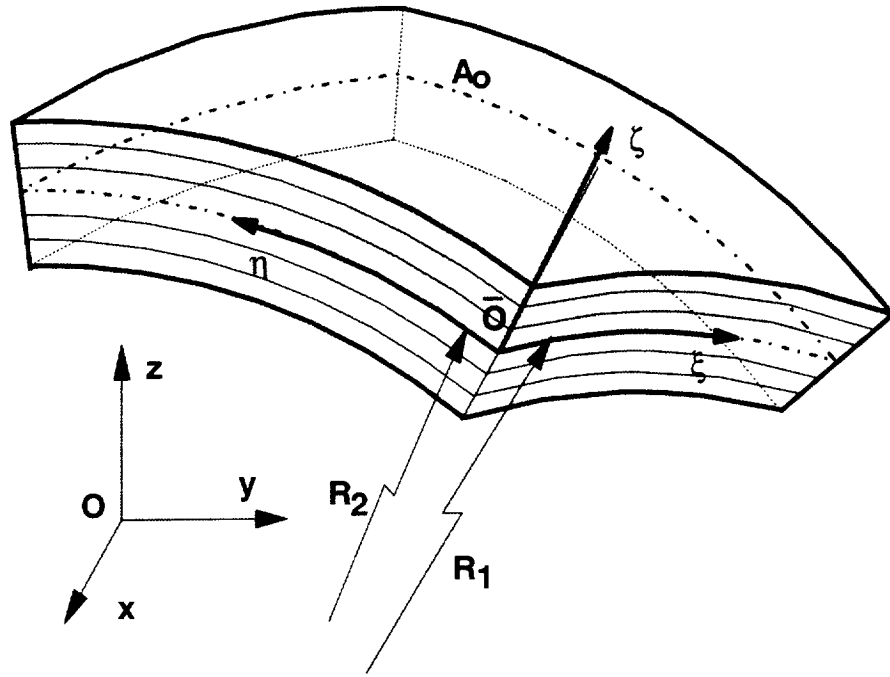


Figure 1: Curvilinear piezoelectric laminate and coordinate systems.

where g_{ii} are the metric tensors and Γ_{ij} are the Christoffel symbols. The following form of the Euclidian metric tensors are employed in the current formulation (Soedel, 1993),

$$g_{11} = \left(1 + \frac{\zeta}{R_1}\right)^2 g_{11}^o \quad (9)$$

$$g_{22} = \left(1 + \frac{\zeta}{R_2}\right)^2 g_{22}^o \quad (10)$$

$$g_{33} = 1 \quad (11)$$

where R_i are the local radii of curvature and g_{ii}^o are the components of the metric tensor on the surface A_0 ($\zeta=0$) defined as

$$g_{11}^o = \sqrt{x_{o,\xi}^2 + y_{o,\xi}^2 + z_{o,\xi}^2} \quad (12)$$

$$g_{22}^o = \sqrt{x_{o,\eta}^2 + y_{o,\eta}^2 + z_{o,\eta}^2} \quad (13)$$

Substituting Equations (9)-(11) into Equation (7) produces the following relationships (Soedel, 1993)

$$S_{11} = \frac{1}{g_{11}^o \left(1 + \frac{\zeta}{R_1}\right)} \left(u_{,\xi} + \frac{g_{11,\eta}^o}{g_{22}^o} v + \frac{g_{11}^o}{R_1} w \right) \quad (14)$$

$$S_{22} = \frac{1}{g_{22}^o \left(1 + \frac{\zeta}{R_2}\right)} \left(\frac{g_{22,\xi}^o}{g_{11}^o} u + v_{,\eta} + \frac{g_{22}^o}{R_2} w \right) \quad (15)$$

$$S_{33} = w_{,\zeta} \quad (16)$$

$$S_{12} = \frac{1}{g_{22}^o \left(1 + \frac{\zeta}{R_2}\right)} \left(u_{,\eta} - \frac{g_{22,\xi}^o}{g_{11}^o} v \right) + \frac{1}{g_{11}^o \left(1 + \frac{\zeta}{R_1}\right)} \left(v_{,\xi} - \frac{g_{11,\eta}^o}{g_{22}^o} u \right) \quad (17)$$

$$S_{13} = u_{,\zeta} + \frac{1}{g_{11}^o \left(1 + \frac{\zeta}{R_1}\right)} \left(w_{,\xi} - \frac{g_{11}^o}{R_1} u \right) \quad (18)$$

$$S_{23} = v_{,\zeta} + \frac{1}{g_{22}^o \left(1 + \frac{\zeta}{R_2}\right)} \left(w_{,\eta} - \frac{g_{22}^o}{R_2} v \right) \quad (19)$$

where u, v, w are the displacements of the curvilinear system. Similarly, introducing Equations (9)-(11) into Equation (8) produces the following relationships

$$E_1 = -\frac{1}{g_{11}^o \left(1 + \frac{\zeta}{R_1}\right)} \varphi_{,\xi} \quad (20)$$

$$E_2 = -\frac{1}{g_{22}^o \left(1 + \frac{\zeta}{R_2}\right)} \varphi_{,\eta} \quad (21)$$

$$E_3 = -\varphi_{,\zeta} \quad (22)$$

3.3 Thermopiezoelectric Constitutive Equations

The constitutive equations for a linear thermopiezoelectric material employing standard contracted notation (Nye, 1964) are

$$S_\alpha = s_{\alpha\beta}^{E,T}(T) \sigma_\beta + d_{\alpha m}^T(T) E_m + \alpha_\alpha^{E,T}(T) \theta \quad (23)$$

$$D_m = d_{m\alpha}^T(T) \sigma_\alpha + \epsilon_{mk}^{\sigma,T}(T) E_k + p_m^{\sigma,T}(T) \theta \quad (24)$$

or in semi-inverted form,

$$\sigma_\alpha = C_{\alpha\beta}^{E,T}(T) S_\beta - e_{\alpha m}^T(T) E_m - \lambda_\alpha^{E,T}(T) \theta \quad (25)$$

$$D_m = e_{m\alpha}^T(T) S_\alpha + \epsilon_{mk}^{S,T}(T) E_k + p_m^{S,T}(T) \theta \quad (26)$$

with the following relationships in the various piezoelectric and thermal properties arising from the inversion,

$$e_{\alpha m}^T(T) = C_{\alpha\beta}^{E,T}(T) d_{\beta m}^T(T) E_m \quad (27)$$

$$\lambda_\alpha^{E,T}(T) = C_{\alpha\beta}^{E,T}(T) \alpha_\beta^{E,T}(T) \quad (28)$$

$$\epsilon_{mk}^{S,T}(T) = \epsilon_{mk}^{\sigma,T}(T) - d_{m\alpha}^T(T) e_{\alpha k}^T(T) \quad (29)$$

$$p_m^{S,T}(T) = p_m^{\sigma,T}(T) - d_{m\alpha}^T(T) \lambda_\alpha^{E,T}(T) \quad (30)$$

where $C_{\alpha\beta}$ and $s_{\alpha\beta}$ are the elastic stiffness and compliance tensors; $d_{\alpha m}$ and $e_{\alpha m}$ are the different forms of the piezoelectric tensor due to inversion; ϵ_{mk} is the electric permittivity tensor; α_α and λ_α are the different forms of the coefficient of thermal expansion due to inversion; p_m is the pyroelectric

constant; $\theta = \Delta T = T - T_0$ is the temperature difference from the current temperature T and the thermally stress free reference temperature T_0 ; and; superscripts E, σ , S, and T, represent constant voltage, constant stress, constant strain, and constant temperature conditions, respectively; $\alpha, \beta = 1, \dots, 6$; and $k, m = 1, 2, 3$.

3.3.1 Piezoelectric Beam

The specific form of the thermopiezoelectric constitutive equations for a piezoelectric beam are simplified since only axial variations of the displacements are assumed,

$$\begin{Bmatrix} S_1 \\ S_5 \end{Bmatrix} = \begin{bmatrix} s_{11} & 0 \\ 0 & s_{55} \end{bmatrix} \begin{Bmatrix} \sigma_1 \\ \sigma_5 \end{Bmatrix} + \begin{bmatrix} 0 & d_{31} \\ d_{15} & 0 \end{bmatrix} \begin{Bmatrix} E_1 \\ E_3 \end{Bmatrix} + \begin{bmatrix} \alpha_1 \\ 0 \end{bmatrix} \theta \quad (31)$$

$$D_3 = d_{31} \sigma_1 + \epsilon_{33} E_3 + p_3 \theta \quad (32)$$

or in semi-inverted form

$$\begin{Bmatrix} \sigma_1 \\ \sigma_5 \end{Bmatrix} = \begin{bmatrix} C_{11} & 0 \\ 0 & C_{55} \end{bmatrix} \begin{Bmatrix} S_1 \\ S_5 \end{Bmatrix} - \begin{bmatrix} 0 & e_{31} \\ e_{15} & 0 \end{bmatrix} \begin{Bmatrix} E_1 \\ E_3 \end{Bmatrix} - \begin{bmatrix} \lambda_1 \\ 0 \end{bmatrix} \theta \quad (33)$$

$$D_3 = e_{31} S_1 + \epsilon_{33} E_3 + p_3 \theta \quad (34)$$

3.3.2 Piezoelectric Plate and Shell

For the piezoelectric plate and shell, the thermopiezoelectric constitutive equations for a monoclinic orthotropic piezoelectric material (Mason, 1950) are used,

$$\begin{Bmatrix} S_1 \\ S_2 \\ S_4 \\ S_5 \\ S_6 \end{Bmatrix} = \begin{bmatrix} s_{11} & s_{12} & 0 & 0 & 0 \\ s_{12} & s_{22} & 0 & 0 & 0 \\ 0 & 0 & s_{44} & 0 & 0 \\ 0 & 0 & 0 & s_{55} & 0 \\ 0 & 0 & 0 & 0 & s_{66} \end{bmatrix} \begin{Bmatrix} \sigma_1 \\ \sigma_2 \\ \sigma_4 \\ \sigma_5 \\ \sigma_6 \end{Bmatrix} + \begin{bmatrix} 0 & 0 & d_{31} \\ 0 & 0 & d_{32} \\ d_{14} & 0 & 0 \\ d_{15} & 0 & 0 \\ 0 & 0 & 0 \end{bmatrix} \begin{Bmatrix} E_1 \\ E_2 \\ E_3 \end{Bmatrix} + \begin{Bmatrix} \alpha_1 \\ \alpha_2 \\ 0 \\ 0 \\ 0 \end{Bmatrix} \theta \quad (35)$$

$$\begin{Bmatrix} D_1 \\ D_2 \\ D_3 \end{Bmatrix} = \begin{bmatrix} 0 & 0 & 0 & d_{15} & 0 \\ 0 & 0 & d_{24} & 0 & 0 \\ d_{31} & d_{32} & 0 & 0 & 0 \end{bmatrix} \begin{Bmatrix} \sigma_1 \\ \sigma_2 \\ \sigma_4 \\ \sigma_5 \\ \sigma_6 \end{Bmatrix} + \begin{bmatrix} \varepsilon_{11} & 0 & 0 \\ 0 & \varepsilon_{22} & 0 \\ 0 & 0 & \varepsilon_{33} \end{bmatrix} \begin{Bmatrix} E_1 \\ E_2 \\ E_3 \end{Bmatrix} + \begin{Bmatrix} p_1 \\ p_2 \\ p_3 \end{Bmatrix} \theta \quad (36)$$

or in semi-inverted form

$$\begin{Bmatrix} \sigma_1 \\ \sigma_2 \\ \sigma_4 \\ \sigma_5 \\ \sigma_6 \end{Bmatrix} = \begin{bmatrix} C_{11} & C_{12} & 0 & 0 & 0 \\ C_{12} & C_{22} & 0 & 0 & 0 \\ 0 & 0 & C_{44} & 0 & 0 \\ 0 & 0 & 0 & C_{55} & 0 \\ 0 & 0 & 0 & 0 & C_{66} \end{bmatrix} \begin{Bmatrix} S_1 \\ S_2 \\ S_4 \\ S_5 \\ S_6 \end{Bmatrix} - \begin{bmatrix} 0 & 0 & e_{31} \\ 0 & 0 & e_{32} \\ 0 & e_{24} & 0 \\ e_{15} & 0 & 0 \\ 0 & 0 & 0 \end{bmatrix} \begin{Bmatrix} E_1 \\ E_2 \\ E_3 \end{Bmatrix} - \begin{Bmatrix} \lambda_1 \\ \lambda_2 \\ 0 \\ 0 \\ 0 \end{Bmatrix} \theta \quad (37)$$

$$\begin{Bmatrix} D_1 \\ D_2 \\ D_3 \end{Bmatrix} = \begin{bmatrix} 0 & 0 & 0 & e_{15} & 0 \\ 0 & 0 & e_{24} & 0 & 0 \\ e_{31} & e_{32} & 0 & 0 & 0 \end{bmatrix} \begin{Bmatrix} S_1 \\ S_2 \\ S_4 \\ S_5 \\ S_6 \end{Bmatrix} + \begin{bmatrix} \varepsilon_{11} & 0 & 0 \\ 0 & \varepsilon_{22} & 0 \\ 0 & 0 & \varepsilon_{33} \end{bmatrix} \begin{Bmatrix} E_1 \\ E_2 \\ E_3 \end{Bmatrix} + \begin{Bmatrix} p_1 \\ p_2 \\ p_3 \end{Bmatrix} \theta \quad (38)$$

CHAPTER 4 LAMINATE MECHANICS

In order to provide more general and accurate analysis of piezoelectric laminates, different theories are implemented for the beam, plate, and shell laminates. A layerwise laminate theory is used as the basis for the different formulations since this theory represents a generalization of other single and higher order laminate theories (Reddy, 1993). The layerwise theory allows separate fields to be assumed for each state variable which provides for more accurate analysis of thick laminates and laminates containing strong inhomogeneities. In the current formulation various simplifying assumptions and approximations are used for the beam, plate, and shell laminates.

4.1 Layerwise Laminate Theory

The general layerwise laminate theory is formulated by introducing piecewise continuous approximations through-the-thickness for each state variable,

$$u(x, y, z, t) = \sum_{j=1}^N u^j(x, y, t) \psi_u^j(z) \quad (39)$$

$$v(x, y, z, t) = \sum_{j=1}^N v^j(x, y, t) \psi_v^j(z) \quad (40)$$

$$w(x, y, z, t) = \sum_{j=1}^N w^j(x, y, t) \psi_w^j(z) \quad (41)$$

$$\varphi(x, y, z, t) = \sum_{j=1}^N \varphi^j(x, y, t) \psi_\varphi^j(z) \quad (42)$$

$$\theta(x, y, z, t) = \sum_{j=1}^N \theta^j(x, y, t) \psi_\theta^j(z) \quad (43)$$

where N is the number of interpolation functions ψ^j and u^j , v^j , w^j , φ^j , and θ^j are the generalized laminate state variables. In general, any order of interpolation functions can be used and different interpolation functions can be selected for each state variable depending on the level of detail desired in the analysis.

4.1.1. Beam Laminate Theory

In deriving the beam laminate theory, only axial and through-the-thickness variations of the state variables are assumed. In addition, the displacement w is assumed to be constant through-the-thickness. This leads to the following simplified approximations from the general layerwise theory,

$$u(x, z, t) = \sum_{j=1}^N u^j(x, t) \psi^j(z) \quad (44)$$

$$w(x, z, t) = w^o(x, t) \quad (45)$$

$$\varphi(x, z, t) = \sum_{j=1}^N \varphi^j(x, t) \psi^j(z) \quad (46)$$

$$\theta(z, t) = \sum_{j=1}^N \theta^j(t) \psi^j(z) \quad (47)$$

$$\psi^j(z) = [1 - \xi \quad \xi] \quad (48)$$

where N is the number of interpolation functions ψ^j , $\xi = z/h$, and h represents the thickness of each discrete layer. In this formulation, the same linear Lagrangian interpolation functions are used for each state variable.

4.1.2 Plate Laminate Theory

The plate laminate theory is formulated with the displacement w assumed to be constant through-the-thickness, which leads to the following simplified approximations from the general layerwise theory,

$$u(x, y, z, t) = \sum_{j=1}^N u^j(x, y, t) \psi^j(z) \quad (49)$$

$$v(x, y, z, t) = \sum_{j=1}^N v^j(x, y, t) \psi^j(z) \quad (50)$$

$$w(x, y, z, t) = w^o(x, y, t) \quad (51)$$

$$\varphi(x, y, z, t) = \sum_{j=1}^N \varphi^j(x, y, t) \psi^j(z) \quad (52)$$

$$\theta(z, t) = \sum_{j=1}^N \theta^j(t) \psi^j(z) \quad (53)$$

$$\psi^j(z) = [1 - \xi \quad \xi] \quad (54)$$

where N is the number of interpolation functions ψ^j and $\xi=z/h$. For the current plate laminate theory, the same linear Lagrangian interpolation functions are used for each state variable.

4.1.3 Shell Laminate Theory

The shell laminate theory combines linear displacement fields through-the-thickness of the laminate for the displacements u and v (along the ξ and η axes respectively) with layerwise electric potential and temperature fields through the laminate, consisting of N discrete continuous segments. Consequently, the present shell theory is specialized for modeling the deformation of thin and moderately thick piezoelectric shells, while maintaining the capability to capture the through-the-thickness electric and thermal inhomogeneities. The various field variables are approximated by the following form,

$$u(\xi, \eta, \zeta, t) = u^o(\xi, \eta, t) + \zeta \beta_{\xi}(\xi, \eta, t) \quad (55)$$

$$v(\xi, \eta, \zeta, t) = v^o(\xi, \eta, t) + \zeta \beta_{\eta}(\xi, \eta, t) \quad (56)$$

$$w(\xi, \eta, \zeta, t) = w^o(\xi, \eta, t) \quad (57)$$

$$\phi(\xi, \eta, \zeta, t) = \sum_{j=1}^N \phi^j(\xi, \eta, t) \Psi^j(\zeta) \quad (58)$$

$$\theta(\xi, \eta, \zeta, t) = \sum_{j=1}^N \theta^j(\xi, \eta, t) \Psi^j(\zeta) \quad (59)$$

$$\psi^j(\zeta) = [1 - \xi \quad \xi] \quad (60)$$

where N is the number of interpolation functions ψ^j , $\xi=\zeta/h$, and β_{ξ} and β_{η} are the flexural rotation

angles. The same linear Lagrangian interpolation functions $\Psi(\zeta)$ are used for the electric potential and temperature state variables.

4.2 Generalized Laminate Matrices

The next step in the development of the formulation is the introduction of the layerwise approximations into the variational form of the equation of motion and the electrostatic equation (Equation 3). By performing an integration through-the-thickness, the dependence of the through-the-thickness coordinate can be separated from the in-plane coordinates into generalized laminate matrices for the density, stiffness, piezoelectric, dielectric permittivity, thermal expansion, and pyroelectric properties.

4.2.1 Beam Laminate Matrices

The equivalent variational form is derived by substituting Equations (4), (5), (20), (21), and (31)-(34) into Equation (3), and integrating through-the-thickness,

$$\begin{aligned}
 & \sum_{k=1}^n \sum_{m=1}^n \int_x \rho_{11}^{km} \ddot{u}^m \delta u^k dx + \int_x \rho_{33} \dot{w} \delta w dx + \\
 & \sum_{k=1}^n \sum_{m=1}^n \int_x \left(D_{11}^{km} \frac{\partial u^m}{\partial x} \frac{\partial \delta u^k}{\partial x} + D_{55}^{km} u^m \delta u^k \right) dx + \\
 & \sum_{k=1}^n \int_x B_{55}^k \left(\frac{\partial w}{\partial x} \delta u^k + u^k \frac{\partial \delta w}{\partial x} \right) dx + \int_x A_{55} \frac{\partial w}{\partial x} \frac{\partial \delta w}{\partial x} dx + \\
 & \sum_{k=1}^n \sum_{m=1}^n \int_x E_{31}^{km} \left(\varphi^m \frac{\partial \delta u^k}{\partial x} + \frac{\partial u^m}{\partial x} \delta \varphi^k \right) dx - \\
 & \sum_{k=1}^n \sum_{m=1}^n \int_x G_{33}^{km} \varphi^m \delta \varphi^k dx - \sum_{k=1}^n \int_x \left(\Lambda_1^k \frac{\partial \delta u^k}{\partial x} - P_3^k \delta \varphi^k \right) dx \\
 & = \int_{\Gamma} t_i \delta u_i d\Gamma + \int_{\Gamma_p} q \delta \varphi d\Gamma
 \end{aligned} \tag{61}$$

in which the dependence of the z-coordinate has been separated into the generalized density matrix $[\rho]$, the stiffness matrices $[A]$, $[B]$, $[D]$, the piezoelectric matrix $[E]$, the dielectric permittivity matrix $[G]$, the thermal expansion matrix $[\Lambda_1]$, and the pyroelectric matrix $[P_3]$.

The laminate density matrices are

$$\rho_{11}^{km} = \sum_{l=1}^L \int_z b \rho \psi^k(z) \psi^m(z) dz \quad (62)$$

$$\rho_{33} = \sum_{l=1}^L \int_z b \rho dz \quad (63)$$

the laminate stiffness matrices are

$$A_{55} = \sum_{l=1}^L \int_z b C_{55} dz \quad (64)$$

$$B_{55}^k = \sum_{l=1}^L \int_z b C_{55} \frac{\partial \psi^k(z)}{\partial z} dz \quad (65)$$

$$D_{11}^{km} = \sum_{l=1}^L \int_z b C_{11} \psi^k(z) \psi^m(z) dz \quad (66)$$

$$D_{55}^{km} = \sum_{l=1}^L \int_z b C_{55} \frac{\partial \psi^k(z)}{\partial z} \frac{\partial \psi^m(z)}{\partial z} dz \quad (67)$$

The piezoelectric laminate matrix is

$$E_{31}^{km} = \sum_{l=1}^L \int_z b e_{31} \psi^k(z) \frac{\partial \psi^m(z)}{\partial z} dz \quad (68)$$

The dielectric permittivity laminate matrix is

$$G_{33}^{km} = \sum_{l=1}^L \int_z b \epsilon_{33} \frac{\partial \psi^k(z)}{\partial z} \frac{\partial \psi^m(z)}{\partial z} dz \quad (69)$$

The laminate thermal force vector is

$$\Lambda_1^k = \sum_{l=1}^L \int_x b \lambda_{1l} \theta^j \psi^j(z) \psi^k(z) dz \quad (70)$$

The laminate thermal electric displacement vector is

$$P_3^k = \sum_{l=1}^L \int_x b p_{3l} \theta^j \psi^j(z) \frac{\partial \psi^k(z)}{\partial z} dz \quad (71)$$

where L is the number of plies and b is the width of the beam.

4.2.2. Plate Laminate Matrices

The equivalent variational form is derived by substituting Equations (4), (5), (24)-(25), and (36)-(40) into Equation (3), and integrating through-the-thickness

$$\begin{aligned}
 & \sum_{k=1}^N \sum_{m=1}^N \int_A (\rho_{11}^{km} \ddot{u}^m \delta u^k + \rho_{22}^{km} \ddot{v}^m \delta v^k) dA + \int_A \rho_{33} \ddot{w} \delta w dA \\
 & \sum_{k=1}^N \sum_{m=1}^N \int_A \{ A_{11}^{km} u_{,x}^m \delta u_{,x}^k + A_{12}^{km} (u_{,x}^m \delta v_{,y}^k + v_{,y}^m \delta u_{,x}^k) + \\
 & A_{16}^{km} (u_{,x}^m \delta u_{,y}^k + u_{,y}^m \delta u_{,x}^k + u_{,x}^m \delta v_{,x}^k + v_{,x}^m \delta u_{,x}^k) + A_{22}^{km} v_{,y}^m \delta v_{,y}^k + \\
 & A_{26}^{km} (u_{,y}^m \delta v_{,y}^k + v_{,y}^m \delta u_{,y}^k + v_{,x}^m \delta v_{,y}^k + v_{,y}^m \delta v_{,x}^k) + \\
 & A_{66}^{km} (u_{,y}^m \delta u_{,y}^k + u_{,y}^m \delta v_{,x}^k + v_{,x}^m \delta v_{,x}^k + v_{,x}^m \delta u_{,y}^k) \} dA + \\
 & \sum_{m=1}^N \int_A \{ B_{44}^m (v^m \delta w_{,y} + w_{,y} \delta v^m) + B_{55}^m (u^m \delta w_{,x} + w_{,x} \delta u^m) + \\
 & B_{45}^m (u^m \delta w_{,y} + v^m \delta w_{,x} + w_{,x} \delta v^m + w_{,y} \delta u^m) \} dA + \\
 & \int_A \{ \overline{C}_{44} w_{,y} \delta w_{,y} + \overline{C}_{45} (w_{,x} \delta w_{,y} + w_{,y} \delta w_{,x}) + \overline{C}_{55} w_{,x} \delta w_{,x} \} dA \tag{72} \\
 & \sum_{k=1}^N \sum_{m=1}^N \int_A \{ D_{44}^{km} v^m \delta v^k + D_{45}^{km} (u^m \delta v^k + v^m \delta u^k) + D_{55}^{km} u^m \delta u^k + \\
 & E_{31}^{km} u_{,x}^m \delta \phi^k + E_{32}^{km} (v_{,y}^m \delta \phi^k + E_{36}^{km} (u_{,y}^m \delta \phi^k + v_{,x}^m \delta \phi^k) + \\
 & \overline{E}_{31}^{km} \phi^m \delta u_{,x}^k + \overline{E}_{32}^{km} \phi^m \delta v_{,y}^k + \overline{E}_{36}^{km} (\phi^m \delta u_{,y}^k + \phi^m \delta v_{,x}^k) \\
 & - G_{11}^{km} \phi_{,x}^m \delta \phi_{,x}^k - G_{22}^{km} \phi_{,y}^m \delta \phi_{,y}^k - G_{33}^{km} \phi^m \delta \phi^k \} dA \\
 & \sum_{m=1}^N \int_A \{ - \Lambda_1^m \delta u_{,x}^m - \Lambda_2^m \delta v_{,y}^m + P_1^m \delta \phi_{,x}^m + P_2^m \delta \phi_{,y}^m + P_3^m \delta \phi^m \} dA \\
 & = \int_{\Gamma} t_i \delta u_i d\Gamma + \int_{\Gamma_p} q \delta \phi d\Gamma
 \end{aligned}$$

in which the dependence of the z-coordinate has been separated into the generalized density matrix $[\rho]$, the stiffness matrices $[A]$, $[B]$, $[C]$, $[D]$, the piezoelectric matrix $[E]$, the dielectric permittivity matrix $[G]$, the thermal expansion matrix $[\Lambda]$, and the pyroelectric matrix $[P]$.

The laminate density matrix is

$$\rho_{ij}^{km} = \sum_{l=1}^L \int_{\bar{z}} \rho \psi^k(z) \psi^m(z) dz \quad (73)$$

for $ij = 11$ and 22 , while

$$\rho_{33} = \sum_{l=1}^L \int_{\bar{z}} \rho dz \quad (74)$$

the laminate stiffness matrices are

$$A_{ij}^{km} = \sum_{l=1}^L \int_{\bar{z}} C_{ij} \psi^k(z) \psi^m(z) dz \quad (75)$$

for $ij = 11, 12, 16, 22, 26, 44$, and 66 ;

$$B_{ij}^{km} = \sum_{l=1}^L \int_{\bar{z}} C_{ij} \frac{\partial \psi^k(z)}{\partial z} dz \quad (76)$$

$$\bar{C}_{ij} = \sum_{l=1}^L \int_{\bar{z}} C_{ij} dz \quad (77)$$

$$D_{ij}^{km} = \sum_{l=1}^L \int_{\bar{z}} C_{ij} \frac{\partial \psi^k(z)}{\partial z} \frac{\partial \psi^m(z)}{\partial z} dz \quad (78)$$

for $ij = 44, 45$, and 55 . The laminate piezoelectric matrices are

$$E_{ij}^{km} = \sum_{l=1}^L \int_{\bar{z}} e_{ij} \psi^k(z) \frac{\partial \psi^m(z)}{\partial z} dz \quad (79)$$

$$\bar{E}_{ij}^{km} = \sum_{l=1}^L \int_{\bar{z}} e_{ij} \psi^m(z) \frac{\partial \psi^k(z)}{\partial z} dz \quad (80)$$

for $ij = 31, 32,$ and 36 . The laminate dielectric permittivity matrix is

$$G_{ij}^{km} = \sum_{l=1}^L \int_z \varepsilon_{ij} \psi^k(z) \psi^m(z) dz \quad (81)$$

for $ij = 11$ and 22 , while

$$G_{33}^{km} = \sum_{l=1}^L \int_z \varepsilon_{33} \frac{\partial \psi^k(z)}{\partial z} \frac{\partial \psi^m(z)}{\partial z} dz \quad (82)$$

The laminate thermal force vector is

$$\Lambda_i^k = \sum_{l=1}^L \int_z \lambda_i \psi_j \theta_j \psi^k(z) dz \quad (83)$$

for $i = 1$ and 2 . The laminate thermal electric displacement vector is

$$P_i^k = \sum_{l=1}^L \int_z p_i \psi_j \theta_j \psi^k(z) dz \quad (84)$$

for $i=1$ and 2 , while

$$P_3^k = \sum_{l=1}^L \int_z p_3 \psi_j \theta_j \frac{\partial \psi^k(z)}{\partial z} dz \quad (85)$$

where L is the number of composite plies and piezoelectric layers.

4.2.3 Shell Laminate Matrices

The equivalent variational form is derived by substituting Equations (11), (12), (24)-(25), and (40)-(45) into Equation (3), and integrating through-the-thickness

$$\begin{aligned}
& \int_A \{ (\rho^A \ddot{u}^o + \rho^B \ddot{\beta}_{\xi}^o) \delta u^o + (\rho^A \ddot{v}^o + \rho^B \ddot{\beta}_{\eta}^o) \delta v^o + \rho^A \ddot{w}^o \delta w^o + \\
& \quad (\rho^B \ddot{u}^o + \rho^D \ddot{\beta}_{\xi}^o) \delta \beta_{\xi}^o + (\rho^B \ddot{v}^o + \rho^D \ddot{\beta}_{\eta}^o) \delta \beta_{\eta}^o \} d\xi d\eta + \\
& \sum_{j=1}^N \int_A \{ (A_{11} S_1^o + A_{12} S_2^o + B_{11} k_1 + B_{12} k_2 + \overline{E}_{31}^j \phi^j - \overline{\Lambda}_1^j \theta^j) \delta S_1^o + \\
& \quad (A_{12} S_1^o + A_{22} S_2^o + B_{12} k_1 + B_{22} k_2 + \overline{E}_{32}^j \phi^j - \overline{\Lambda}_2^j \theta^j) \delta S_2^o + \\
& \quad (A_{44} S_4^o + E_{24}^j \frac{\phi_{,\xi}^j}{g_{11}^o}) \delta S_4^o + (A_{66} S_6^o + B_{66} k_6) \delta S_6^o + (B_{66} S_6^o + D_{66} k_6) \delta k_6 \} + \\
& \quad (B_{11} S_1^o + B_{12} S_2^o + D_{11} k_1 + D_{12} k_2 + \hat{E}_{31}^j \phi^j - \hat{\Lambda}_1^j \theta^j) \delta k_1 + \\
& \quad (B_{12} S_1^o + B_{22} S_2^o + D_{12} k_1 + D_{22} k_2 + \hat{E}_{32}^j \phi^j - \hat{\Lambda}_2^j \theta^j) \delta k_2 + \\
& \quad \sum_{j=1}^N \sum_{k=1}^N \int_A \{ (E_{15}^j \frac{S_5^o}{g_{11}^o} - G_{11}^{jk} \frac{\phi_{,\xi}^k}{(g_{11}^o)^2} + P_1^{jk} \frac{\theta^j}{g_{11}^o}) \delta \phi_{,\xi}^k + \\
& \quad (E_{24}^j \frac{S_4^o}{g_{22}^o} - G_{22}^{jk} \frac{\phi_{,\eta}^k}{(g_{11}^o)^2} + P_2^{jk} \frac{\theta^j}{g_{22}^o}) \delta \phi_{,\eta}^k + \\
& \quad (\overline{E}_{31}^j S_1^o + \overline{E}_{32}^j S_2^o + \hat{E}_{31}^j k_1 + \hat{E}_{32}^j k_2 - G_{33}^{jk} \phi^k + P_3^{jk} \theta^k) \delta \phi^j \} d\xi d\eta \\
& \quad = \int_{\Gamma} t_i \delta u_i d\Gamma + \int_{\Gamma_p} q \delta \phi d\Gamma
\end{aligned} \tag{86}$$

in which the dependence of the z-coordinate has been separated into the generalized density matrix $[\rho]$, the stiffness matrices $[A]$, $[B]$, $[C]$, $[D]$, the piezoelectric matrix $[E]$, the dielectric permittivity matrix $[G]$, the thermal expansion matrix $[\Lambda]$, and the pyroelectric matrix $[P]$.

The laminate density matrix is

$$\rho^A = g_{11}^o g_{22}^o \sum_{l=1}^L \int_{\zeta} \rho d\zeta \tag{87}$$

$$\rho^B = g_{11}^o g_{22}^o \sum_{l=1}^L \int_{\zeta} \zeta \rho d\zeta \tag{88}$$

$$\rho^D = g_{11}^o g_{22}^o \sum_{l=1}^L \int_{\zeta} \zeta^2 \rho d\zeta \tag{89}$$

The laminate stiffness matrices are

$$A_{ij} = g_{11}^o g_{22}^o \sum_{l=1}^L \int_{\zeta} C_{ij} d\zeta \quad (90)$$

for $ij = 11, 12, 22, 44, 55, 66$

$$B_{ij} = g_{11}^o g_{22}^o \sum_{l=1}^L \int_{\zeta} \zeta C_{ij} d\zeta \quad (91)$$

$$D_{ij} = g_{11}^o g_{22}^o \sum_{l=1}^L \int_{\zeta} \zeta^2 C_{ij} d\zeta \quad (92)$$

for $ij = 11, 12,$ and 22 . The laminate piezoelectric matrices are

$$E_{ij}^k = g_{11}^o g_{22}^o \sum_{l=1}^L \int_{\zeta} e_{ij} \psi^k(\zeta) d\zeta \quad (93)$$

for $ij = 14, 15,$ and 24 .

$$\overline{E}_{ij}^k = g_{11}^o g_{22}^o \sum_{l=1}^L \int_{\zeta} e_{ij} \frac{\partial \psi^k(\zeta)}{\partial \zeta} d\zeta \quad (94)$$

$$\hat{E}_{ij}^k = g_{11}^o g_{22}^o \sum_{l=1}^L \int_{\zeta} \zeta e_{ij} \frac{\partial \psi^k(\zeta)}{\partial \zeta} d\zeta \quad (95)$$

for $ij = 31, 32,$ and 36 . The laminate dielectric permittivity matrix is

$$G_{ij}^{km} = g_{11}^o g_{22}^o \sum_{l=1}^L \int_{\zeta} \epsilon_{ij} \psi^k(\zeta) \psi^m(\zeta) d\zeta \quad (96)$$

for $ij = 11$ and 22 , while

$$G_{33}^{km} = g_{11}^o g_{22}^o \sum_{l=1}^L \int_{\zeta} \epsilon_{33} \frac{\partial \psi^k(\zeta)}{\partial \zeta} \frac{\partial \psi^m(\zeta)}{\partial \zeta} d\zeta \quad (97)$$

The laminate thermal force vector is

$$\overline{\Lambda}_i^k = g_{11}^o g_{22}^o \sum_{l=1}^L \int_{\zeta} \lambda_i \psi^k(\zeta) d\zeta \quad (98)$$

$$\hat{\Lambda}_i^k = g_{11}^o g_{22}^o \sum_{l=1}^L \int_{\zeta} \zeta \lambda_i \psi^k(\zeta) d\zeta \quad (99)$$

for $i = 1$ and 2 . The laminate thermal electric displacement vector is

$$P_i^{km} = g_{11}^o g_{22}^o \sum_{l=1}^L \int_{\zeta} p_k \psi^k(\zeta) \psi^m(\zeta) d\zeta \quad (100)$$

$$P_3^{km} = g_{11}^o g_{22}^o \sum_{l=1}^L \int_{\zeta} p_3 \frac{\partial \psi^k(\zeta)}{\partial \zeta} \psi^m(\zeta) d\zeta \quad (101)$$

for $i=1$ and 2 , while where L is the number of composite plies and piezoelectric layers.

CHAPTER 5
FINITE ELEMENT FORMULATION

Finite element based solutions for structural problems are obtained by incorporating additional local in-plane approximations as detailed in Hughes (1987) and Cook et al. (1989). For piezoelectric materials, the following approximations are made for the generalized laminate state variables introduced in Equations (39)-(42),

$$u^j(x, y, t) = \sum_{i=1}^M u^{ji}(t) N_u^i(x, y) \quad (102)$$

$$v^j(x, y, t) = \sum_{i=1}^M v^{ji}(t) N_v^i(x, y) \quad (103)$$

$$w^j(x, y, t) = \sum_{i=1}^M w^{ji}(t) N_w^i(x, y) \quad (104)$$

$$\phi^j(x, y, t) = \sum_{i=1}^M \phi^{ji}(t) N_\phi^i(x, y) \quad (105)$$

$$\theta^j(x, y, t) = \sum_{i=1}^M \theta^{ji}(t) N_\theta^i(x, y) \quad (106)$$

where M is the number of in-plane shape functions N. Typically, any order of shape functions can be used and different shape functions can be selected for each state variable, depending on the level of detail desired in the analysis.

By implementing the in-plane approximations for the state variables into the variational form of Equation (3) and collecting the coefficients, the following discrete matrix form can be obtained,

$$\begin{bmatrix} [M_{uu}] & 0 \\ 0 & 0 \end{bmatrix} \begin{Bmatrix} \{\ddot{u}\} \\ \{\ddot{\phi}\} \end{Bmatrix} + \begin{bmatrix} [K_{uu}] & [K_{u\phi}] \\ [K_{\phi u}] & [K_{\phi\phi}] \end{bmatrix} \begin{Bmatrix} \{u\} \\ \{\phi\} \end{Bmatrix} = \begin{Bmatrix} \{F(t)\} - [K_{u\theta}]\{\theta\} \\ \{Q(t)\} - [K_{\phi\theta}]\{\theta\} \end{Bmatrix} \quad (107)$$

where the submatrices K_{uu} , $K_{u\phi}$ and $K_{\phi\phi}$ indicate the elastic, piezoelectric and permittivity matrices; $K_{u\theta}$ and $K_{\phi\theta}$ are the thermal expansion and pyroelectric matrices of the structure; M_{uu} is the mass matrix; F are the applied mechanical loads; and Q are the applied voltages.

The coupled finite element formulation can also be expressed in a compact form with the electric potential partitioned into active and sensory components such that

$$\begin{bmatrix} [M_{uu}] & 0 \\ 0 & 0 \end{bmatrix} \begin{Bmatrix} \{\ddot{u}\} \\ \{\ddot{\phi}^F\} \end{Bmatrix} + \begin{bmatrix} [K_{uu}] & [K_{u\phi}^{FF}] \\ [K_{\phi u}^{FF}] & [K_{\phi\phi}^{FF}] \end{bmatrix} \begin{Bmatrix} \{u\} \\ \{\phi^F\} \end{Bmatrix} = \begin{Bmatrix} \{F(t)\} - [K_{u\phi}^{FA}]\{\phi^A\} - [K_{u\theta}]\{\theta\} \\ \{Q^F(t)\} - [K_{\phi\phi}^{FA}]\{\phi^A\} - [K_{\phi\theta}]\{\theta\} \end{Bmatrix} \quad (108)$$

where superscripts F and A indicate the partitioned submatrices in accordance with the sensory (free) and active electric potential components, respectively. Thus, the left-hand side includes the unknown electromechanical responses of the structure, u and ϕ^F (i.e. the resultant displacements and voltage at the sensors, respectively). The right-hand includes the known excitations of the structure by the mechanical loads, applied voltages on the actuators, applied temperature loads, and electric charges.

The matrix equations can also be condensed into the following independent equations for the sensory electric potentials,

$$\{\phi^F\} = [K_{\phi\phi}^{FF}]^{-1} ([K_{\phi\phi}^{FA}]\{\phi^A\} + [K_{\phi\theta}]\{\theta\} - [K_{\phi u}^{FF}]\{u\} - \{Q^F(t)\}) \quad (109)$$

and the structural displacements,

$$\begin{aligned} [M_{uu}]\{\ddot{u}\} + ([K_{uu}] - [K_{u\phi}^{FF}][K_{\phi\phi}^{FF}]^{-1}[K_{\phi u}^{FF}])\{u\} = \\ \{F(t)\} - ([K_{u\phi}^{FF}][K_{\phi\phi}^{FF}]^{-1}[K_{\phi\phi}^{FA}] + [K_{u\phi}^{FA}])\{\phi^A\} + \\ [K_{u\phi}^{FF}][K_{\phi\phi}^{FF}]^{-1}\{Q^F(t)\} - ([K_{u\phi}^{FF}][K_{\phi\phi}^{FF}]^{-1}[K_{\phi\theta}] + [K_{u\theta}])\{\theta\} \end{aligned} \quad (110)$$

5.1 Beam Element

The piezoelectric beam element formulation is obtained by incorporating the following in-plane approximations to the state variables,

$$u^j(x, t) = \sum_{i=1}^M u^{ji}(t) N^i(x) \quad (111)$$

$$w^j(x, t) = \sum_{i=1}^M w^{ji}(t) N^i(x) \quad (112)$$

$$\phi^j(x, t) = \sum_{i=1}^M \phi^{ji}(t) N^i(x) \quad (113)$$

$$N^i(x) = [1-\xi \quad \xi] \quad (114)$$

where M is the number of in-plane linear shape functions N , $\xi=x/L$, and L is the length of the element. A selectively reduced integration scheme is also implemented for the second stiffness term (containing D_{55}) of Equation (67) in order to eliminate locking.

Incorporating Equations (111)-(114) into Equation (61) results in the following specific forms of the submatrices defined in Equation (107) for the beam element, where the submatrices are defined using the beam laminate matrices of Equations (62)-(71). The mass matrix is

$$[M_{uu}] = \int_x [N]^T \begin{bmatrix} [\rho_{11}] & 0 \\ 0 & [\rho_{33}] \end{bmatrix} [N] dx \quad (115)$$

The stiffness matrices are

$$[K_{uu}] = \int_x \begin{bmatrix} [N_{,x}]^T [D_{11}] [N_{,x}] + [N]^T [D_{55}] [N] & [N]^T [B_{55}] [N_{,x}] \\ [N]^T [B_{55}] [N_{,x}] & [N_{,x}]^T [A_{55}] [N_{,x}] \end{bmatrix} dx \quad (116)$$

$$[K_{u\phi}] = \int_x [N]^T [E_{31}] [N_{,x}] dx \quad (117)$$

$$[K_{u\theta}] = \int_x [N]^T [\Lambda_1] dx \quad (118)$$

$$[K_{\phi\phi}] = \int_x [N]^T [G_{33}] [N] dx \quad (119)$$

$$[K_{\phi\theta}] = \int_x [N]^T [P_3] dx \quad (120)$$

5.2 Plate Element

The piezoelectric plate element implements the following in-plane approximations to the state variables,

$$u^j(x,y,t) = \sum_{i=1}^M u^{ji}(t) N^i(x,y) \quad (121)$$

$$v^j(x,y,t) = \sum_{i=1}^M v^{ji}(t) N^i(x,y) \quad (122)$$

$$w^j(x,y,t) = \sum_{i=1}^M w^{ji}(t) N^i(x,y) \quad (123)$$

$$\phi^j(x,y,t) = \sum_{i=1}^M \phi^{ji}(t) N^i(x,y) \quad (124)$$

$$N^i(x,y) = \frac{1}{4} [(1-\xi)(1-\eta) \quad (1+\xi)(1-\eta) \quad (1+\xi)(1+\eta) \quad (1-\xi)(1+\eta)] \quad (125)$$

where M is the number of in-plane bi-linear shape functions N , $\xi=x/a$, and $\eta=y/b$.

Implementing Equations (121)-(125) into Equation (72) leads to the following finite element submatrices for the plate element, where the submatrices are defined using the plate laminate matrices in Equations (73)-(85). The mass submatrices are

$$[M_{uu}] = \int_A [N]^T \begin{bmatrix} [\rho_{11}] & 0 & 0 \\ 0 & [\rho_{22}] & 0 \\ 0 & 0 & [\rho_{33}] \end{bmatrix} [N] dA \quad (126)$$

The stiffness submatrices are

$$[K_{uu}] = \begin{bmatrix} [K_{11}] & [K_{12}] & [K_{13}] \\ [K_{12}] & [K_{22}] & [K_{23}] \\ [K_{13}] & [K_{23}] & [K_{33}] \end{bmatrix} \quad (127)$$

where

$$[K_{11}] = \int_A \{ [N_{,x}]^T [A_{11}] [N_{,x}] + [N_{,x}]^T [A_{16}] [N_{,y}] + [N_{,y}]^T [A_{16}] [N_{,x}] + [N]^T [D_{55}] [N] + [N_{,y}]^T [A_{66}] [N_{,y}] \} dA \quad (128)$$

$$[K_{12}] = \int_A \{ [N_{,x}]^T [A_{12}] [N_{,y}] + [N_{,x}]^T [A_{16}] [N_{,x}] + [N_{,y}]^T [A_{26}] [N_{,y}] + [N]^T [D_{45}] [N] + [N_{,y}]^T [A_{66}] [N_{,x}] \} dA \quad (129)$$

$$[K_{13}] = \int_A \{ [N]^T [B_{45}] [N_{,y}] + [N]^T [B_{55}] [N_{,x}] \} dA \quad (130)$$

$$[K_{22}] = \int_A \{ [N_{,y}]^T [A_{22}] [N_{,y}] + [N_{,x}]^T [A_{26}] [N_{,y}] + [N_{,y}]^T [A_{26}] [N_{,x}] + [N]^T [D_{44}] [N] + [N_{,x}]^T [A_{66}] [N_{,x}] \} dA \quad (131)$$

$$[K_{23}] = \int_A \{ [N]^T [B_{44}] [N_{,y}] + [N]^T [B_{45}] [N_{,x}] \} dA \quad (132)$$

$$[K_{33}] = \int_A \{ [N_{,y}]^T [\overline{C}_{44}] [N_{,y}] + [N_{,x}]^T [\overline{C}_{45}] [N_{,y}] + [N_{,y}]^T [\overline{C}_{45}] [N_{,x}] + [N_{,x}]^T [\overline{C}_{55}] [N_{,x}] \} dA \quad (133)$$

$$[K_{u\phi}] = \int_A \begin{bmatrix} [N_{,x}]^T [E_{31}] [N] + [N_{,y}]^T [E_{36}] [N] \\ [N_{,y}]^T [E_{32}] [N] + [N_{,x}]^T [E_{36}] [N] \end{bmatrix} dA \quad (134)$$

$$[K_{u\theta}] = \int_A \begin{bmatrix} [N_{,x}]^T [\Lambda_1] \\ [N_{,y}]^T [\Lambda_2] \end{bmatrix} dA \quad (135)$$

$$[K_{\varphi\varphi}] = \int_A \{ [N_{,x}]^T [G_{11}] [N_{,x}] + [N_{,y}]^T [G_{22}] [N_{,y}] + [N]^T [G_{33}] [N] \} dA \quad (136)$$

$$[K_{\varphi 0}] = \int_A \{ [N_{,x}]^T [P_1] + [N_{,y}]^T [P_2] + [N]^T [P_3] \} dA \quad (137)$$

5.3 Shell Element

The piezoelectric shell element implements the following in-plane approximations to the state variables,

$$u_j^o(\xi, \eta, t) = \sum_{i=1}^M u_j^{oi}(t) N^i(\xi, \eta) \quad (138)$$

$$\beta_\alpha(\xi, \eta, t) = \sum_{i=1}^M \beta_\alpha^i(t) N^i(\xi, \eta) \quad (139)$$

$$\varphi^m(\xi, \eta, t) = \sum_{i=1}^M \varphi^{mi}(t) N^i(\xi, \eta) \quad (140)$$

$$\theta^m(\xi, \eta, t) = \sum_{i=1}^M \theta^{mi}(t) N^i(\xi, \eta) \quad (141)$$

$$N^i(\xi, \eta) = \frac{1}{4} \begin{bmatrix} (1-\xi)(1-\eta) - (1-\xi^2)(1-\eta) - (1-\xi)(1-\eta^2) \\ (1+\xi)(1-\eta) - (1-\xi^2)(1-\eta) - (1+\xi)(1-\eta^2) \\ (1+\xi)(1+\eta) - (1+\xi)(1-\eta^2) - (1-\xi^2)(1+\eta) \\ (1-\xi)(1+\eta) - (1-\xi^2)(1+\eta) - (1-\xi)(1-\eta^2) \\ (1-\xi^2)(1-\eta) \\ (1+\xi)(1-\eta^2) \\ (1-\xi^2)(1+\eta) \\ (1-\xi)(1-\eta^2) \end{bmatrix}^T \quad (142)$$

where M is the number of in-plane shape functions N for an eight-noded Serendipity element.

By introducing Equations (138)-(142) into Equation (86), the following finite element submatrices for the shell element are calculated in accordance with the shell laminate matrices defined in Equations (87)-(101). The mass submatrix is

$$[M_{uu}] = \int_A [N]^T \begin{bmatrix} [\rho_A] & [\rho_B] \\ [\rho_B] & [\rho_D] \end{bmatrix} [N] d\xi d\eta \quad (143)$$

The stiffness submatrices are

$$[K_{uu}] = \begin{bmatrix} [K_{11}] & [K_{12}] & [K_{13}] & [K_{14}] & [K_{15}] \\ [K_{12}] & [K_{22}] & [K_{23}] & [K_{24}] & [K_{25}] \\ [K_{13}] & [K_{23}] & [K_{33}] & [K_{34}] & [K_{35}] \\ [K_{14}] & [K_{24}] & [K_{34}] & [K_{44}] & [K_{45}] \\ [K_{15}] & [K_{25}] & [K_{35}] & [K_{45}] & [K_{55}] \end{bmatrix} \quad (144)$$

where

$$[K_{11}] = \int_A \left\{ \frac{1}{(g_{11}^o)^2} [N_{,\xi}]^T [A_{11}] [N_{,\xi}] + \frac{2g_{22,\xi}^o}{(g_{11}^o)^2 g_{22}^o} [N]^T [A_{12}] [N_{,\xi}] + \frac{(g_{22,\xi}^o)^2}{(g_{11}^o g_{22}^o)^2} [N]^T [A_{22}] [N] + \frac{1}{(R_1)^2} [N]^T [A_{55}] [N] + \frac{1}{(g_{22}^o)^2} \left([N_{,\eta}] - \frac{g_{11,\eta}^o}{g_{11}^o} [N] \right)^T [A_{66}] \left([N_{,\eta}] - \frac{g_{11,\eta}^o}{g_{11}^o} [N] \right) \right\} d\xi d\eta \quad (145)$$

$$\begin{aligned}
[K_{12}] = \int_A \{ & \frac{g_{11,\eta}^{\circ}}{(g_{11}^{\circ})^2 g_{22}^{\circ}} [N_{,\xi}]^T [A_{11}] [N] + \frac{1}{g_{11}^{\circ} g_{22}^{\circ}} [N_{,\xi}]^T [A_{12}] [N_{,\eta}] + \\
& \frac{g_{11,\eta}^{\circ} g_{22,\xi}^{\circ}}{(g_{11}^{\circ} g_{22}^{\circ})^2} [N]^T [A_{12}] [N] + \frac{g_{22,\eta}^{\circ}}{g_{11}^{\circ} (g_{22}^{\circ})^2} [N]^T [A_{22}] [N_{,\eta}] + \\
& \frac{1}{g_{11}^{\circ} g_{22}^{\circ}} ([N_{,\eta}] - \frac{g_{11,\eta}^{\circ}}{g_{11}^{\circ}} [N])^T [A_{66}] ([N_{,\xi}] - \frac{g_{22,\xi}^{\circ}}{g_{22}^{\circ}} [N]) \} d\xi d\eta
\end{aligned} \tag{146}$$

$$\begin{aligned}
[K_{13}] = \int_A \{ & \frac{1}{g_{11}^{\circ} R_1} [N_{,\xi}]^T [A_{11}] [N] + \frac{1}{g_{11}^{\circ} R_2} [N_{,\xi}]^T [A_{12}] [N] + \\
& \frac{g_{22,\xi}^{\circ}}{g_{11}^{\circ} g_{22}^{\circ} R_1} [N]^T [A_{12}] [N] + \frac{g_{22,\xi}^{\circ}}{g_{11}^{\circ} g_{22}^{\circ} R_2} [N]^T [A_{22}] [N] + \\
& \frac{1}{g_{11}^{\circ} g_{22}^{\circ}} ([N_{,\eta}] - g_{11,\eta}^{\circ} [N])^T [A_{55}] [N_{,\xi}] \} d\xi d\eta
\end{aligned} \tag{147}$$

$$\begin{aligned}
[K_{14}] = \int_A \{ & \frac{1}{(g_{11}^{\circ})^2} [N_{,\xi}]^T [B_{11}] [N_{,\xi}] + \frac{2g_{22,\xi}^{\circ}}{(g_{11}^{\circ})^2 g_{22}^{\circ}} [N_{,\xi}]^T [B_{12}] [N] + \\
& \frac{(g_{22,\xi}^{\circ})^2}{(g_{11}^{\circ} g_{22}^{\circ})^2} [N]^T [B_{22}] [N] - \frac{1}{R_1} [N]^T [A_{55}] [N] + \\
& \frac{1}{g_{22}^{\circ}} ([N_{,\eta}] - \frac{g_{11,\eta}^{\circ}}{g_{11}^{\circ}} [N])^T [B_{66}] ([N_{,\eta}] - \frac{g_{11,\eta}^{\circ}}{g_{11}^{\circ}} [N]) \} d\xi d\eta
\end{aligned} \tag{148}$$

$$\begin{aligned}
[K_{15}] = \int_A \{ & \frac{g_{11,\eta}^{\circ}}{(g_{11}^{\circ})^2 g_{22}^{\circ}} [N_{,\xi}]^T [B_{11}] [N] + \frac{1}{g_{11}^{\circ} g_{22}^{\circ}} [N_{,\xi}]^T [B_{12}] [N_{,\eta}] + \\
& \frac{g_{11,\eta}^{\circ} g_{22,\xi}^{\circ}}{(g_{11}^{\circ} g_{22}^{\circ})^2} [N]^T [B_{12}] [N] + \frac{g_{22,\xi}^{\circ}}{g_{11}^{\circ} (g_{22}^{\circ})^2} [N]^T [B_{22}] [N_{,\eta}] + \\
& \frac{1}{g_{11}^{\circ} g_{22}^{\circ}} ([N_{,\eta}] - \frac{g_{11,\eta}^{\circ}}{g_{11}^{\circ}} [N])^T [B_{66}] ([N_{,\xi}] - \frac{g_{22,\xi}^{\circ}}{g_{22}^{\circ}} [N]) \} d\xi d\eta
\end{aligned} \tag{149}$$

$$\begin{aligned}
[K_{22}] = \int_A \{ & \frac{(g_{11,\eta}^{\circ})^2}{(g_{11}^{\circ} g_{22}^{\circ})^2} [N]^T [A_{11}] [N] + \frac{2g_{11,\eta}^{\circ}}{g_{11}^{\circ} (g_{22}^{\circ})^2} [N]^T [A_{12}] [N_{,\eta}] + \\
& \frac{1}{(g_{22}^{\circ})^2} [N_{,\eta}]^T [A_{22}] [N_{,\eta}] + \frac{1}{(R_2)^2} [N]^T [A_{44}] [N] + \\
& \frac{1}{(g_{11}^{\circ})^2} ([N_{,\xi}] - \frac{g_{22,\xi}^{\circ}}{g_{22}^{\circ}} [N])^T [A_{66}] ([N_{,\xi}] - \frac{g_{22,\xi}^{\circ}}{g_{22}^{\circ}} [N]) \} d\xi d\eta
\end{aligned} \tag{150}$$

$$\begin{aligned}
[K_{23}] = \int_A \{ & \frac{g_{11,\eta}^{\circ}}{g_{11}^{\circ} g_{22}^{\circ} R_1} [N]^T [A_{11}] [N] + \frac{g_{11,\eta}^{\circ}}{g_{11}^{\circ} g_{22}^{\circ} R_2} [N]^T [A_{12}] [N] + \\
& \frac{1}{g_{22}^{\circ} R_1} [N_{,\eta}]^T [A_{12}] [N] + \frac{1}{g_{22}^{\circ} R_2} [N_{,\eta}]^T [A_{22}] [N] - \\
& \frac{1}{g_{22}^{\circ} R_2} [N]^T [A_{44}] [N] \} d\xi d\eta
\end{aligned} \tag{151}$$

$$\begin{aligned}
[K_{24}] = \int_A \{ & \frac{g_{11,\eta}^o}{(g_{11}^o)^2 g_{22}^o} [N]^T [B_{11}] [N_{,\xi}] + \frac{g_{11,\eta}^o g_{22,\xi}^o}{(g_{11}^o g_{22}^o)^2} [N]^T [B_{12}] [N] + \\
& \frac{1}{g_{11}^o g_{22}^o} [N_{,\eta}]^T [B_{12}] [N_{,\xi}] + \frac{g_{22,\xi}^o}{g_{11}^o (g_{22}^o)^2} [N_{,\eta}]^T [B_{22}] [N] + \\
& \frac{1}{g_{11}^o g_{22}^o} ([N_{,\xi}] - \frac{g_{22,\xi}^o}{g_{22}^o} [N])^T [B_{66}] ([N_{,\eta}] - \frac{g_{11,\eta}^o}{g_{11}^o} [N]) \} d\xi d\eta
\end{aligned} \tag{152}$$

$$\begin{aligned}
[K_{25}] = \int_A \{ & \frac{(g_{11,\eta}^o)^2}{(g_{11}^o g_{22}^o)^2} [N]^T [B_{11}] [N] + \frac{2g_{11,\eta}^o}{g_{11}^o (g_{22}^o)^2} [N]^T [B_{12}] [N_{,\eta}] + \\
& \frac{1}{(g_{22}^o)^2} [N_{,\eta}]^T [B_{22}] [N_{,\eta}] - \frac{1}{R_2} [N]^T [A_{44}] [N] + \\
& \frac{1}{(g_{11}^o g_{22}^o)^2} ([N_{,\xi}] - \frac{g_{22,\xi}^o}{g_{22}^o} [N])^T [B_{66}] ([N_{,\xi}] - \frac{g_{22,\xi}^o}{g_{22}^o} [N]) \} d\xi d\eta
\end{aligned} \tag{153}$$

$$\begin{aligned}
[K_{33}] = \int_A \{ & \frac{1}{R_1^2} [N]^T [A_{11}] [N] + \frac{2}{R_1 R_2} [N]^T [A_{12}] [N] + \\
& \frac{1}{R_2^2} [N]^T [A_{22}] [N] + \frac{1}{(g_{22}^o)^2} [N_{,\eta}]^T [A_{44}] [N_{,\eta}] + \\
& \frac{1}{(g_{11}^o)^2} [N_{,\xi}]^T [A_{55}] [N_{,\xi}] \} d\xi d\eta
\end{aligned} \tag{154}$$

$$\begin{aligned}
[K_{34}] = \int_A \{ & \frac{1}{(g_{11}^{\circ}) R_1} [N]^T [B_{11}] [N_{,\xi}] + \frac{g_{22,\xi}^{\circ}}{g_{11}^{\circ} g_{22}^{\circ} R_1} [N]^T [B_{12}] [N] + \\
& \frac{1}{g_{11}^{\circ} R_2} [N]^T [B_{12}] [N_{,\xi}] + \frac{g_{22,\xi}^{\circ}}{g_{11}^{\circ} g_{22}^{\circ} R_2} [N]^T [B_{22}] [N] + \\
& \left. \frac{1}{g_{11}^{\circ}} [N_{,\xi}]^T [A_{55}] [N] \right\} d\xi d\eta
\end{aligned} \tag{155}$$

$$\begin{aligned}
[K_{35}] = \int_A \{ & \frac{g_{11,\eta}^{\circ}}{g_{11}^{\circ} g_{22}^{\circ} R_1} [N]^T [B_{11}] [N] + \frac{1}{g_{22}^{\circ} R_1} [N]^T [B_{12}] [N_{,\eta}] + \\
& \frac{g_{11,\eta}^{\circ}}{g_{11}^{\circ} g_{22}^{\circ} R_2} [N]^T [B_{12}] [N] + \frac{1}{g_{22}^{\circ} R_2} [N]^T [B_{22}] [N_{,\eta}] + \\
& \left. \frac{1}{g_{22}^{\circ}} [N_{,\eta}]^T [A_{44}] [N] \right\} d\xi d\eta
\end{aligned} \tag{156}$$

$$\begin{aligned}
[K_{44}] = \int_A \{ & [N]^T [A_{55}] [N] + \frac{1}{(g_{11}^{\circ})^2} [N_{,\xi}]^T [D_{11}] [N_{,\xi}] + \\
& \frac{2 g_{22,\xi}^{\circ}}{(g_{11}^{\circ})^2 g_{22}^{\circ}} [N_{,\xi}]^T [D_{12}] [N] + \frac{(g_{22,\xi}^{\circ})^2}{(g_{11}^{\circ} g_{22}^{\circ})^2} [N]^T [D_{22}] [N] + \\
& \left. \frac{1}{(g_{22}^{\circ})^2} ([N_{,\eta}] - g_{11,\eta}^{\circ} [N])^T [D_{66}] ([N_{,\eta}] - g_{11,\eta}^{\circ} [N]) \right\} d\xi d\eta
\end{aligned} \tag{157}$$

$$\begin{aligned}
[K_{45}] = \int_A & \left\{ \frac{g_{11,\eta}^{\circ}}{(g_{11}^{\circ})^2 g_{22}^{\circ}} [N_{,\xi}]^T [D_{11}] [N] + \frac{1}{g_{11}^{\circ} g_{22}^{\circ}} [N_{,\xi}]^T [D_{12}] [N_{,\eta}] + \right. \\
& \frac{g_{11,\eta}^{\circ} g_{22,\xi}^{\circ}}{(g_{11}^{\circ} g_{22}^{\circ})^2} [N]^T [D_{12}] [N] + \frac{g_{22,\xi}^{\circ}}{g_{11}^{\circ} (g_{22}^{\circ})^2} [N]^T [D_{22}] [N] + \\
& \left. \frac{1}{g_{11}^{\circ} g_{22}^{\circ}} \left([N_{,\eta}] - \frac{g_{11,\eta}^{\circ}}{g_{11}^{\circ}} [N] \right)^T [D_{66}] \left([N_{,\xi}] - \frac{g_{22,\xi}^{\circ}}{g_{22}^{\circ}} [N] \right) \right\} d\xi d\eta
\end{aligned} \tag{158}$$

$$\begin{aligned}
[K_{55}] = \int_A & \left\{ [N]^T [A_{44}] [N] + \frac{(g_{11,\eta}^{\circ})^2}{(g_{11}^{\circ} g_{22}^{\circ})^2} [N]^T [D_{11}] [N] + \right. \\
& \frac{2g_{11,\eta}^{\circ}}{g_{11}^{\circ} (g_{22}^{\circ})^2} [N_{,\xi}]^T [D_{12}] [N] + \frac{1}{(g_{22}^{\circ})^2} [N_{,\eta}]^T [D_{22}] [N_{,\eta}] + \\
& \left. \frac{1}{g_{11}^{\circ}} \left([N_{,\eta}] - \frac{g_{22,\xi}^{\circ}}{g_{22}^{\circ}} [N] \right)^T [D_{66}] \left([N_{,\eta}] - \frac{g_{22,\xi}^{\circ}}{g_{22}^{\circ}} [N] \right) \right\} d\xi d\eta
\end{aligned} \tag{159}$$

$$\begin{aligned}
[K_{u\phi}] = \int_A & \left[\begin{aligned}
& [N_{,\xi}]^T \frac{[E_{31}]}{g_{11}^{\circ}} [N] + [N]^T \frac{g_{22,\xi}^{\circ} [\overline{E}_{32}]}{g_{11}^{\circ} g_{22}^{\circ}} [N] - [N]^T \frac{[E_{15}]}{g_{11}^{\circ} R_1} [N] \\
& [N]^T \frac{g_{11,\eta}^{\circ} [\overline{E}_{31}]}{g_{11}^{\circ} G_{22}^{\circ}} [N] + [N_{,\eta}]^T \frac{[\overline{E}_{32}]}{g_{22}^{\circ}} [N] - [N]^T \frac{[E_{24}]}{g_{22}^{\circ} R_2} [N] \\
& [N]^T \left(\frac{[\overline{E}_{31}]}{R_1} + \frac{[\overline{E}_{32}]}{R_2} \right) [N] + [N_{,\eta}]^T \frac{[E_{24}]}{(g_{22}^{\circ})^2} [N] + [N_{,\xi}]^T \frac{[E_{15}]}{(g_{11}^{\circ})^2} [N] \\
& [N]^T \frac{[E_{15}]}{g_{11}^{\circ}} [N] + [N_{,\xi}]^T \frac{[\hat{E}_{31}]}{g_{11}^{\circ}} [N] + [N]^T \frac{[g_{22,\xi}^{\circ} \hat{E}_{32}]}{g_{11}^{\circ} g_{22}^{\circ}} [N] \\
& [N]^T \frac{[E_{24}]}{g_{22}^{\circ}} [N] + [N]^T \frac{[g_{11,\eta}^{\circ} \hat{E}_{31}]}{g_{11}^{\circ} g_{22}^{\circ}} [N] [N_{,\eta}]^T \frac{[\hat{E}_{32}]}{g_{22}^{\circ}} [N]
\end{aligned} \right] d\xi d\eta
\end{aligned} \tag{160}$$

$$[K_{u\theta}] = \int_A \left[\begin{array}{l} [N]^T \frac{[\bar{\Lambda}_1]}{g_{11}^o} [N_{,\xi}] + [N]^T \frac{g_{22,\xi}^o [\bar{\Lambda}_2]}{g_{11}^o g_{22}^o} [N] \\ [N]^T \frac{g_{11,\eta}^o [\bar{\Lambda}_1]}{g_{11}^o g_{22}^o} [N] + [N_{,\eta}]^T \frac{[\bar{\Lambda}_2]}{g_{22}^o} [N] \\ [N]^T \left(\frac{[\bar{\Lambda}_1]}{R_1} + \frac{[\bar{\Lambda}_2]}{R_2} \right) [N] \\ [N]^T \frac{[\hat{\Lambda}_1]}{g_{11}^o} [N_{,\xi}] + [N]^T \frac{g_{22,\xi}^o [\hat{\Lambda}_2]}{g_{11}^o g_{22}^o} [N] \\ [N]^T \frac{g_{11,\eta}^o [\hat{\Lambda}_1]}{g_{11}^o g_{22}^o} [N] + [N_{,\eta}]^T \frac{[\hat{\Lambda}_2]}{g_{22}^o} [N] \end{array} \right] d\xi d\eta \quad (161)$$

$$[K_{\varphi\varphi}] = \int_A \left\{ [N]^T \left(\frac{[G_{11}]}{(g_{11}^o)^2} + \frac{[G_{22}]}{(g_{22}^o)^2} + [G_{33}] \right) [N] \right\} d\xi d\eta \quad (162)$$

$$[K_{\varphi\theta}] = \int_A \left\{ [N]^T \frac{[P_1]}{g_{11}^o} [N_{,\xi}] + [N]^T \frac{[P_2]}{g_{22}^o} [N_{,\eta}] + [N]^T [P_3] [N] \right\} d\xi d\eta \quad (163)$$

CHAPTER 6 CASE STUDIES AND DISCUSSION OF RESULTS

Results from representative problems for a variety of different beam, plate, and shell structures are presented in this section. The accuracy of the current analytical formulation is verified with comparisons from published experimental data and other analytical models. Additional numerical studies are also conducted to demonstrate the capabilities of the current formulation to model the sensory and active behavior of piezoelectric composite materials.

6.1 Comparisons with Room Temperature Experimental Results

Results from previously published room temperature experimental studies are used to verify the developed analytical formulation. The problems examined consist of a cantilevered piezoelectric bimorph beam examined by Lee and Moon (1989) and a clamped composite plate with attached discrete piezoelectric patches studied by Crawley and Lazarus (1991).

6.1.1 Piezoelectric Bimorph Beam

The cantilevered piezoelectric bimorph beam problem examined by Lee and Moon (1989) is shown in Figure 2. The bimorph is created by bonding two layers of a piezoelectric polymer together such that the poling directions are opposite in each layer. In this configuration, the application of an external voltage will result in a pure bending deformation. The beam has a length (L) of 8 cm, a width of 1 cm, and a height of 220 μm . The material properties of the polyvinylidene fluoride (PVDF) piezoelectric polymer used in the experiment are listed in Table 1. A finite element analysis of the bimorph beam problem is performed using the developed beam, plate, and shell elements using sixteen elements along the length of the beam with two discrete layers through-the-thickness. All three elements produced similar results, so only one set of predictions are presented. Figure 3 illustrates the predicted free end (at $x/L = 1$) displacement obtained by applying active voltages of between 0-500 Volts, along with the experimental results of Lee and Moon (1989). Good agreement is observed between the predicted results of the current analytical formulation and the experimental data.

6.1.2 Composite Plate with Piezoelectric Patches

The cantilevered composite plate problem examined by Crawley and Lazarus (1991) is shown in Figure 4. The plate is constructed using AS4/3501 Graphite/Epoxy with a length (L) of 29.2 cm, a width (b) of 15.2 cm, and a thickness of 0.83 mm. Two laminate configurations, $[0/\pm 45]_s$ and $[30/0_2]_s$, are examined with fifteen G-1195 piezoceramic patches with a thickness of 0.25 mm bonded on both the top and bottom surfaces of the plate. Figure 4 also depicts the finite element mesh used in the analysis: a 16 by 9 mesh with 8 discrete layers (one for each composite and piezoelectric layer through-the-thickness) is used for both the plate and shell elements. Only one set of results is presented since similar results are obtained using each element. The material properties of the composite and piezoelectric material are listed in Table 2. The purpose of the experimental

studies was to investigate the resulting deflections of the plate when active voltages are applied to the piezoceramic patches. The experimental displacements along the centerline ($y/b=0.5$) of the plate are shown in Figure 5 for the $[0/\pm 45]_s$ plate with an applied voltage of 394 V/mm and in Figure 6 for the $[30/0_2]_s$ plate with an applied voltage of 472 V/mm. Good agreement is observed between the predictions of the current analytical formulation and the experimental results.

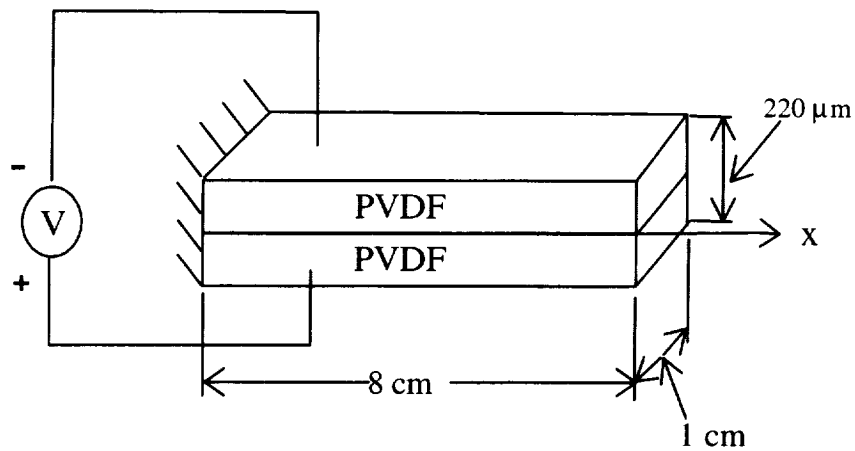


Figure 2: Cantilevered piezoelectric PVDF bimorph beam (Lee and Moon, 1989).

Table 1: Material properties of PVDF piezoelectric polymer (Lee and Moon, 1989).

Property	PVDF
Elastic Modulus, E (10^9 Pa):	2.0
Poisson's Ratio, ν :	0.29
Shear Modulus, G (10^9 Pa):	0.8
Piezoelectric Charge Constants (10^{-12} m/V):	
d_{31}	23.0
d_{32}	3.0

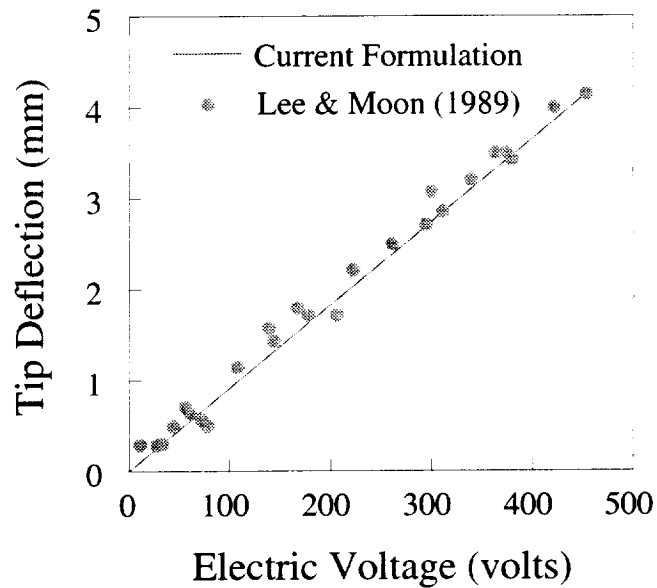


Figure 3: Comparison of tip deflections of a PVDF bimorph beam under applied active electric voltages of 0-500 Volts at room temperature.

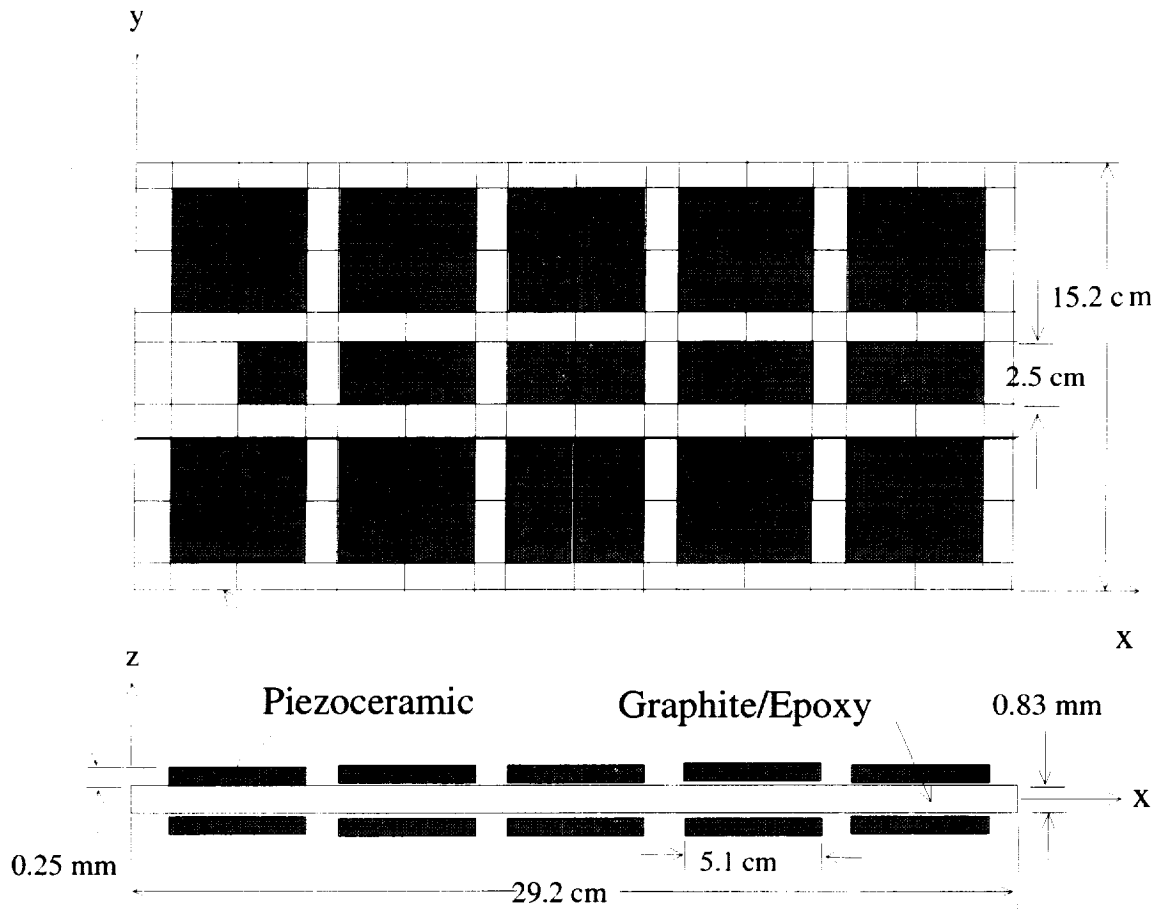


Figure 4: Cantilevered AS4/3501 composite plate with 30 attached discrete G-1195 piezoelectric patches (Crawley and Lazarus, 1991).

Table 2: Material properties of piezoceramic (G-1195) and Graphite/Epoxy (AS4/3501) (Crawley and Lazarus, 1991).

Property	Piezoceramic	Graphite/Epoxy
Elastic Moduli (10^9 Pa):		
E_{11}	63.0	143.0
E_{22}	63.0	9.7
E_{33}	63.0	9.7
Poisson's Ratio:		
ν_{12}	0.3	0.3
ν_{23}	0.3	0.3
ν_{31}	0.3	0.3
Shear Moduli (10^9 Pa):		
G_{12}	24.2	6.0
G_{23}	24.2	2.5
G_{31}	24.2	6.0
Piezoelectric Charge Constant (10^{-12} m/V) :		
d_{31}	254.	----
d_{32}	254.	----
Electric Permittivity (10^{-9} f/m):		
ϵ_{11}	15.3	----
ϵ_{22}	15.3	----
ϵ_{33}	15.0	----

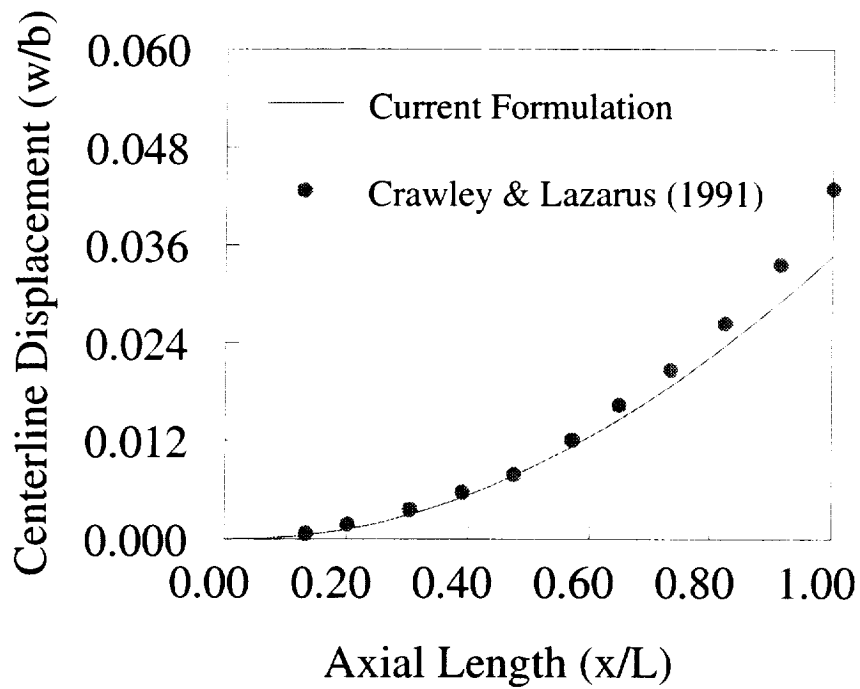


Figure 5: Comparisons of centerline displacement of an AS4/3501 $[0/\pm 45]_s$ plate with attached G-1195 piezoelectric patches under 394 V/mm at room temperature.

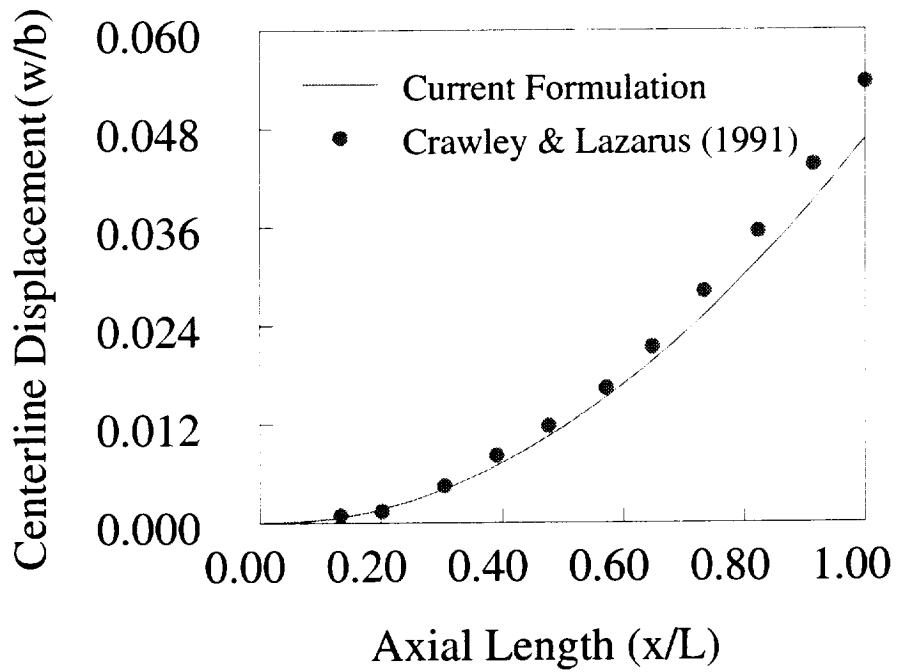


Figure 6: Comparisons of centerline displacement of an AS4/3501 [30/0₂]_s plate with attached G-1195 piezoelectric patches under 472 V/mm at room temperature.

6.2 Comparisons with Analytical Results for Temperature Effects

Results from previously published high temperature analytical studies are used to verify the developed analytical formulation. The problems examined consist of a cantilevered piezoelectric bimorph beam examined by Sunar and Rao (1997) and a simply supported composite plate with attached discrete piezoelectric patches investigated by Ha et al. (1992). These problems present slight variations on the room temperature experimental studies of Lee and Moon (1989) and Crawley and Lazarus (1991) to analytically quantify the influence of temperature effects.

6.2.1 Piezoelectric Bimorph Beam

The cantilevered piezoelectric bimorph beam problem examined by Sunar and Rao (1997) is shown in Figure 7. The bimorph has a length (L) of 100 mm, a width of 5 mm, and a height of 1 mm. The material properties of the polyvinylidene fluoride (PVDF) piezoelectric polymer at 27°C and at 77°C are listed in Table 3. An applied electric voltage of 250 Volts was applied to the bimorph beam at 27°C to induce a bending deformation. The impact of thermal effects on the deflection of the bimorph is subsequently examined by applying a uniform 50°C temperature increase. The current finite element analysis is performed using 20 elements along the length of the beam with two discrete layers through-the-thickness. All three elements (i.e. beam, plate, and shell) produced similar results, so only one set of predictions are presented. Figure 8 shows the predicted deflection of the bimorph along the length of the beam under an applied active voltages of 250 Volts at 27°C and 77°C , along with the corresponding analytical results of Sunar and Rao (1997). Good agreement is observed between the two sets of results, which demonstrate the impact of temperature effects on the deflection of the bimorph beam.

6.2.2 Composite Plate with Piezoelectric Patches

The simply supported composite plate problem examined by Ha et al. (1992) is shown in Figure 9. The $[0/\pm 45]_s$ plate has a length (L) of 37.2 cm, a width (b) of 22.8 cm, and a thickness of 0.75 mm. Fifteen equally sized G-1195 piezoceramic patches with a length of 6 cm, a width of 6 cm, and a thickness of 0.13 mm are bonded on both surfaces of the plate. Figure 9 also depicts the finite element mesh used in the analysis: a 16 by 10 mesh with 8 discrete layers (one for each composite and piezoelectric layer through-the-thickness) used for both the plate and shell elements. Only one set of results is presented since similar results are obtained using each element. The material properties of the composite and piezoelectric material are listed in Table 4. Analytical studies were performed to investigate the capability to achieve thermal distortion management by applying active voltages to the piezoelectric patches to eliminate the bending deflection induced by applying a 100°C linear thermal gradient through-the-thickness of the plate (50°C on the top surface and -50°C on the bottom surface). The predicted displacements along the centerline ($y/b=0.5$) of the plate along with corresponding applied active voltages to produce this deflection are shown in Figure 10, along with the corresponding results from Ha et al. (1992). Good agreement is observed between the two predictions. The results demonstrate the capability to achieve shape control of the thermally induced bending deformation by the application of increasing active voltages to the piezoelectric actuators.

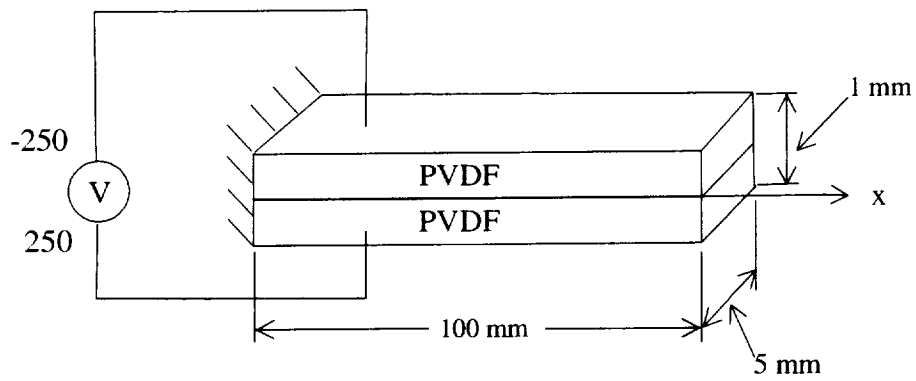


Figure 7: Cantilevered piezoelectric PVDF bimorph beam (Sunar and Rao, 1997).

Table 3: Material properties of PVDF piezoelectric polymer (Sunar and Rao, 1997).

Property	27°C	77°C
Elastic Compliance, c_{11} (10^9 Pa):	3.8	1.8
Thermal Expansion, α (10^{-6} m/m°C):	150.	215.
Piezoelectric Constant, e_{31} (C/m ²):	0.046	0.049
Electric Permittivity, ϵ (10^{-9} f/m):	0.1026	0.1553
Pyroelectric Constant, P (10^{-3} C/m ² °C):	0.04	0.055
Reference Temperature, T_0 (°C):	27.0	27.0

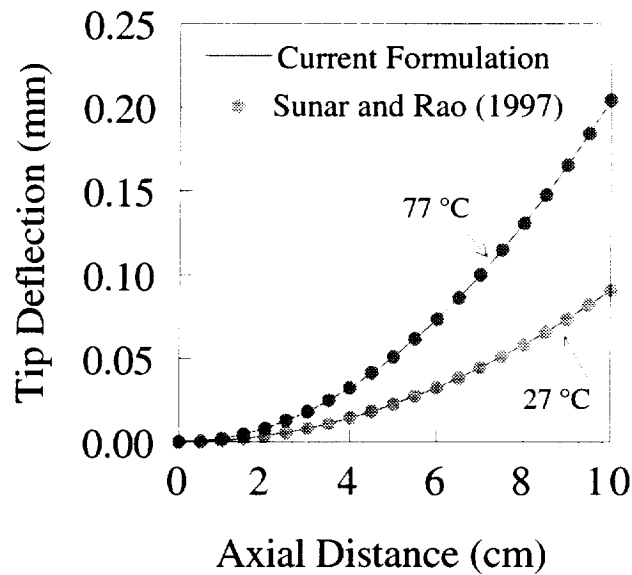


Figure 8: Comparison of tip deflections of a PVDF bimorph beam under an applied active electric voltages of 250 V at 27°C and 77°C.

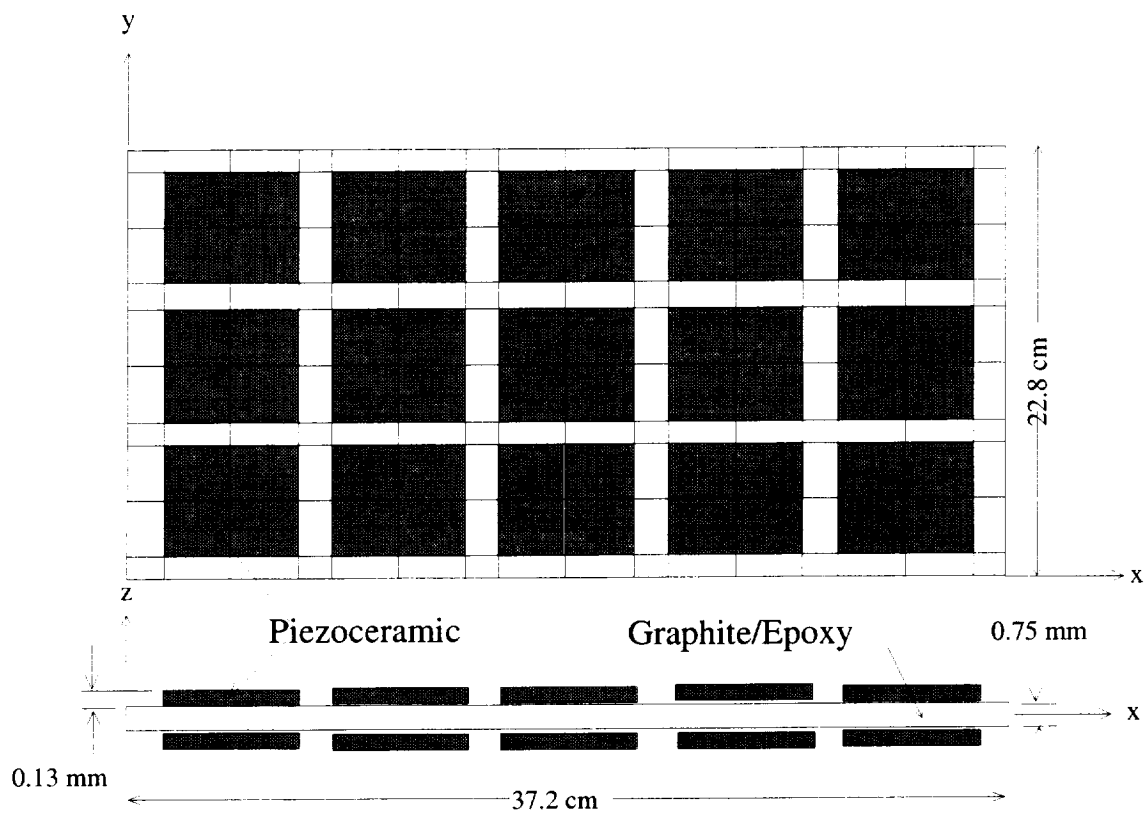


Figure 9: Simply supported AS4/3501 composite plate with 30 attached discrete G-1195 piezoelectric patches (Ha et al., 1992).

Table 4: Material properties of piezoceramic (G-1195) and Graphite/Epoxy (AS4/3501) (Ha et al., 1992).

Property	Piezoceramic	Graphite/Epoxy
Elastic Moduli (10^9 Pa):		
E_{11}	63.0	150.0
E_{22}	63.0	9.0
E_{33}	63.0	9.0
Poisson's Ratio:		
ν_{12}	0.3	0.3
ν_{23}	0.3	0.3
ν_{31}	0.3	0.3
Shear Moduli (10^9 Pa):		
G_{12}	24.2	7.1
G_{23}	24.2	2.5
G_{31}	24.2	7.1
Piezoelectric Charge Constant (10^{-12} m/V) :		
d_{31}	254.	----
d_{32}	254.	----
Electric Permittivity (10^{-9} f/m):		
ϵ_{11}	15.3	----
ϵ_{22}	15.3	----
ϵ_{33}	15.0	----
Thermal Expansion (10^{-6} m/m $^{\circ}$ C):		
α_{11}	0.9	1.1
α_{22}	0.9	25.2
α_{33}	0.9	25.2
Reference Temperature, T_0 ($^{\circ}$ C):	20.0	20.0

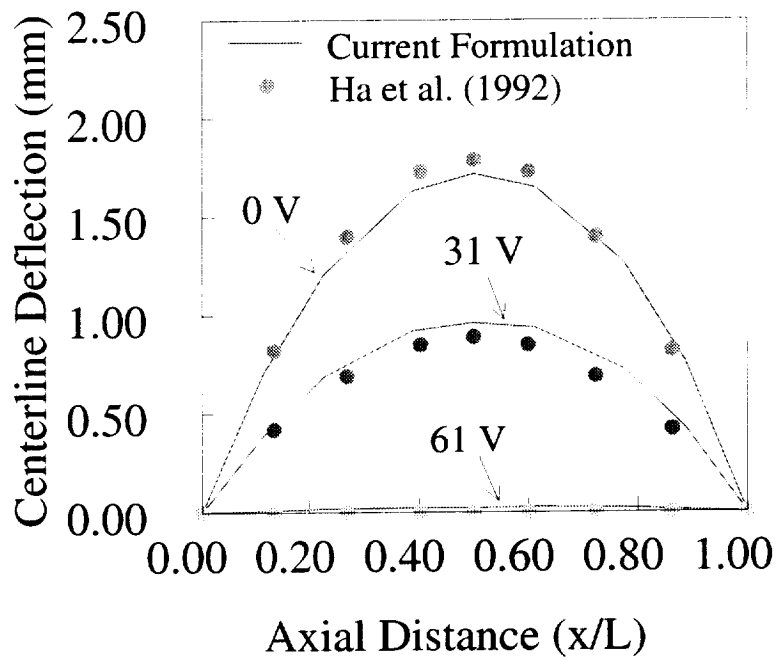


Figure 10: Comparisons of centerline displacement of an AS4/3501 [0/±45]_s plate with attached G-1195 piezoelectric patches under a 100°C thermal gradient through-the-thickness (50°C on top, -50°C on bottom) with 0, 31, and 61 V applied active voltages.

6.3 Comparisons with a Commercial Finite Element Analysis Program

Evaluations of the developed analytical formulation for both the sensory and active responses are verified with corresponding results from a commercial finite element analysis program, ABAQUS (1996). In order to represent the location of piezoelectric layers, the standard laminate notation is expanded, such that the piezoelectric layer is indicated by the letter p. The problem examined consists of a Carbon/Epoxy composite plate with an attached layer of piezoceramic material. The $[0_8/p]$ plate has a length (a) of 50.8 mm, a width (b) of 25.4mm, and a height (h) of 5.08 mm, as shown in Figure 11. The plate is clamped on one side and is subjected to a uniform thermal load of 50°C. The material properties used are listed in Table 5. A 20 x 10 mesh with two discrete layers (one for the Carbon/Epoxy and one for the piezoelectric layer) is used for both the plate and shell elements from the current formulation, while a 10 x 5 x 2 mesh is used for the 20 noded continuum elements in ABAQUS. Only one set of results is presented for the current formulation, since similar results were obtained for both the plate and shell elements. Pyroelectric effects are intentionally neglected (i.e. set to zero) in the current formulation, since ABAQUS neglects such effects.

6.3.1 Sensory Mode

The piezoelectric layer can be utilized in either a sensory or active mode. In the sensory mode, the piezoelectric layer is free to develop a corresponding electric potential in response to the thermally induced deformation of the plate through the direct piezoelectric effect. The resulting displacements along the centerline of the plate (along $y/b = 0.5$) are shown in Figure 12, while the corresponding electric potentials which develop in the piezoelectric layer are shown in Figure 13. There is good overall agreement between the current formulation and the ABAQUS results. The differences in the sensory electric potentials arise due to the consideration of the through-the-thickness Poisson's effect in ABAQUS, which are neglected in the current formulation. In typical health monitoring applications, these sensory voltages would be used to provide the essential feedback necessary to infer the current state of deformation in the structure.

6.3.2 Active Mode

The piezoelectric layer can also be operated as an actuator by applying a voltage differential to the piezoelectric layer and utilizing the converse piezoelectric effect to produce a corresponding structural deformation. Figure 14 shows the centerline deflection (along $y/b = 0.5$) for three different applied electric potentials (0, 250, and 500 Volts). Good agreement is observed between the current formulation and the ABAQUS predictions. The results also demonstrate the potential of piezoelectric actuators to completely alter the initial thermally induced deformation of the plate by the application of increasing electric potentials in order to achieve thermal shape control.

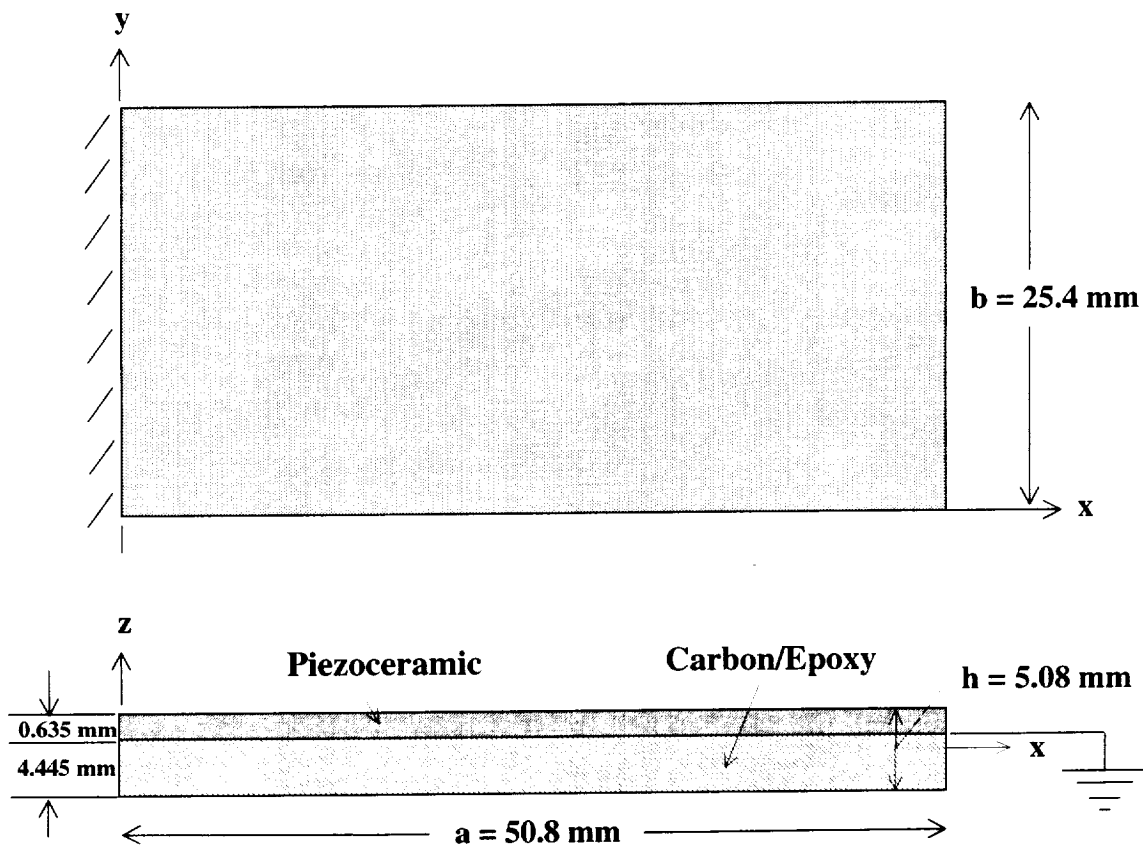


Figure 11: Clamped Carbon/Epoxy composite plate with an attached piezoceramic layer.

Table 5: Material properties of piezoceramic and Carbon/Epoxy.

Property	Piezoceramic	Carbon/Epoxy (Daniel and Ishai, 1994)
Elastic Moduli (10^9 Pa):		
E_{11}	69.0	142.0
E_{22}	69.0	10.3
E_{33}	69.0	10.3
Poisson's Ratio:		
ν_{12}	0.3	0.27
ν_{23}	0.3	0.27
ν_{31}	0.3	0.20
Shear Moduli (10^9 Pa):		
G_{12}	26.5	7.20
G_{23}	26.5	4.29
G_{31}	26.5	7.20
Piezoelectric Charge Constant (10^{-12} m/V) :		
d_{31}	-154.	----
Electric Permittivity (10^{-9} f/m):		
ϵ_{11}	15.05	----
ϵ_{22}	15.05	----
ϵ_{33}	15.05	----
Thermal Expansion (10^{-6} m/m $^{\circ}$ C):		
α_{11}	1.2	-0.9
α_{22}	1.2	27.0
Reference Temperature, T_0 ($^{\circ}$ C):	20.0	20.0

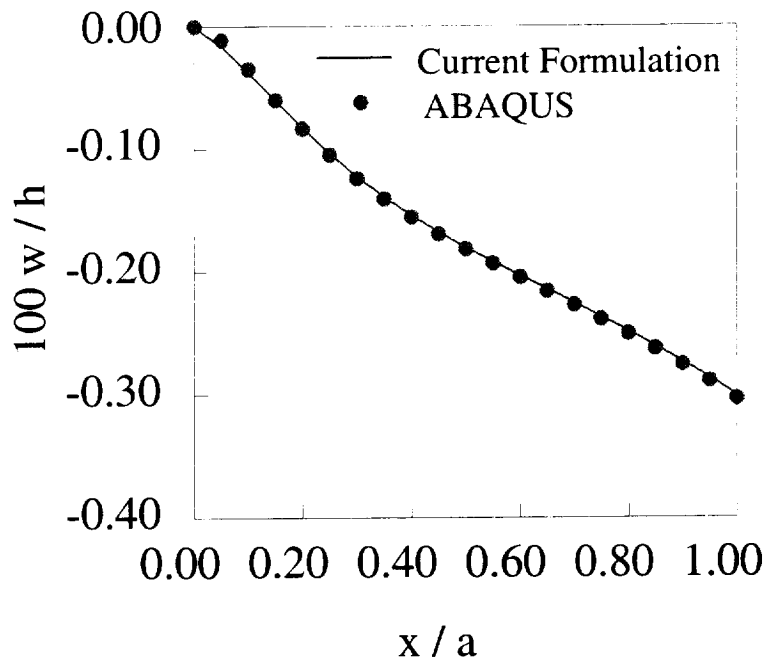


Figure 12: Comparison of centerline sensory deflections of a clamped $[0_g/p]$ Carbon/Epoxy plate with a piezoceramic layer under a uniform 50°C load.

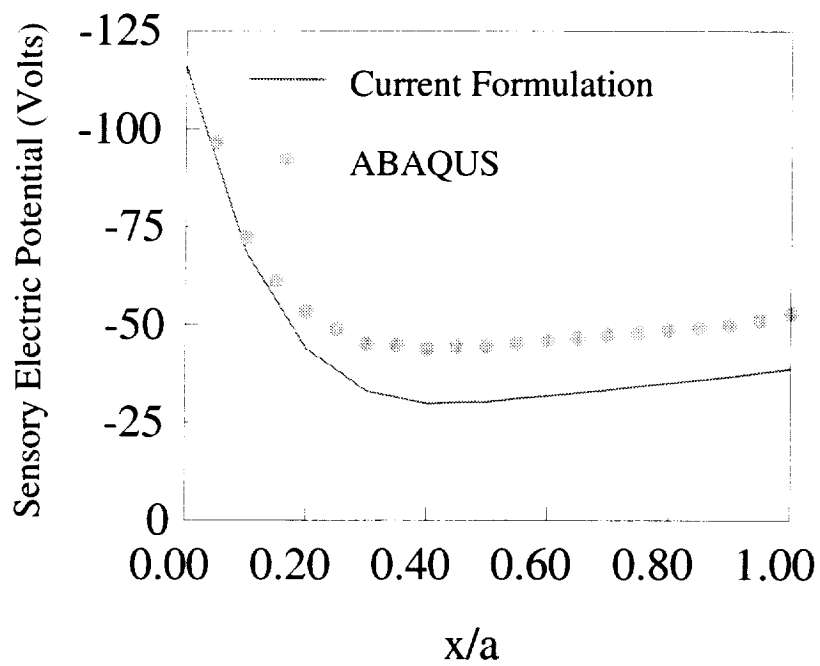


Figure 13: Comparison of centerline sensory electric potentials of a clamped $[0_8/p]$ Carbon/Epoxy plate with a piezoceramic layer under a uniform 50°C load.

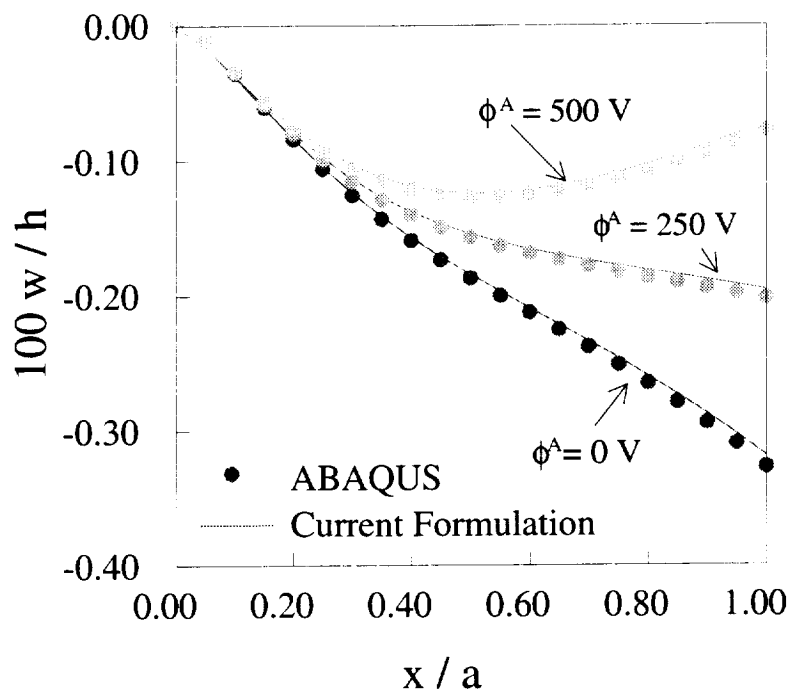


Figure 14: Comparison of centerline deflections of a clamped $[0_8/p]$ Carbon/Epoxy plate with a piezoceramic layer under a uniform 50°C load with applied active voltages of 0, 250, and 500 V.

6.4 Additional Numerical Studies

Results from numerical studies are presented to demonstrate additional capabilities of the current formulation to model the behavior of piezoelectric composite structures. The capabilities investigated include: incorporating pyroelectric effects and temperature dependent material properties into the analysis and evaluating the significance of these effects on the thermal response; demonstrating capabilities to achieve selective shape control of thermally induced bending and twisting deformations; assessing the improved accuracy of layerwise models in predicting thermal stresses; and determining the influence of curvature on the sensory and active responses.

6.4.1 Pyroelectric Effects

Pyroelectric effects arise in piezoelectric material due to temperature dependent changes in the electrical properties. This behavior is analogous to the change in mechanical strains observed in elastic materials due to thermal expansion. In order to demonstrate the effect of incorporating pyroelectric effects, the clamped plate problem shown in Figure 11 is re-examined incorporating pyroelectric effects. The problem details remain the same as before except for the consideration of non-zero pyroelectric constants in the piezoelectric material properties as listed in Table 6. The influence of the pyroelectric effects on the centerline deflection of the plate when the piezoelectric layer is operating in a sensory mode is shown in Figure 15 along with the corresponding result when the pyroelectric constant is neglected. The corresponding results for the sensory electric potential which develops is shown in Figure 16. Both figures demonstrate that pyroelectric effects can have a significant impact on both the displacements and electric potentials of piezoelectric composite structures in thermal environments.

Table 6: Material properties of piezoceramic and Carbon/Epoxy.

Property	Piezoceramic	Carbon/Epoxy (Daniel and Ishai, 1994)
Elastic Moduli (10^9 Pa):		
E_{11}	69.0	142.0
E_{22}	69.0	10.3
E_{33}	69.0	10.3
Poisson's Ratio:		
ν_{12}	0.3	0.27
ν_{23}	0.3	0.27
ν_{31}	0.3	0.20
Shear Moduli (10^9 Pa):		
G_{12}	26.5	7.20
G_{23}	26.5	4.29
G_{31}	26.5	7.20
Piezoelectric Charge Constant (10^{-12} m/V) :		
d_{31}	-154.	----
Electric Permittivity (10^9 f/m):		
ϵ_{11}	15.05	----
ϵ_{22}	15.05	----
ϵ_{33}	15.05	----
Thermal Expansion (10^{-6} m/m °C):		
α_{11}	1.2	-0.9
α_{22}	1.2	27.0
Pyroelectric Constant (10^{-3} C/m ² °C):		
P_3	-0.2	----
Reference Temperature, T_0 (°C):		
	20.0	20.0

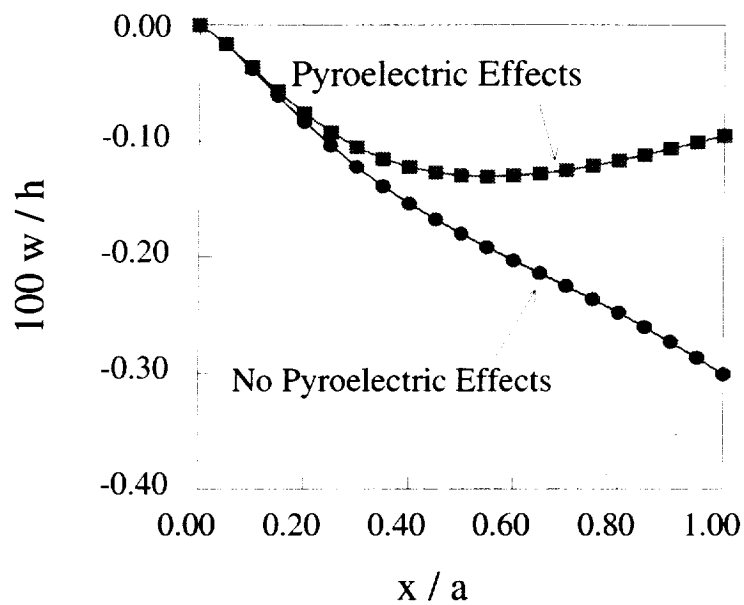


Figure 15: Pyroelectric effects on the centerline sensory deflections of a clamped $[0_8/p]$ Carbon/Epoxy plate with an attached piezoceramic layer under a uniform 50°C load.

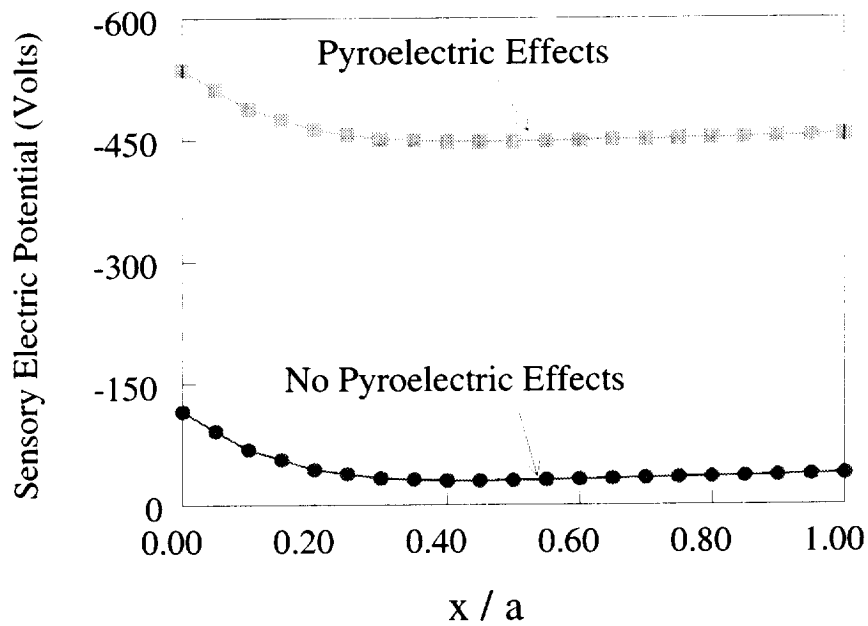


Figure 16: Pyroelectric effects on the centerline sensory electric potentials of a clamped $[0_8/p]$ Carbon/Epoxy plate with an attached piezoceramic layer under a uniform 50°C load.

6.4.2 Temperature Dependent Material Properties

The various elastic, dielectric, piezoelectric, and pyroelectric material properties of piezoelectric materials are influenced differently by temperature variations. In addition, piezoelectric materials also possess a characteristic limiting temperature, called the Curie temperature, beyond which the material loses its piezoelectric properties. Thus, in typical applications the operating temperature of piezoelectric materials must be considerably lower than the Curie temperature. In the current study, the temperature dependent variations of an AS4/3501-6 Carbon/Epoxy composite and a PZT-5A piezoceramic were implemented using a piecewise linear representation in the constitutive equations (Equations 23-26). The temperature dependence of the AS4/3501-6 moduli and α_{22} are depicted in Figure 17, while the variation of the PZT-5A properties d_{31} and ϵ_{33} are shown in Figure 18, while α_{11} , and p_3 are shown in Figure 19. All properties are nondimensionalized with their respective room temperature values shown in Table 7. The simply supported plate with discrete piezoelectric patches examined in Figure 9 is used to demonstrate the effects of temperature dependent material properties. Linear thermal gradients of different values are applied through-the-thickness of the plate with the bottom surface ($z/h = -0.5$) fixed at 20°C and the upper surface ($z/h = 0.5$) varying from 45° to 170°C .

The first case utilizes a combined active/sensory configuration of the piezoceramic patches, in which the upper patches are utilized as sensors and the lower patches are used as actuators with zero volts applied. All the piezoceramic patches are grounded on the surface in contact with the carbon/epoxy plate. The resulting thermally induced deflection at the center of the plate is shown in Figure 20 for different applied thermal gradients. The deflections are nondimensionalized with respect to the total laminate thickness ($H = 1.01$ mm). The results show that when material properties are assumed to remain constant with temperature, a linear variation in deflection occurs. In contrast, a nonlinear variation in the deflection is observed when the temperature dependent properties are incorporated. Larger discrepancies occur between the two cases as larger thermal gradients are applied. The corresponding sensory voltages at the central piezoceramic patch on the upper surface of the plate is shown in Figure 21. As with the deflections, the assumption of constant material properties leads to a linear variation of the voltages, while nonlinearities are introduced when temperature dependent properties are modeled. Closer agreement is observed in this case.

A fully active configuration of the piezoceramic patches is used to investigate the effect of temperature dependent material properties on thermal shape control. Equal voltages are applied to all the piezoceramics. The applied voltages required to equally minimize the deflection at the center of the plate to zero for different applied voltages are shown in Figure 22. Once again, a nonlinear variation is predicted by the temperature dependent case and an increasing discrepancy is observed as the thermal gradient increases. This discrepancy corresponds to the trend observed for the center deflection of the plate (Figure 20). Since larger deflections occur for the temperature dependent case, this in part justifies the larger applied voltages required to minimize the deflections.

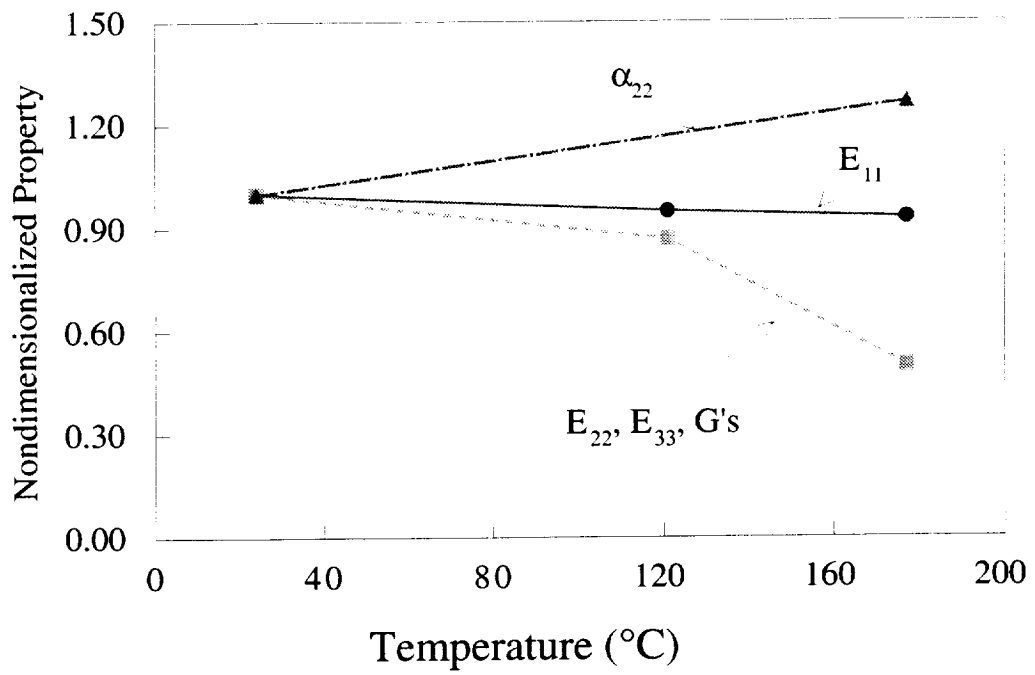


Figure 17: Temperature dependence of AS4/3501-6 Carbon/Epoxy properties (Daniel and Ishai, 1994).

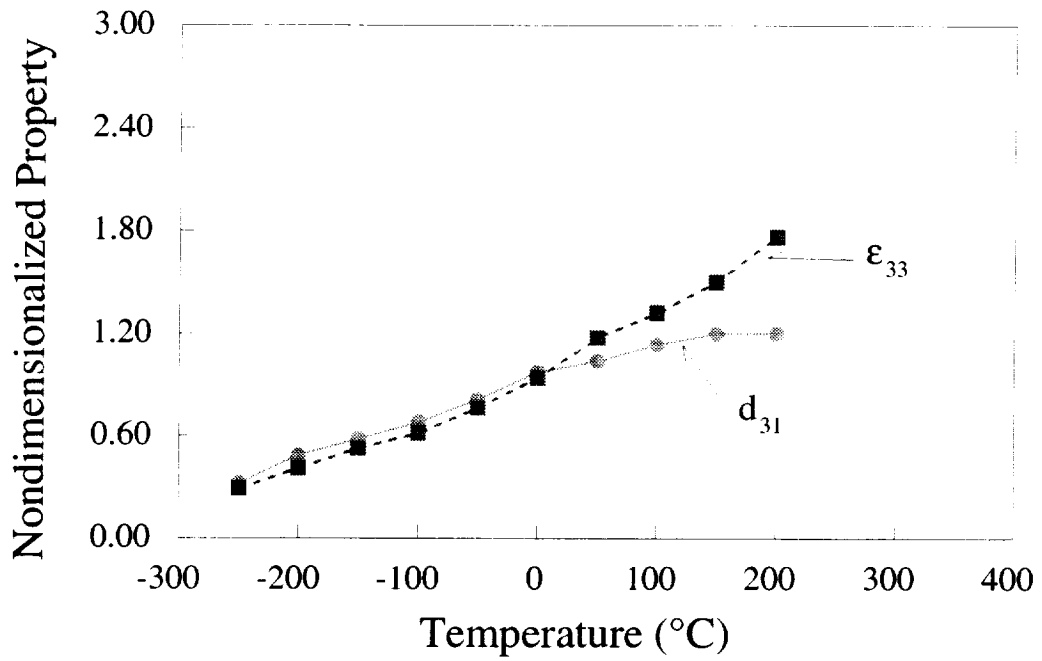


Figure 18: Temperature dependence of PZT-5A properties d_{31} and ϵ_{33} .

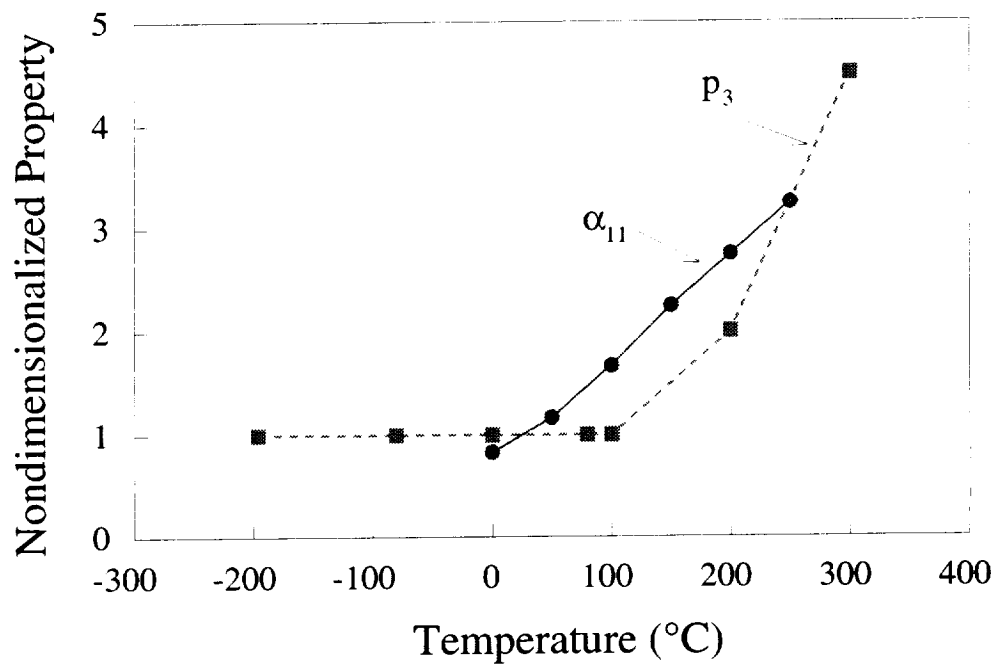


Figure 19: Temperature dependence of PZT-5A properties α_{11} and p_3 .

Table 7: Material properties of piezoceramic (PZT-5A) and Carbon/Epoxy (AS4/3501-6) composite.

	Piezoceramic	Carbon/Epoxy (Daniel and Ishai, 1994)
Elastic Moduli (10^9 Pa):		
E_{11}	69.0	142.0
E_{22}	69.0	10.3
E_{33}	53.0	10.3
Poisson's Ratio:		
ν_{12}	0.31	0.27
ν_{23}	0.44	0.20
ν_{31}	0.38	0.02
Shear Moduli (10^9 Pa):		
G_{12}	23.3	7.2
G_{23}	21.1	4.29
G_{31}	21.1	7.2
Thermal Expansion (10^{-6} m/m °C):		
α_{11}	1.2	-0.9
α_{22}	1.2	27.0
Piezoelectric Charge Constant (10^{-12} m/V):		
d_{31}	-154.	----
Electric Permittivity (10^9 f/m):		
ϵ_{33}	15.05	----
Pyroelectric Constant (10^{-3} C/m ² °C):		
P_3	-2.0	----
Reference Temperature, T_o , (°C):	20.	20.
Curie Temperature, T_c , (°C):	365.	----

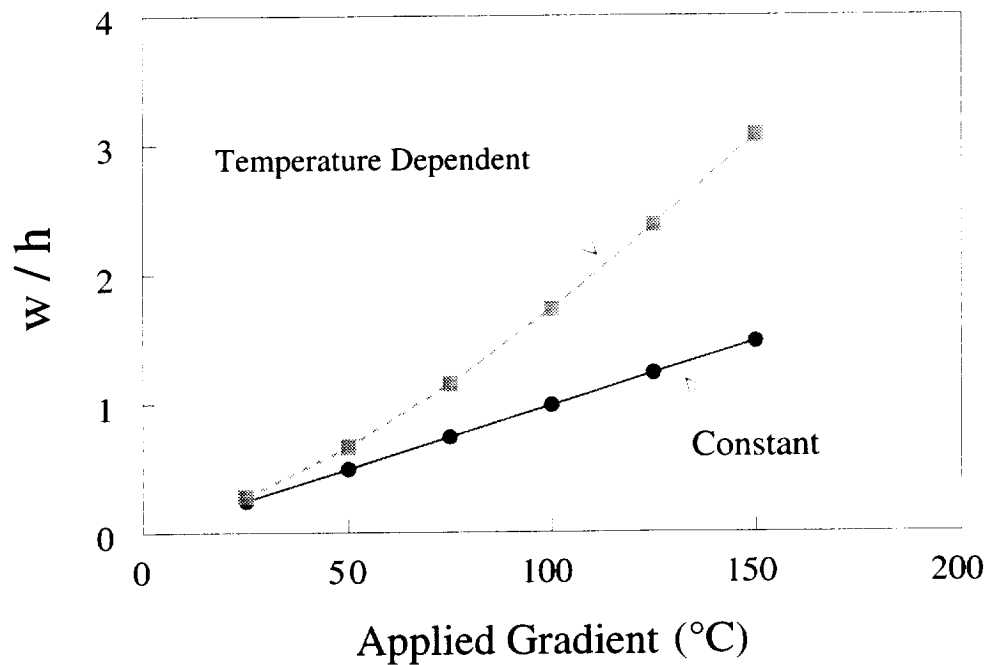


Figure 20: Influence of temperature dependent material properties on the deflections at the center of a $[0/\pm 45]_s$ Carbon/Epoxy plate with 30 attached piezoceramic patches in an active/sensory mode with varying applied thermal gradients through-the-thickness (25°C to 150°C).

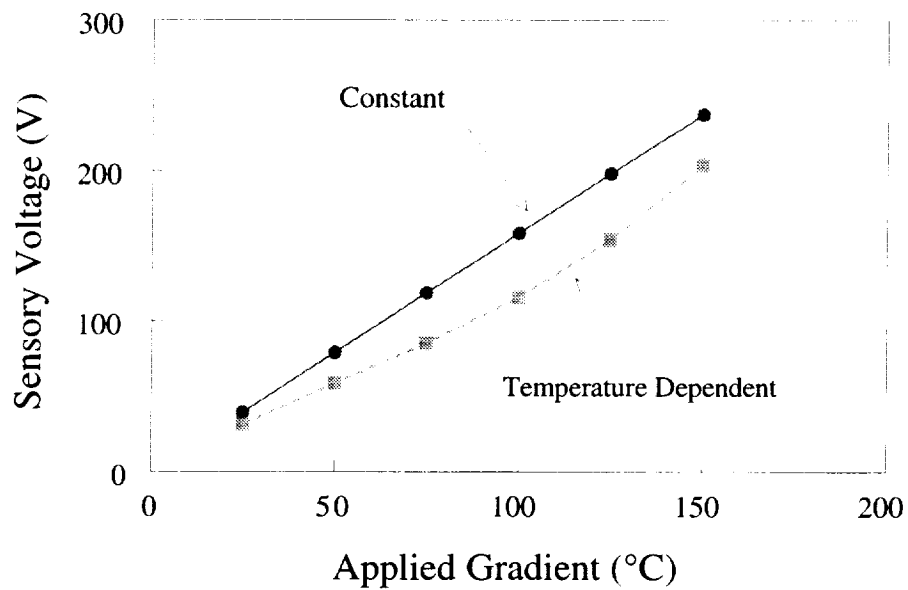


Figure 21: Influence of temperature dependent material properties on the electric potentials at the center of a $[0/\pm 45]_s$ Carbon/Epoxy plate with 30 attached piezoceramic patches in an active/sensory mode with varying applied thermal gradients through-the-thickness (25°C to 150°C).

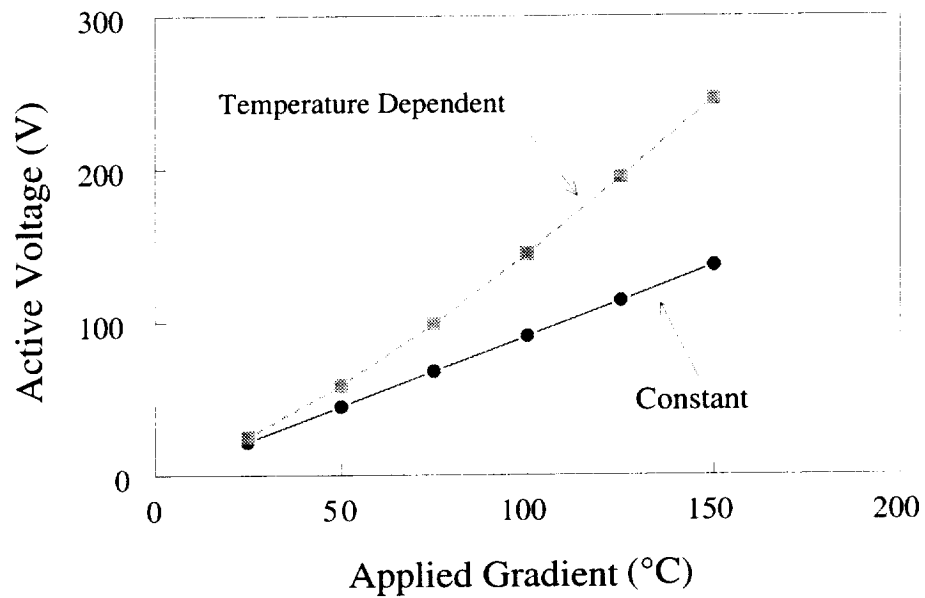


Figure 22: Influence of temperature dependent material properties on the active voltages to minimize deflections at the center of a $[0/\pm 45]_s$ Carbon/Epoxy plate with 30 attached piezoceramic patches in an active/active mode with varying applied thermal gradients through-the-thickness (25°C to 150°C).

6.4.3 Selective Shape Control of Bending and Twisting

The potential of piezoelectric actuators to selectively minimize thermally induced deformations is demonstrated on a clamped $[45_3/-45_3]$ plate with attached piezoelectric patches. The geometry and material properties remain the same as in Figure 9 and Table 4, respectively. The plate is clamped along $x=0$ and a 30°C thermal gradient is applied through-the-thickness with the piezoelectric patches operating as actuators. The temperature dependence of material properties is neglected in this study. The resulting initial deformation is shown in Figure 23 and shows a combined bending and twisting deformation induced by the thermal gradient. The bending deformation can be selectively minimized by applying the same voltages to the top and bottom piezoceramic patches. The resulting deformation when 40 V is applied is shown in Figure 24. The twisting deformation remains unaffected and is now more apparent due to the removal of the bending. In a similar manner, the twisting deformation can be minimized without affecting the bending behavior. This is accomplished by applying voltages of opposite polarities on the top and bottom surface piezoceramic patches. The deformation produced by the application of 145 V on the top piezoceramic patches and -145 V on the bottom piezoceramic patches is shown in Figure 25. The bending deformation is more apparent due to the removal of the twisting. In order to minimize both the bending and twisting deformations simultaneously, the previous two cases can be superimposed. Thus, by applying 185 V on the top actuators and -105 V on the bottom actuators, all deformations in the plate can be eliminated as shown in Figure 26.

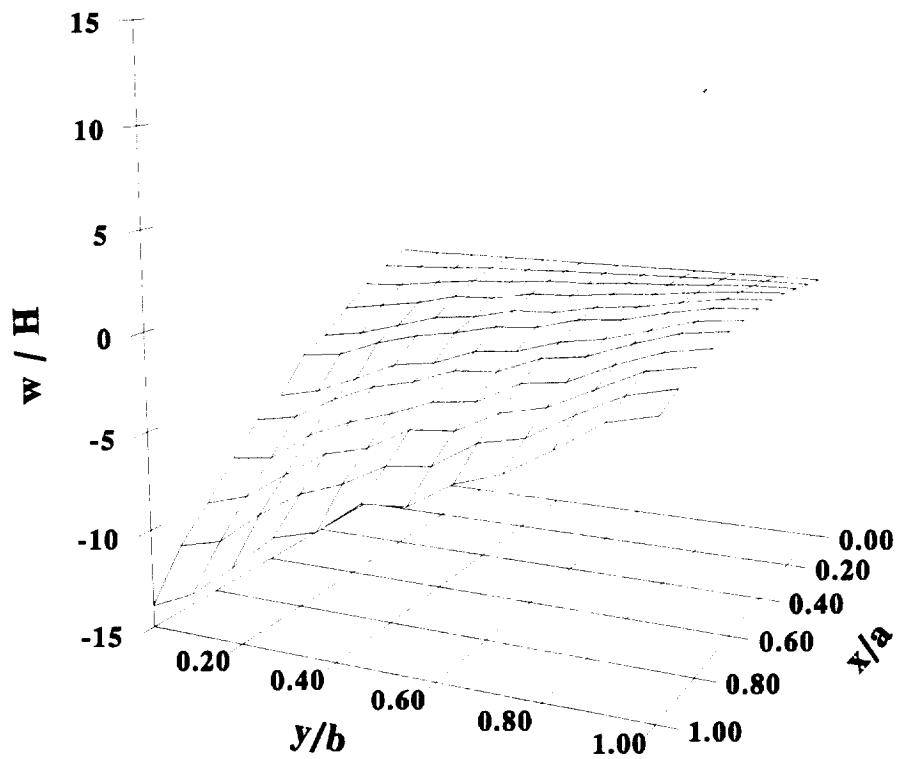


Figure 23: Initial bending and twisting deformation of a clamped [45₃/45₃] AS4/3501 plate with 30 attached discrete G-1195 piezoelectric patches under a 30°C thermal gradient through-the-thickness.

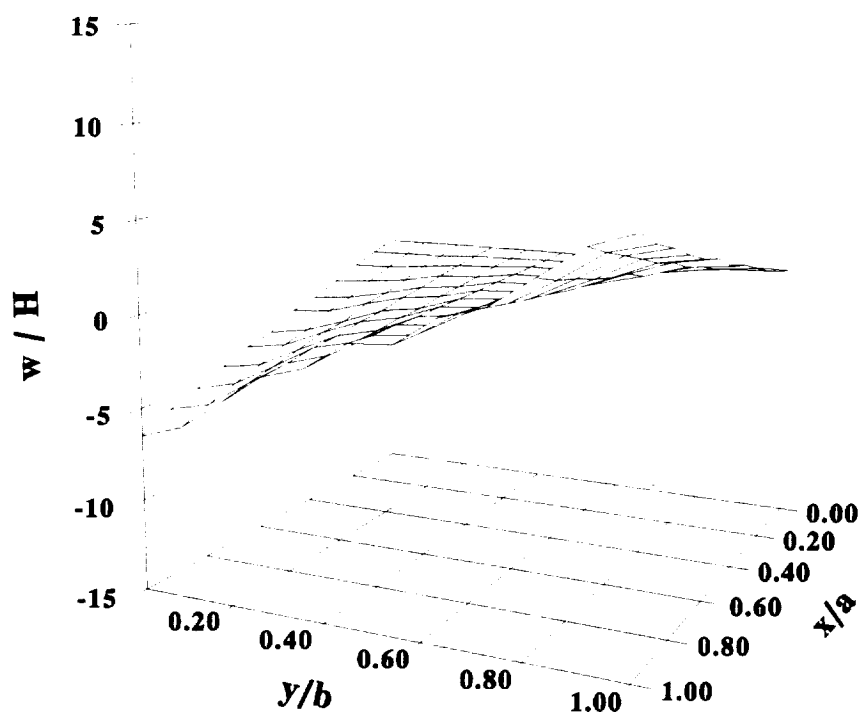


Figure 24: Selective shape control of the bending deformation of a clamped $[45_3/45_{-3}]$ AS4/3501 plate with 30 attached discrete G-1195 piezoelectric patches under a 30°C thermal gradient through-the-thickness by applying 40 V to all piezoceramic patches.

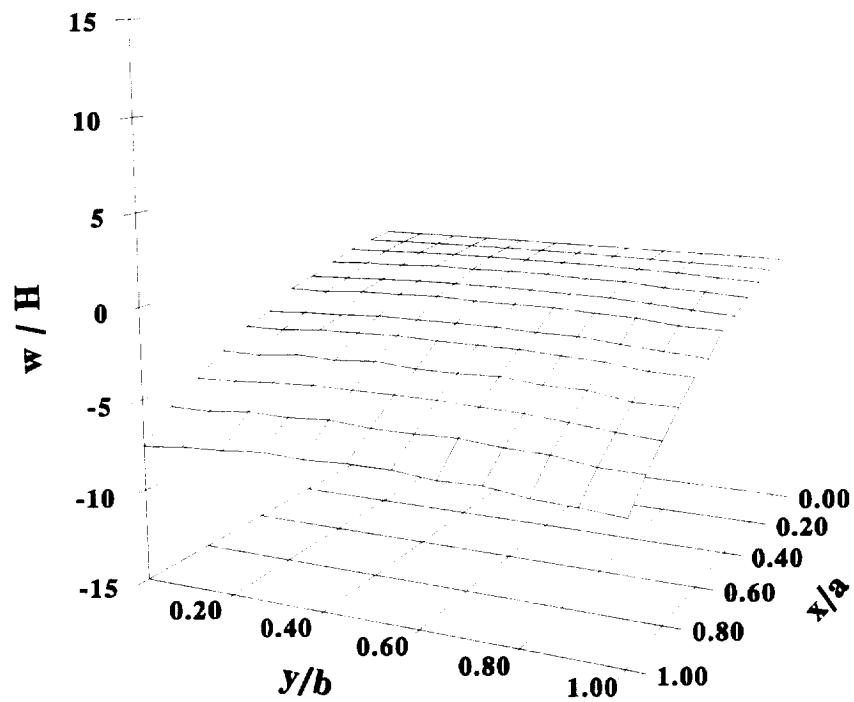


Figure 25: Selective shape control of the twisting deformation of a clamped $[45_3/45_{.3}]$ AS4/3501 plate with 30 attached discrete G-1195 piezoelectric patches under a 30°C thermal gradient through-the-thickness by applying 145 V to top patches and -145 V to bottom patches.

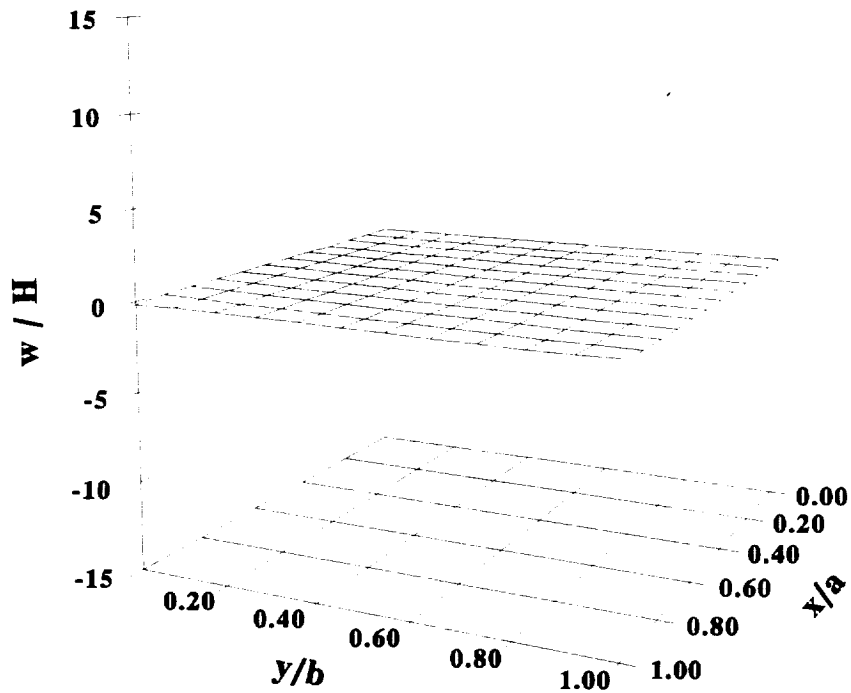


Figure 26: Shape control of both bending and twisting deformation of a clamped $[45_3/45_{-3}]$ AS4/3501 plate with 30 attached discrete G-1195 piezoelectric patches under a 30°C thermal gradient through-the-thickness by applying 185 V to top patches and -105 V to bottom patches.

6.4.4 Thermal Stresses

The increased accuracy gained from implementing a layerwise laminate theory is demonstrated by examining the thermal stresses in a cantilevered $[0_8/p]$ beam. The beam is depicted in Figure 27 and has a length (L) of 25.4 cm and a width (b) of 2.54 cm. Two thicknesses (H) are examined; a thin beam ($H = 0.1143$ cm) with an aspect ratio (L/H) of ~ 200 and a thick beam ($H = 11.43$ cm) with an aspect ratio (L/H) of ~ 2 . The beam is composed of eight unidirectional E-Glass/Epoxy plies and one piezoelectric layer. The material properties are listed in Table 8. The beam element is used to conduct the analysis using 30 elements along the length of the beam, with one discrete layer modeled through-the-thickness for each piezoelectric and E-Glass/Epoxy ply. A uniform temperature rise of 100°C is applied with the piezoelectric layer grounded (i.e. 0 V applied). The predicted normal stress, σ_{11} , near the middle of the beam ($x/L = 0.5$) is shown in Figure 28 for both the thin and thick beams, along with the corresponding results predicted by classical laminate theory (CLT). The normal stress is nondimensionalized using the equivalent laminate modulus, $E_{L11} = 42.2 \cdot 10^9$ Pa. The CLT predicts the same stress regardless of the thickness of the beam. At this location of the beam, there is good agreement between the current formulation and CLT regardless of the beam thickness. The predicted normal stress, σ_{11} , at the free end of the beam ($x/L = 1.0$) is shown in Figure 29 and shows that CLT is only accurate for the thin beam. The predicted shear stress, σ_{13} , at the free end of the beam ($x/L = 1.0$) is shown in Figure 30. The shear stress is nondimensionalized using the equivalent laminate modulus, $G_{L13} = 6.3 \cdot 10^9$ Pa. The results show that the CLT assumption of neglecting shear stresses is only accurate for the thin beam case. These results help demonstrate the improved accuracy in stress predictions achieved by using the layerwise laminate theory, especially for thick laminates.

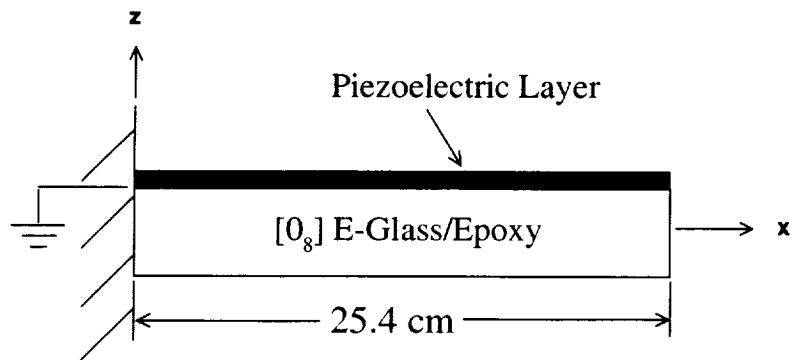


Figure 27: Cantilevered [0_p/p] E-Glass/Epoxy and piezoelectric beam

Table 8: Material properties of piezoelectric and E-Glass/Epoxy.

	Piezoelectric	E-Glass/Epoxy (Daniel and Ishai, 1994)
Elastic Moduli (10^9 Pa):		
E_{11}	68.0	39.0
E_{33}	68.0	8.6
Poisson's Ratio:		
ν_{13}	0.30	0.28
Shear Modulus (10^9 Pa):		
G_{13}	26.2	3.8
Thermal Expansion (10^{-6} m/m $^{\circ}$ C):		
α_{11}	3.8	7.0
α_{33}	3.8	21.0
Piezoelectric Charge Constant (10^{-12} m/V) :		
d_{31}	-125.	----
Electric Permittivity (10^{-9} f/m):		
ϵ_{33}	11.06	----
Pyroelectric Constant (10^{-3} C/m 2 $^{\circ}$ C):		
p_3	-2.5	----
Reference Temperature, T_0 , ($^{\circ}$ C):	20.	20.

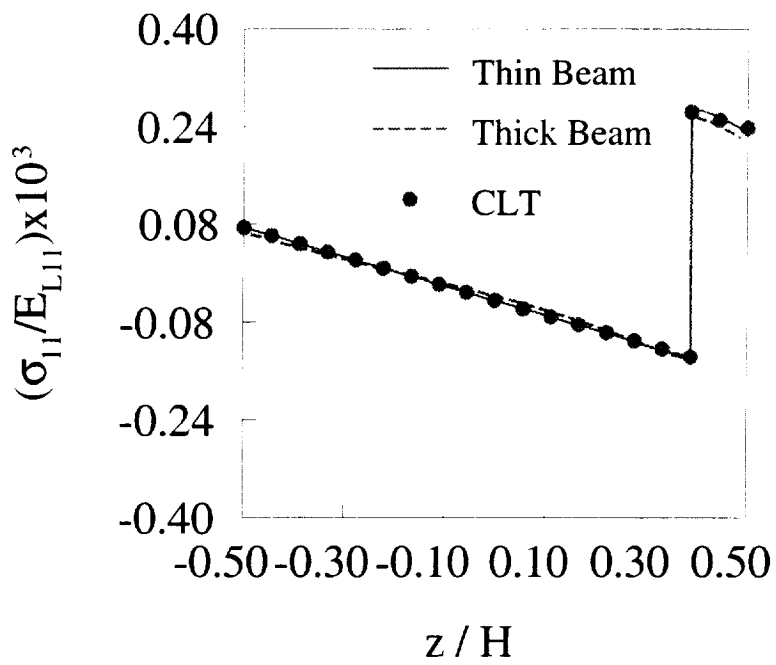


Figure 28: Comparison of normal stresses at the middle ($x/L=0.5$) of a $[0_g/p]$ E-Glass/Epoxy and piezoelectric beam under a uniform 100°C load for two aspect ratios (thin=200 and thick=2).

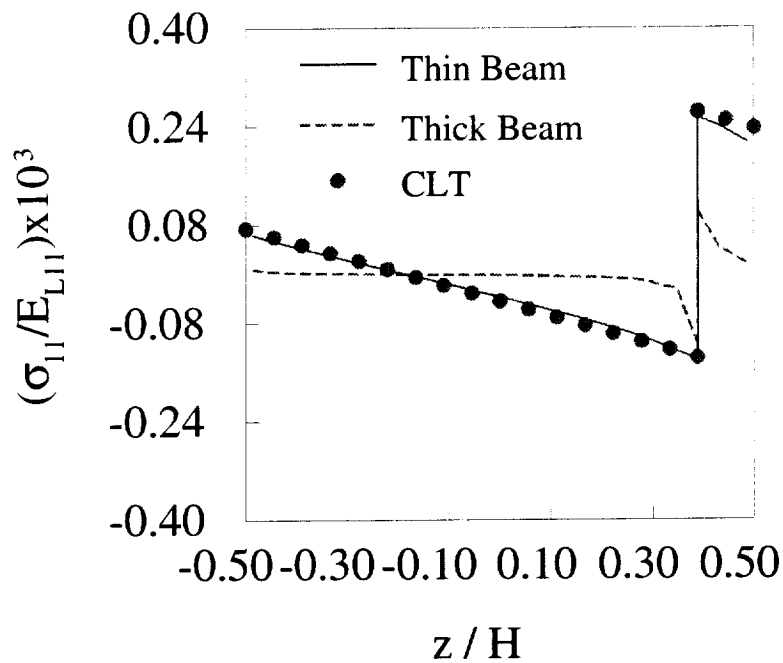


Figure 29: Comparison of normal stresses at the free end ($x/L=1.0$) of a $[0_8/p]$ E-Glass/Epoxy and piezoelectric beam under a uniform 100°C load for two aspect ratios (thin=200 and thick=2).

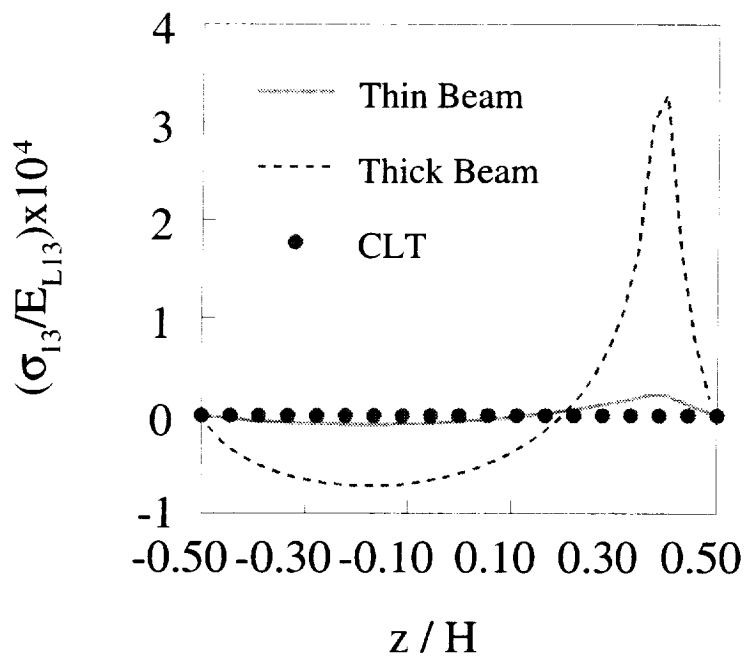


Figure 30: Comparison of shear stresses at the free end ($x/L=1.0$) of a $[0_g/p]$ E-Glass/Epoxy and piezoelectric beam under a uniform 100°C load for two aspect ratios (thin=200 and thick=2).

6.4.5 Influence of Curvature on Active and Sensory Response

The problem examined consists of a $[0_p/p]$ (where 0° is along the ξ axis) circular cylinder with a radius (R) of 0.76 m, a length (L) of 1.524 m, and a thickness (h) of 7.62 mm as depicted in Figure 31. The cylinder is composed of nine unidirectional Carbon/Epoxy plies and one piezoceramic layer. The material properties are listed in Table 6. Due to the symmetry of the problem, only $1/8$ of the cylinder is modeled using a 10×10 mesh with two discrete layers (one for the Carbon/Epoxy and one for the piezoceramic). A clamped-clamped configuration in which both ends of the cylinder ($z/L = 0$ and $z/L = 1$) are fixed is examined. The cylinder is subjected to three different types of thermal loads (a uniform thermal load and two types of sinusoidally varying temperatures along the hoop direction) as shown in Figure 32. Results from the current shell element are presented to investigate the influence of the curved structure on the sensory and active response under the different applied thermal loads. All displacements (w) and electric potentials (ϕ) presented in this section are along the hoop direction at $z/L = 0.5$ and $r/R = 1.0$ of the cylinder.

The influence of pyroelectric effects on the displacements and sensory electric potentials of the cylinder under the three different applied thermal loads are presented in Figures 33-38. Each figure contains results for two cases to show the effects of incorporating the pyroelectric constant in the analysis (the $p_3=0$ case neglects pyroelectric effects). Figures 33 and 34 show, respectively, the displacement and sensory electric potential induced from applying a uniform thermal load of 50°C . A uniform deflection of the cylinder is achieved, which maintains the original circular shape. The sensory electric potential also shows a uniform response that corresponds to the displacement. The incorporation of pyroelectric effects produces larger displacements and electric potentials. The results from applying a cosine varying temperature are shown in Figures 35 and 36. The deflection of the cylinder now shows a sinusoidal pattern that translates into either an oval-shaped or figure eight shaped circumferential displacement, depending on whether pyroelectric effects are modeled. The electric potential only displays a sinusoidal pattern when pyroelectric effects are included and becomes almost zero when the pyroelectric effect is neglected. Figures 37 and 38 show the results of applying a double cosine varying thermal load. A sinusoidally varying displacement and electric potential pattern is produced which corresponds to an oval-shaped deflection of the cylinder. Once again, incorporating the pyroelectric effect leads to increased displacements and electric potentials.

The active response of the cylinder under the three applied thermal loads is examined in Figures 39-41. Each figure shows the displacement of the cylinder for three configurations of the piezoelectric layers: a sensory mode, a grounded configuration (zero electric potential applied), and an active mode. The magnitude of the applied electric potential remains the same for all three cases, although the form of the electric potential varies to correspond to the type of thermal load. Figure 39 shows the deflection of the cylinder under a uniform thermal load (50°C). Application of increasing uniform applied electric potentials produces a noticeable decrease in the thermally induced sensory deflection. Figure 40 depicts the displacement of the cylinder under a cosine varying thermal load and shows that although some changes in the overall shape of the cylinder can be obtained by applying active electric potentials, no significant overall reduction of the thermal deflection is achieved. Figure 41 illustrates the deflections produced under a double cosine variation of the thermal load. For this case, the double cosine applied electric potential effectively minimizes the thermal deflection.

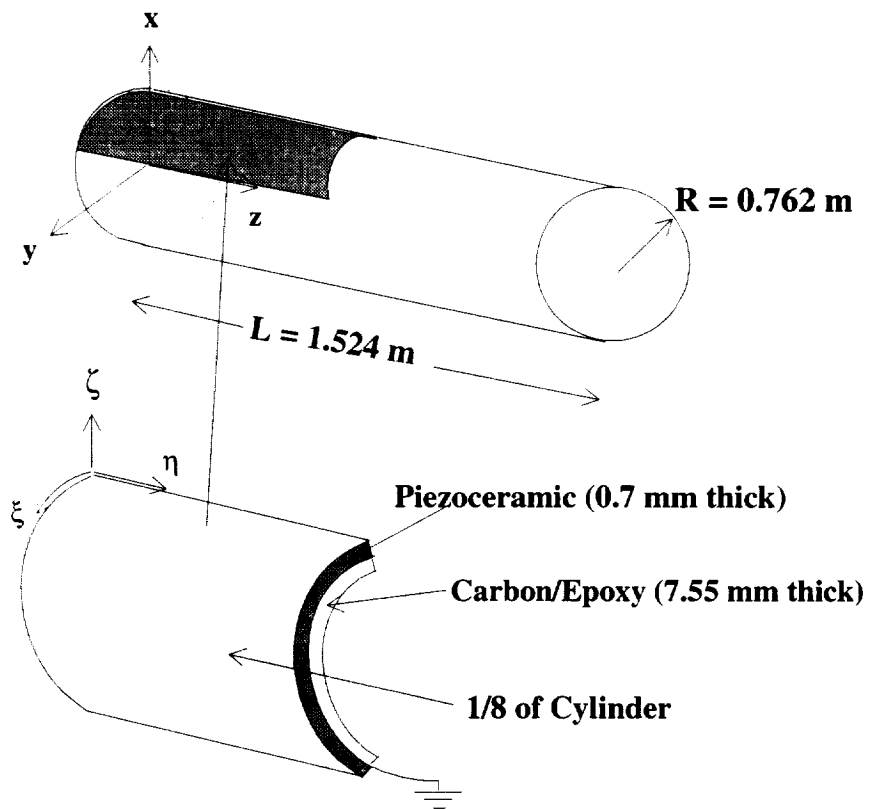


Figure 31: Geometry of a [0_θ/p] Carbon/Epoxy circular cylinder with an attached piezoceramic layer.

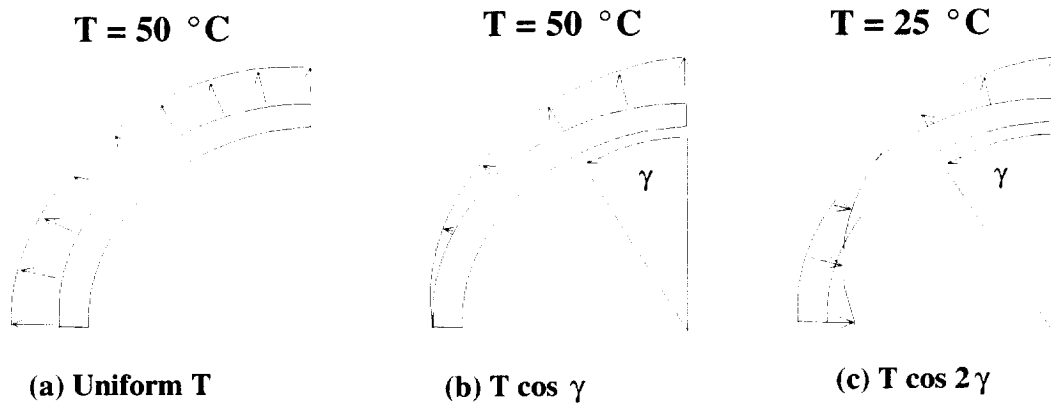


Figure 32: Different types of applied thermal loads applied to the cylinder:
 a) 50°C uniform thermal load; b) 50°C cosine varying load; and
 c) 25°C double cosine varying load.

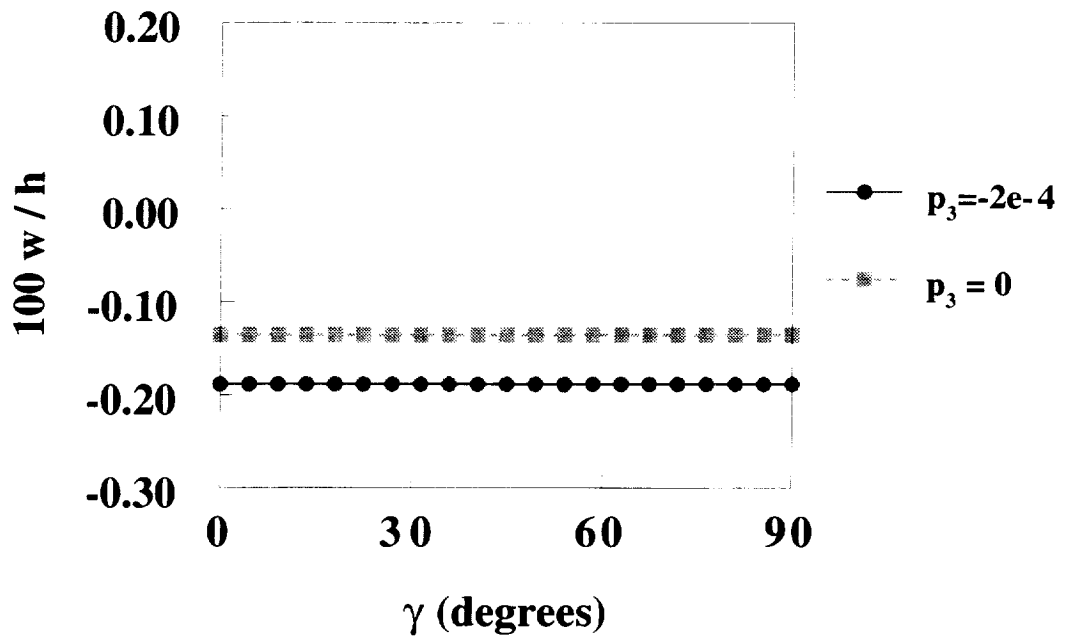


Figure 33: Influence of pyroelectric effects on the displacements of a $[0_g/p]$ Carbon/Epoxy circular cylinder with a piezoceramic layer under a 50°C uniform thermal load.

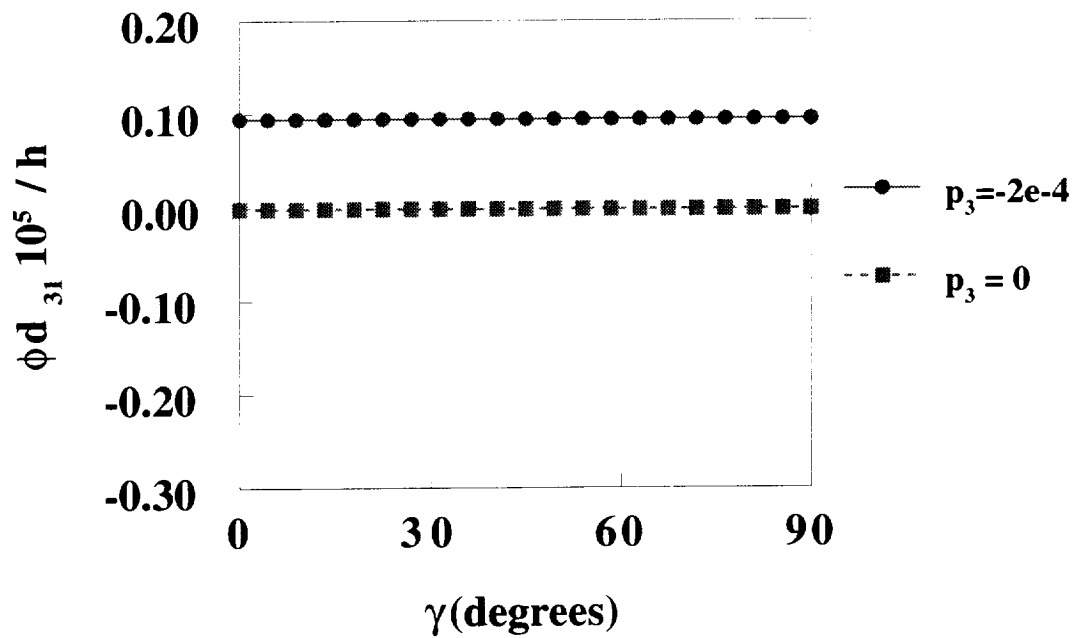


Figure 34: Influence of pyroelectric effects on the sensory electric potentials of a [0_p/p] Carbon/Epoxy circular cylinder with a piezoceramic layer under a 50°C uniform thermal load.

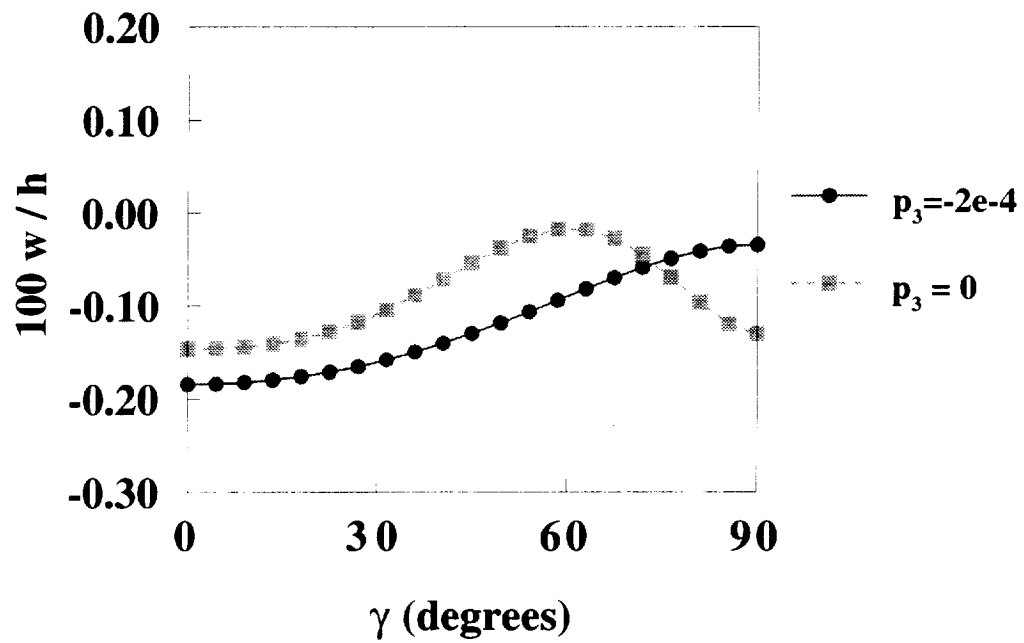


Figure 35: Influence of pyroelectric effects on the displacements of a $[0_p/p]$ Carbon/Epoxy circular cylinder with a piezoceramic layer under a 50°C cosine varying thermal load.

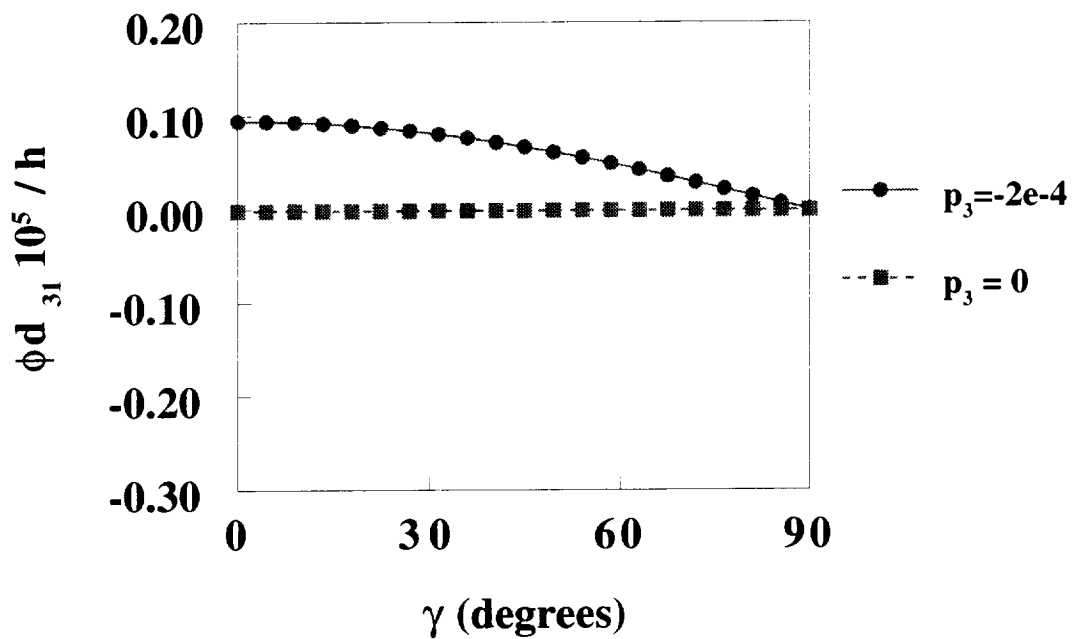


Figure 36: Influence of pyroelectric effects on the sensory electric potentials of a $[0_p/p]$ Carbon/Epoxy circular cylinder with a piezoceramic layer under a 50°C cosine varying thermal load.

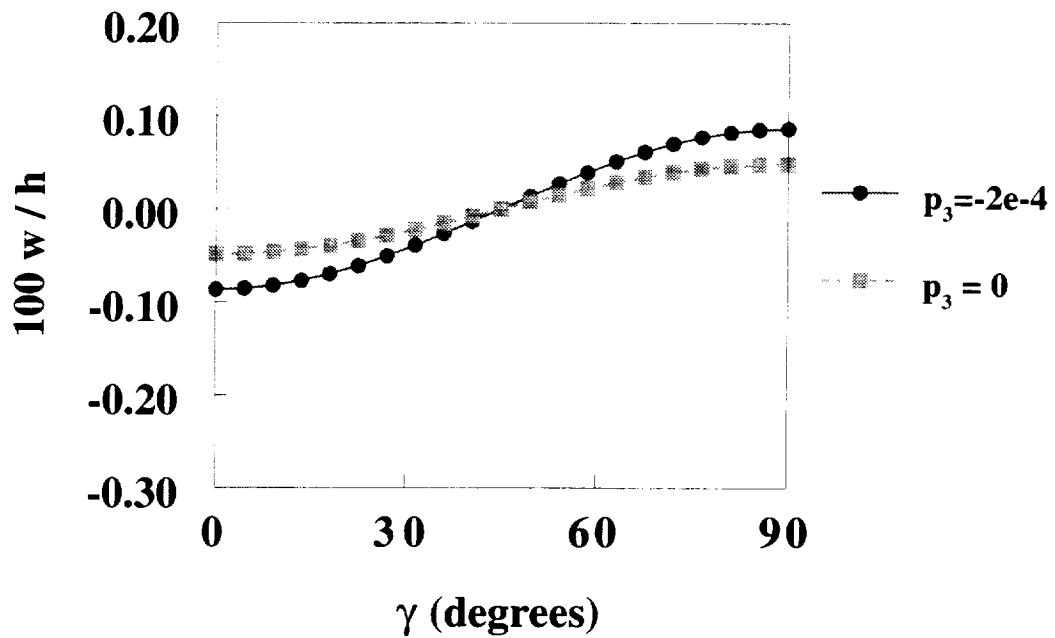


Figure 37: Influence of pyroelectric effects on the displacements of a $[0_\theta/p]$ Carbon/Epoxy circular cylinder with a piezoceramic layer under a 25°C double cosine varying thermal load.

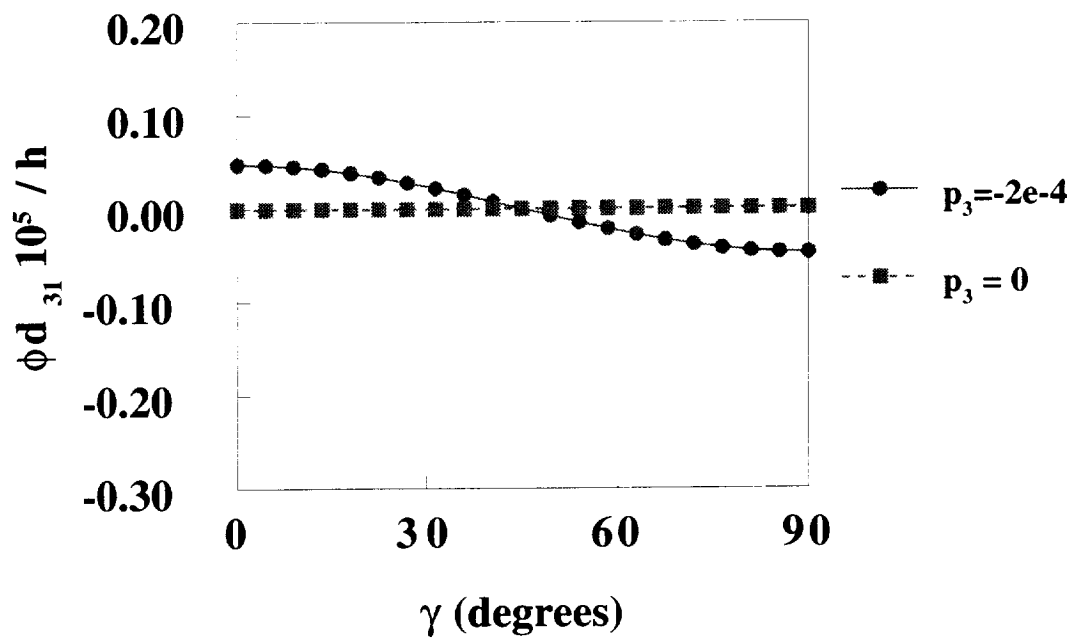


Figure 38: Influence of pyroelectric effects on the sensory electric potentials of a [0/p] Carbon/Epoxy circular cylinder with a piezoceramic layer under a 25°C double cosine varying thermal load.

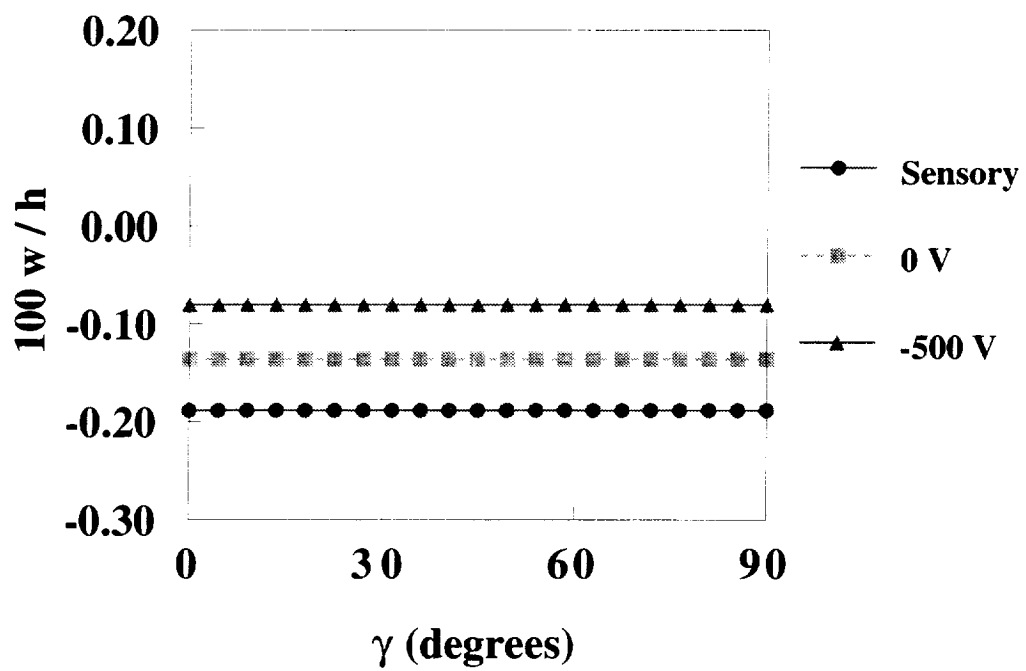


Figure 39: Comparison of displacements of a $[0_p/p]$ Carbon/Epoxy circular cylinder with a piezoceramic layer in sensory, grounded, and active modes under a 50°C uniform thermal load.

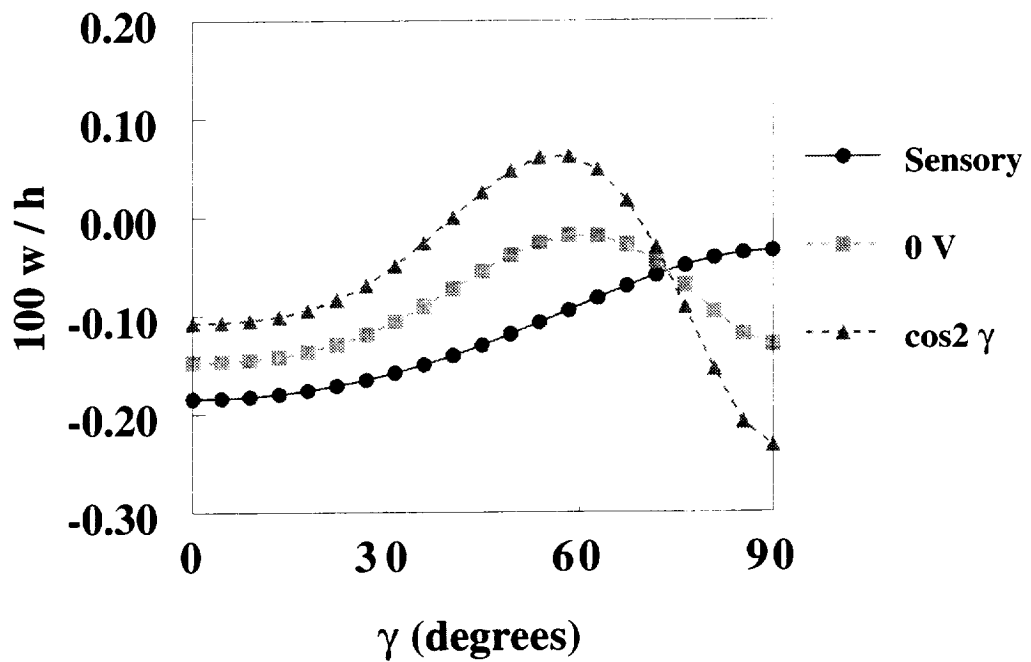


Figure 40: Comparison of displacements of a $[0_p/p]$ Carbon/Epoxy circular cylinder with a piezoceramic layer in sensory, grounded, and active modes under a 50°C cosine varying thermal load.

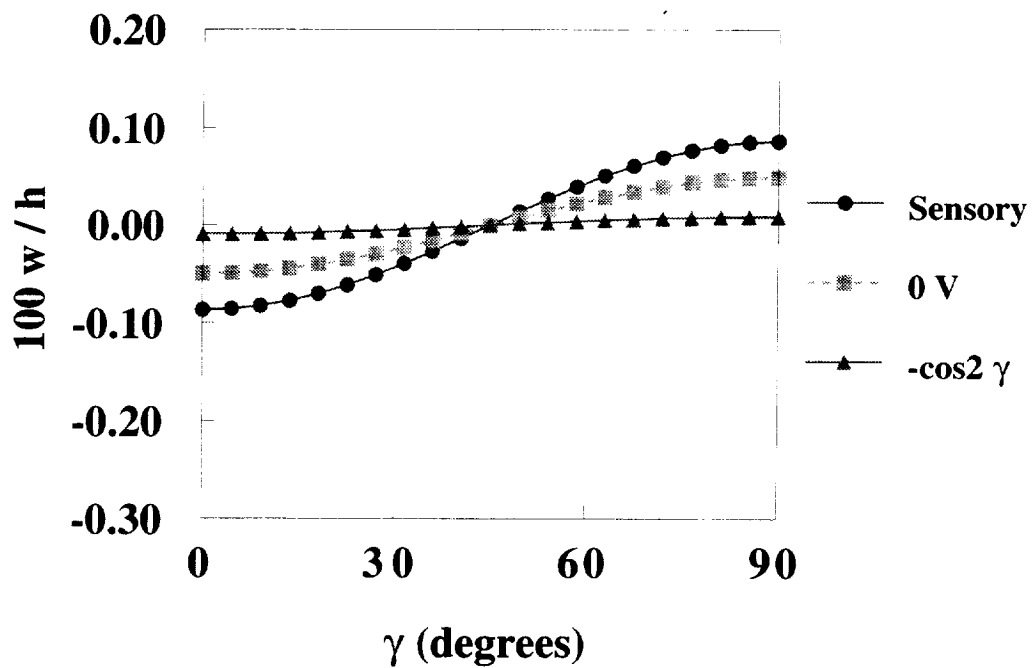


Figure 41: Comparison of displacements of a $[0_6/p]$ Carbon/Epoxy circular cylinder with a piezoceramic layer in sensory, grounded, and active modes under a 25°C double cosine varying thermal load.

CHAPTER 7 CONCLUSION AND SUGGESTIONS FOR FUTURE WORK

New analytical formulations and mechanics are developed to characterize the coupled mechanical, electrical, and thermal behavior of piezoelectric composite materials. The coupled thermopiezoelectric behavior is captured at the material level through the constitutive equations and the displacements, electric potential, and temperature are introduced as state variables in the formulation. The equations of motion are developed in both cartesian and curvilinear coordinates and a layerwise laminate theory is incorporated to provide more accurate predictions of interlaminar and intralaminar effects, especially for thick laminates. Thermal effects arising from thermal expansion mismatch, pyroelectric effects, and temperature dependent material properties are incorporated in the formulation. Corresponding finite element equations are developed and implemented into stand alone computer programs for beam, plate, and shell elements. The accuracy of the formulation is verified with comparisons from published experimental data and other analytical methods. Additional numerical studies are also conducted to demonstrate additional capabilities of the formulation to predict the sensory and active behavior of piezoelectric composite materials. The verification and numerical studies have helped to demonstrate the effectiveness and accuracy of the developed mechanics and finite elements. However, future experimental studies will help to complement this work by contributing to additional verification studies.

7.1 Suggested Plan of Future Experimental Studies

In order to verify the accuracy of the developed analytical formulation in more detail, the following plan of experimental studies are outlined. As illustrated in the previous sections, previous researchers have conducted numerous room temperature static experimental studies along with some limited high temperature studies. However, dynamic studies, and in particular high temperature dynamic experiments, have received less attention. Thus, the development of an experimental setup for conducting high temperature dynamic studies will help to more fully characterize the behavior of piezoelectric composite materials and determine the feasibility of applying these materials in extreme temperature environments.

A generic dynamic experimental setup is shown in Figure 39. A beam specimen with an attached piezoelectric patch will be excited by an electromagnetic shaker and the corresponding response of the beam measured by an accelerometer. For high temperature tests, the beam will be placed inside an oven or furnace. The time varying responses of the beam and piezoelectric patch are passed through various test measurement devices including signal conditioners, amplifiers, and oscilloscopes to increase the signal strength and gain, as well as to monitor and measure the dynamic waveforms. The time signals are then passed on to a PC based dynamic data acquisition system which contains hardware to acquire the signals and software to calculate the frequency response of the data. The resulting output will include the natural frequencies of the beam, the mode shapes, and the sensor output.

A series of tests will be performed to investigate the individual sensory and active dynamic responses of piezoelectric composite materials at high temperature. The first test configuration will consist of a beam with a single piezoelectric patch as shown in Figure 40. A series of tests will be

performed as listed in Table 9 to determine the sensory and active responses individually. A room temperature baseline test will be performed to determine the natural frequencies of the beam with the piezoelectric patch grounded. The piezoelectric patch will then be tested in a sensory mode to demonstrate the capability to monitor modal frequencies through measurement of the sensory voltages, and to determine the effect of the sensory mode on the natural frequencies. Next, the piezoelectric patch will be configured as an actuator and electric voltages applied to measure the capability to actively control the vibration of the beam. These experiments will then be repeated at higher temperature to assess thermal effects on the sensory and active responses. A series of different beam materials from metals to composites can be studied, as well as different types of piezoelectric materials from piezopolymers to piezoceramics, in order to determine the most effective sensor and actuator materials. In addition, the size and location of the piezoelectric patch can be varied to assess the influence of coverage area and location on sensing and actuation.

The next test configuration will consist of a beam with two piezoelectric patches, as shown in Figure 41, to investigate combined sensory/active and active/active modes of operation. A series of tests will be performed as shown in Table 10 to determine capabilities for combined sensory and actuator operations. The baseline case will consist of a room temperature test with both piezoelectric patches grounded to determine the natural frequencies of the beam. A combined sensory/active configuration will then be studied, in which various voltages will be applied to the actuator patch to reduce the natural frequencies, while the sensor patch monitors the response. The next case will involve both patches operating as actuators to determine whether multiple actuators can more effectively reduce the beam vibrations than a single actuator. These experiments will then be repeated at higher temperature to determine thermal effects on the combined sensory/active and active/active configurations. Additional cases with different beam and piezoelectric materials, as well as different sized patches and locations will also be studied to determine the optimal combinations for combined sensory/active and active/active operations.

Additional studies will also be conducted on a flat plate with multiple piezoelectric patches (Figure 42) and a curved plate with multiple piezoelectric patches (Figure 43). The flat plate will provide additional information on two-dimensional geometry effects on sensing and actuation, as well as to determine capabilities to utilize patches at specific locations to sense and actuate certain natural frequencies. A similar study will also be performed on a cylindrical shell to determine the effect of curvature on actuation and sensing. As in previous problems, the baseline case will involve determining the room temperature natural frequencies with the piezoelectric patches inoperative. A variety of different sensor and actuator configurations will be examined at room and high temperatures, for different beam and piezoelectric materials.

Throughout the experimental studies, the developed finite element codes will be used to provide design guidelines to reduce the number of experiments. Even for the simple beam configurations studied in Figures 40 and 41, there a large number of different experiments required to determine the influence of different materials, patch sizes, and locations. As more complicated geometries are considered in Figures 42 and 43, the number of experimental tests will increase substantially. Thus, in order to keep experimental testing time and costs reasonable, a combined analytical and experimental approach is essential.

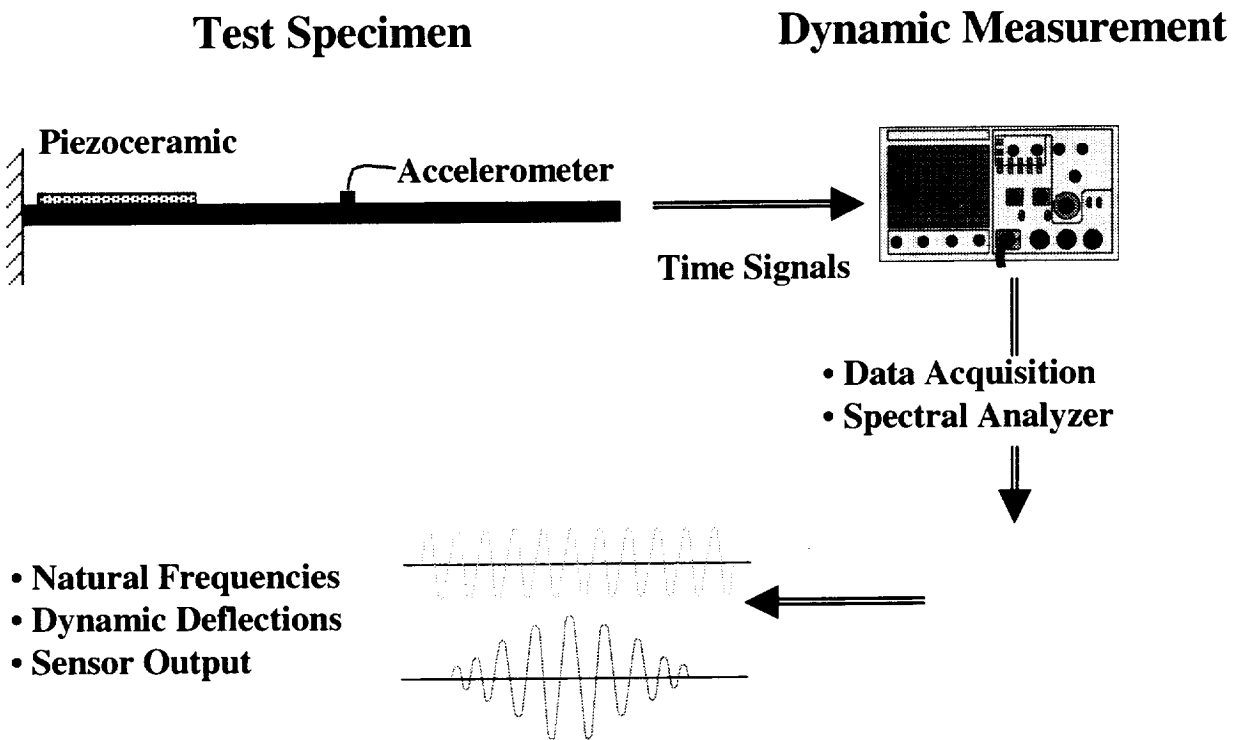


Figure 39: Dynamic experimental setup.

Testing Configuration

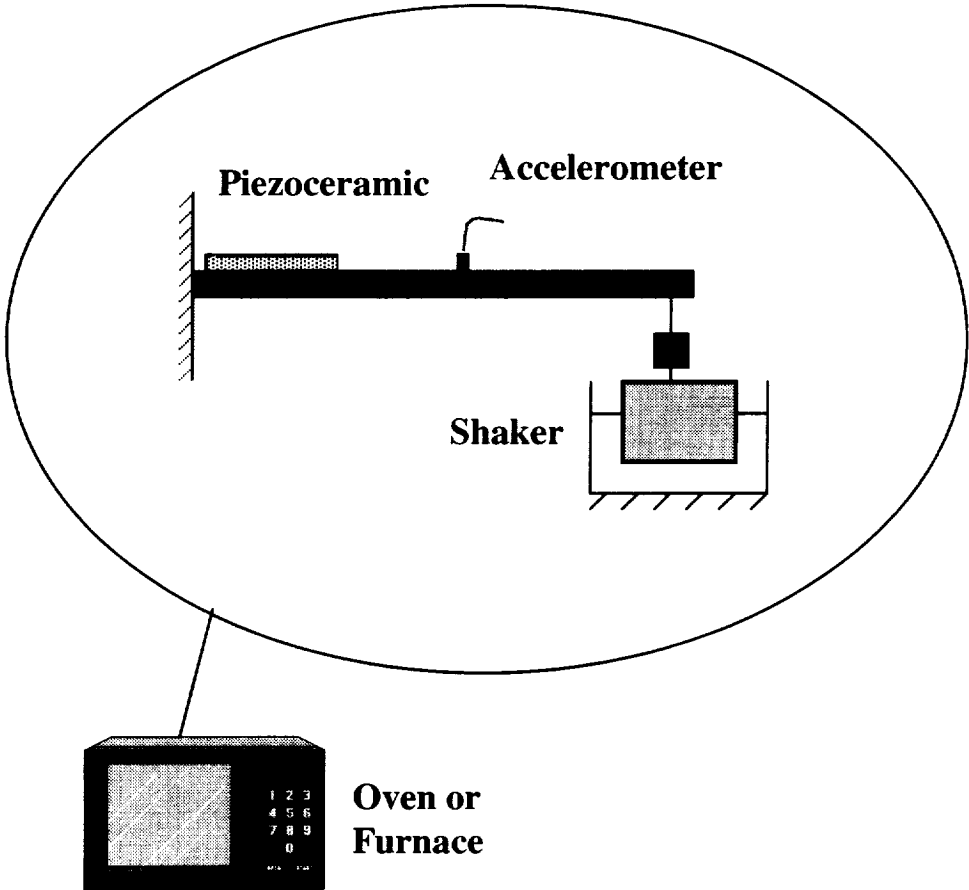


Figure 40: High temperature test configuration for a cantilevered beam with one piezoelectric patch to examine sensory and active modes individually.

Table 9: Series of tests for a cantilevered beam with one piezoelectric patch.

		Beam and Piezoelectric Materials					
		Aluminum Beam		[0 ₈] Graphite/Epoxy Beam		[0 ₂ /90 ₂] _s Graphite/Epoxy Beam	
Temp.	Piezo Mode	PZT Patch	PVDF Patch	PZT Patch	PVDF Patch	PZT Patch	PVDF Patch
Room	Grounded						
Room	Sensory						
Room	Active						
Elevated	Grounded						
Elevated	Sensory						
Elevated	Active						

Testing Configuration

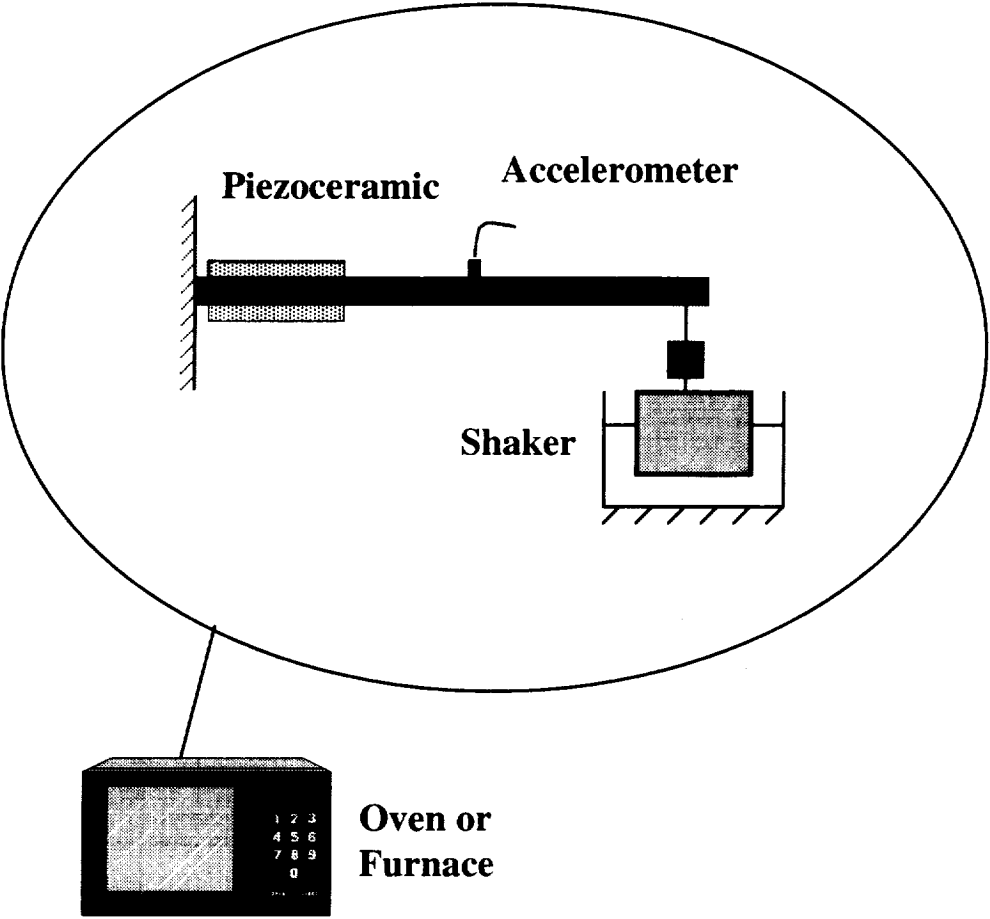


Figure 41: High temperature test configuration for a cantilevered beam with two piezoelectric patches to examine combined sensory/active and active/active modes of operation.

Table 10: Series of tests for a cantilevered beam with two piezoelectric patches.

		Beam and Piezoelectric Materials								
		Aluminum Beam			[0 _s] Graphite/Epoxy Beam			[0 ₂ /90 ₂] _s Graphite/Epoxy Beam		
Temp.	Piezo. Mode	PZT/ PZT	PVDF/ PVDF	PZT/ PVDF	PZT/ PZT	PVDF/ PVDF	PZT/ PVDF	PZT/ PZT	PVDF/ PVDF	PZT/ PVDF
Room	Grounded									
Room	Active/ Sensory									
Room	Active/ Active									
High	Grounded									
High	Active/ Sensory									
High	Active/ Active									

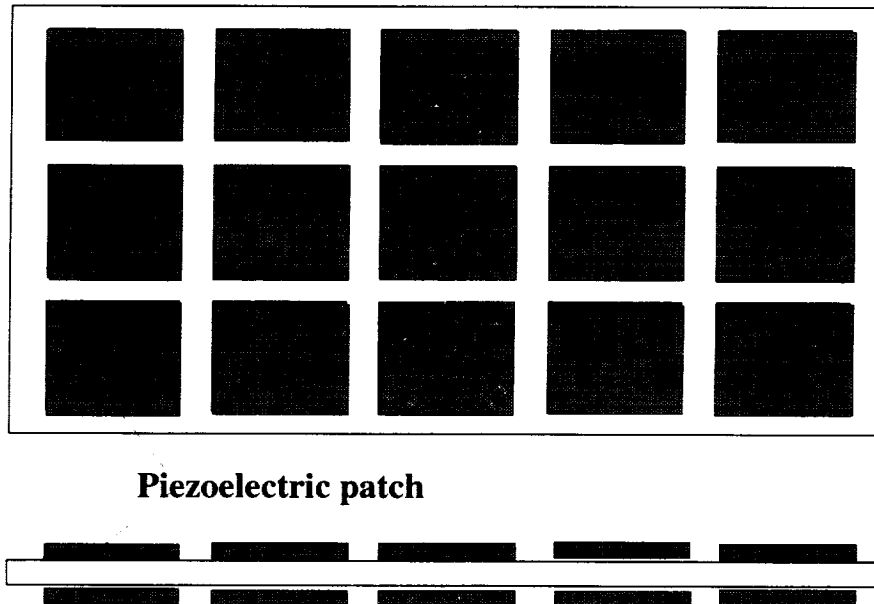


Figure 42: Test configuration of a flat plate with attached piezoelectric patches to investigate two-dimensional effects on combined sensory and active operations.

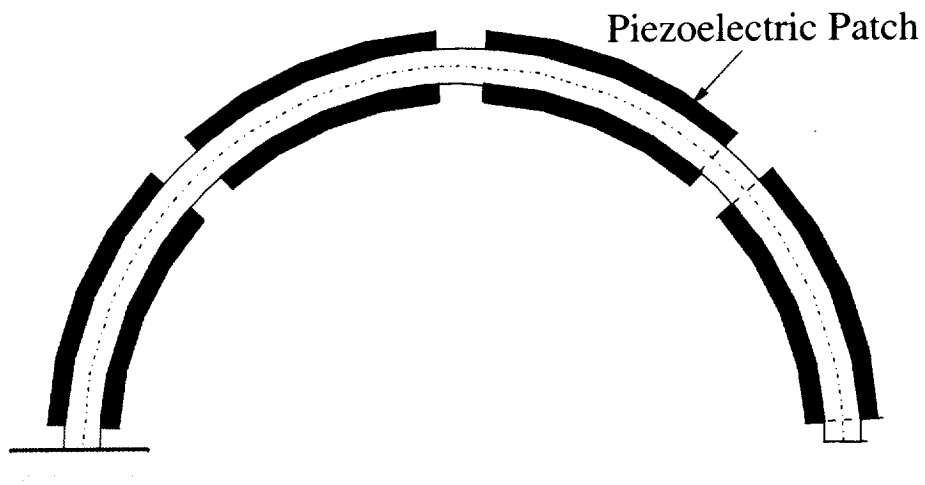


Figure 43: Test configuration of a curved cylinder with attached piezoelectric patches to investigate curvature effects on combined sensory and active operations

REFERENCES

- ABAQUS. 1996. *MSC/ABAQUS User's Manual Version 5.6, Volumes I-III*. Los Angeles: MacNeal-Schwendler Corporation.
- Allik, H. and T.J.R. Hughes. 1970. Finite element method for piezoelectric vibration. *International Journal for Numerical Methods in Engineering* 2:151-157.
- Bailey, T. and J.E. Hubbard. 1985. Distributed piezoelectric-polymer active vibration control of a cantilever beam. *Journal of Guidance* 8:605-611.
- Batra, R.C. and X. Q. Liang. 1997. The vibration of a rectangular laminated elastic plate with embedded piezoelectric sensors and actuators. *Computers and Structures* 63:203-216.
- Baz, A. and S. Poh. 1988. Performance of an active control system with piezoelectric actuators. *Journal of Sound and Vibration* 126:327-343.
- Bhattacharya, P., H. Suhail, and P.K. Sinha. 1998. Finite element free vibration analysis of smart laminated composite beams and plates. *Journal of Intelligent Material Systems and Structures* 9:20-28.
- Cady, W.G. 1964. *Piezoelectricity*. Rev. Ed. New York: Dover Press.
- Chandrashekhara, K. and A.N. Agarwal. 1993. Active vibration control of laminated composite plates using piezoelectric devices: a finite element approach. *Journal of Intelligent Material Systems and Structures* 4:496-508.
- Chandrashekhara, K. and R. Tenneti. 1995. Thermally induced vibration suppression of laminated plates with piezoelectric sensors and actuators. *Smart Materials and Structures* 4:281-290.
- Chandrashekhara, K. and S. Varadarajan. 1997. Adaptive shape control of composite beams with piezoelectric actuators. *Journal of Intelligent Material Systems and Structures* 8:112-124.
- Chattopadhyay, A., H. Gu, and D. Dragomir-Daescu. 1999. Dynamics of delaminated composite plates with piezoelectric actuators. *AIAA Journal* 37:248-254.
- Chattopadhyay, A. and C. Seeley. 1997. A higher order theory for modeling composite laminates with induced strain actuators. *Composites Part B* 28B:243-252.
- Charette, F., A. Berry, and C. Guigou. 1997. Dynamic effects of piezoelectric actuators on the vibrational response of a plate. *Journal of Intelligent Material Systems and Structures* 8:513-524.
- Clark, R.L., M.R. Flemming, and C.R. Fuller. 1993. Piezoelectric actuators for distributed vibration excitation of thin plates: a comparison between theory and experiment. *Journal of Vibration and Acoustics* 115:332-339.

- Clark, R.L., C.R. Fuller, and A. Wicks. 1991. Characterization of multiple piezoelectric actuators for structural excitation. *Journal of the Acoustical Society of America* 90:346-357.
- Cook, R.D., D.S. Malkus, and M.E. Plesha. 1989. *Concepts and Applications of Finite Element Analysis, Third Edition*. New York: John Wiley & Sons.
- Crawley, E.F. 1994. Intelligent structures for aerospace: a technology overview and assessment. *AIAA Journal* 32:1689-1699.
- Crawley, E.F. and E.H. Anderson. 1990. Detailed models of piezoceramic actuation of beams. *Journal of Intelligent Material Systems and Structures* 1:4-25.
- Crawley, E.F. and J. de Luis. 1987. Use of piezoelectric actuators as elements of intelligent structures. *AIAA Journal* 25:1373-1385.
- Crawley, E.F. and K. B. Lazarus. 1991. Induced strain actuation of isotropic and anisotropic plates. *AIAA Journal* 29:944-951.
- Daniel, I.M. and O. Ishai. 1994. *Engineering Mechanics of Composite Materials*. New York: Oxford University Press.
- Dimitriadis, E.K., C.R. Fuller and C.A. Rogers. 1991. Piezoelectric actuators for distributed vibration excitation of thin plates. *Journal of Vibration and Acoustics* 113:100-107.
- Donthireddy, P. and K. Chandrashekhara. 1996. Modeling and shape control of composite beams with embedded piezoelectric actuators. *Composite Structures* 35:237-244.
- Friswell, M.I., D.J. Inman, and R.W. Rietz. 1997. Active damping of thermally induced vibrations. *Journal of Intelligent Material Systems and Structures* 8:678-685.
- Fung, Y.C. 1965. *Foundations of solid mechanics*. Englewood Cliffs, New Jersey: Prentice-Hall, Inc.
- Ha, S.K., C. Keilers and F-K. Chang. 1992. Finite element analysis of composite structures containing distributed piezoceramic sensors and actuators. *AIAA Journal* 30:772-780.
- Heyliger, P.R., K.C. Pei, and D.A. Saravanos. 1996. Layerwise mechanics and finite element model for laminated piezoelectric shells. *AIAA Journal* 34:2353-2360.
- Heyliger, P.R., G. Ramirez, and D. Saravanos. 1994. Coupled discrete-layer finite elements for laminated piezoelectric plates. *Communications in Numerical Methods in Engineering* 10:971-981.

- Heyliger, P.R. and D.A. Saravanos. 1995. Exact free-vibration analysis of laminated plates with embedded piezoelectric layers. *Journal of the Acoustical Society of America* 98:1-11.
- Hong, C.-H. and I. Chopra. 1999. Modeling and validation of induced strain actuation of composite coupled plates. *AIAA Journal* 37:372-377.
- Hughes, T.J.R. 1987. *The Finite Element Method, Third Edition*. Englewood Cliffs, New Jersey: Prentice-Hall, Inc.
- Hwang, W.-S. and H.C. Park. 1993. Finite element modeling of piezoelectric sensors and actuators. *AIAA Journal* 31:930-937.
- Im, S. and S.N. Atluri. 1989. Effects of a piezo-actuator on a finitely deformed beam subjected to general loading. *AIAA Journal* 27:1801-1807.
- Jonnalagadda, K.D., G.E. Blandford, and T.R. Tauchert. 1994. Piezothermoelastic composite plate analysis using first-order shear deformation theory. *Computers and Structures* 51:79-89.
- Kim, J., V.V. Varadan, and V.K. Varadan. 1997. Finite element modelling of structures including piezoelectric active devices. *International Journal for Numerical Methods in Engineering* 40:817-832.
- Kim, J., V.V. Varadan, V.K. Varadan and X.-Q. Bao. 1996. Finite-element modeling of a smart cantilever plate and comparison with experiments. *Smart Materials and Structures* 5:165-170.
- Koconis, D.B., L.P. Kollar, and G.S. Springer. 1994a. Shape control of composite plates and shells with embedded actuators. I. Voltages specified. *Journal of Composite Materials* 28:415-458.
- Koconis, D.B., L.P. Kollar, and G.S. Springer. 1994b. Shape control of composite plates and shells with embedded actuators. II. Desired shape specified. *Journal of Composite Materials* 28:459-483.
- Lam, K.Y., X.Q. Peg, G.R. Liu, and J.N. Reddy. 1997. A finite-element model for piezoelectric composite laminates. *Smart Materials and Structures* 6:583-591.
- Lammering, R. 1991. The application of a finite shell element for composites containing piezo-electric polymers in vibration control. *Computers and Structures* 41:1101-1109.
- Lee, C.-K. 1990. Theory of laminated piezoelectric plates for the design of distributed sensors/actuators. Part I: Governing equations and reciprocal relationships. *Journal of the Acoustical Society of America* 87:1144-1158.
- Lee, C.-K., W.-W. Chiang, and T.C. O'Sullivan. 1991. Piezoelectric modal sensor/actuator pairs for critical active damping vibration control. *Journal of the Acoustical Society of America* 90:374-384.

- Lee, C.-K. and F.C. Moon. 1989. Laminated piezopolymer plates for torsion and bending sensors and actuators. *Journal of the Acoustical Society of America* 85:2432-2439.
- Lee, H.-J. And D.A. Saravanos. 1996. Coupled layerwise analysis of thermopiezoelectric composite beams. *AIAA Journal* 34:1231-1237.
- Lee, H.-J. And D.A. Saravanos. 1997. Generalized finite element formulation for smart multilayered thermal piezoelectric composite plates. *International Journal of Solids and Structures* 34:3355-3371.
- Lee, H.-J. And D.A. Saravanos. 1998. The effect of temperature dependent material properties on the response of piezoelectric composite materials. *Journal of Intelligent Material Systems and Structures* 9:503-508.
- Lee, H.-J. And D.A. Saravanos. 2000. A mixed multi-field finite element formulation for thermo-piezoelectric composite shells. *International Journal of Solids and Structures* 37:4949-4967.
- Lerch, R. 1990. Simulation of piezoelectric devices by two- and three-dimensional finite elements. *IEEE Transactions on Ultrasonics, Ferroelectrics, and Frequency Control* 37:233-247.
- Librescu, L., L. Meirovitch and S.S. Na. 1997. Control of cantilever vibration via structural tailoring and adaptive materials. *AIAA Journal* 35:1309-1315.
- Lin, C.-C., C.-Y. Hsu and H.-N. Huang. 1996. Finite element analysis on deflection control of plates with piezoelectric actuators. *Composite Structures* 35:423-433.
- Liu, G.R., X.Q. Peng and K.Y. Lam. 1999. Vibration control simulation of laminated composite plates with integrated piezoelectrics. *Journal of Sound and Vibration* 220:827-846.
- Loewy, R.G. 1997. Recent developments in smart structures with aeronautical applications. *Smart Materials and Structures* 6:R11-R42.
- Mason, W.P. 1950. *Piezoelectric crystals and their application to ultrasonics*. New York: D. Van Nostrand Company, Inc.
- Mindlin, R.D. 1974. Equations of high frequency vibrations of thermopiezoelectric crystal plates. *International Journal of Solids and Structures* 10:625-637.
- Mitchell, J.A. and J.N. Reddy. 1995a. A refined hybrid plate theory for composite laminates with piezoelectric laminae. *International Journal of Solids and Structures* 32:2345-2367.
- Mitchell, J.A. and J.N. Reddy. 1995b. A study of embedded piezoelectric layers in composite cylinders. *Journal of Applied Mechanics* 62:166-173.

Naillon, M., R.H. Coursant, and F. Besnier. 1983. Analysis of piezoelectric structures by a finite element method. *ACTA Electronica* 25:341-362.

Nye, J.F. 1964. *Physical properties of crystals*. Oxford: The Clarendon Press.

Oguamanam, D.C.D., S.F.M. Almeida, and J.S. Hansen. 1998. Stress stiffening effects in laminated beams with piezoelectric actuators. *Journal of Intelligent Material Systems and Structures* 9:137-145.

Pai, P.F., A.H. Nayfeh, K. Oh and D.T. Mook. 1993. A refined nonlinear model of composite plates with integrated piezoelectric actuators and sensors. *International Journal of Solids and Structures* 30:1603-1630.

Park, C. and I. Chopra. 1996. Modeling piezoceramic actuation of beams in torsion. *AIAA Journal* 34:2582-2589.

Parton, V.Z. and B.A. Kudryavtsev. 1988. *Electromagnetoelasticity*. New York: Gordon and Breach Science Publishers.

Peng, X.Q., K.Y. Lam, and G.R. Liu. 1998. Active vibration control of composite beams with piezoelectrics: a finite element model with third order theory. *Journal of Sound and Vibration* 209:635-650.

Pletner, B. and H. Abramovich. 1997. Consistent methodology for the modeling of piezolaminated shells. *AIAA Journal* 35:1316-1326.

Rao, S.S. and M. Sunar. 1993. Analysis of distributed thermopiezoelectric sensors and actuators in advanced intelligent structures. *AIAA Journal* 31:1280-1286.

Ray, M.C., R. Bhattacharyya, and B. Samanta. 1994. Static analysis of an intelligent structure by the finite element method. *Computers and Structures* 52:617-631.

Reddy, J.N. 1993. An evaluation of equivalent-single-layer and layerwise theories of composite laminates. *Composite Structures* 25:21-35.

Robbins, D.H. and J.N. Reddy. 1991. Analysis of piezoelectrically actuated beams using a layer-wise displacement theory. *Computers and Structures* 41:265-279.

Samanta, B., M.C. Ray and R. Bhattacharyya. 1996. Finite element model for active control of intelligent structures. *AIAA Journal* 34:1885-1893.

Saravanos, D.A. 1997. Mixed laminate theory and finite element for smart piezoelectric composite shell structures. *AIAA Journal* 35:1327-1333.

Saravanos, D.A. and P.R. Heyliger. 1995. Coupled layerwise analysis of composite beams with embedded piezoelectric sensors and actuators. *Journal of Intelligent Material Systems and Structures* 6:350-363.

Shen, M.-H. 1995. A new modeling technique for piezoelectrically actuated beams. *Computers and Structures* 57:361-366.

Shen, Y.-C. and C.-I Weng. 1995. Deformation control of laminated composite plates containing piezoelectric layers under thermal loading. *Journal of Thermal Stresses* 18:449-464.

Shieh, R.C. 1994. Governing equations and finite element models for multiaxial piezoelectric beam sensors/actuators. *AIAA Journal* 32:1250-1258.

Soedel, W. 1993. *Deep shell equations, vibrations of shells and plates*. New York: Marcel Dekker, Inc.

Sonti, V.R. and J.D. Jones. 1996. Curved piezoactuator model for active vibration control of cylindrical shells. *AIAA Journal* 34:1034-1040.

Stam, M. and G. Carman. 1996. Electrothermoelastic behavior of piezoelectric coupled cylinders. *AIAA Journal* 34:1612-1618.

Suleman, A. and V.B. Venkayya. 1995. A simple finite element formulation for a laminated composite plate with piezoelectric layers. *Journal of Intelligent Material Systems and Structures* 6:776-782.

Sunar, M. and S.S. Rao. 1997. Thermopiezoelectric control design and actuator placement. *AIAA Journal* 35:534-539.

Sung, C.K., T.F. Chen and S.G. Chen. 1996. Piezoelectric modal sensor/actuator design for monitoring/generating flexural and torsional vibrations of cylindrical shells. *Journal of Vibration and Acoustics* 118:48-55.

Tang, Y.Y. and K. Xu. 1995. Dynamic analysis of a piezothermoelastic laminate plate. *Journal of Thermal Stresses* 18:87-104.

Tauchert, T.R. 1992. Piezothermoelastic behavior of a laminated plate. *Journal of Thermal Stresses* 15:25-37.

Tiersten, H.F. 1969. *Linear piezoelectric plate vibrations*. New York: Plenum Press.

Tong, D., R. Williams II, and S.K. Agrawal. 1998. Optimal shape control of composite thin plates with piezoelectric actuators. *Journal of Intelligent Material Systems and Structures* 9:458-467.

Tzou, H.S. and Y. Bao. 1995. A theory on anisotropic piezothermoelastic shell laminates with sensors/actuator applications. *Journal of Sound and Vibration* 184:453-473.

Tzou, H.S. and M. Gadre. 1989. Theoretical analysis of a multi-layered thin shell coupled with piezoelectric shell actuators for distributed vibration controls. *Journal of Sound and Vibration* 132:433-450.

Tzou, H.S. and R.V. Howard. 1994. A piezothermoelastic thin shell theory applied to active structures. *Journal of Vibration and Acoustics* 116:295-302.

Tzou, H.S. and C.I. Tseng. 1990. Distributed piezoelectric sensor/actuator design for dynamic measurement/control of distributed parameter systems: a piezoelectric finite element approach. *Journal of Sound and Vibration* 138:17-34.

Tzou, H.S. and R. Ye. 1994. Piezothermoelasticity and precision control of piezoelectric systems: theory and finite element analysis. *Journal of Vibration and Acoustics* 116:489-495.

Wang, B-T. and C.A. Rogers. 1991. Laminate plate theory for spatially distributed induced strain actuators. *Journal of Composite Materials* 25:433-452.

REPORT DOCUMENTATION PAGE

Form Approved
OMB No. 0704-0188

Public reporting burden for this collection of information is estimated to average 1 hour per response, including the time for reviewing instructions, searching existing data sources, gathering and maintaining the data needed, and completing and reviewing the collection of information. Send comments regarding this burden estimate or any other aspect of this collection of information, including suggestions for reducing this burden, to Washington Headquarters Services, Directorate for Information Operations and Reports, 1215 Jefferson Davis Highway, Suite 1204, Arlington, VA 22202-4302, and to the Office of Management and Budget, Paperwork Reduction Project (0704-0188), Washington, DC 20503.

1. AGENCY USE ONLY (Leave blank)	2. REPORT DATE May 2001	3. REPORT TYPE AND DATES COVERED Technical Memorandum	
4. TITLE AND SUBTITLE Finite Element Analysis of Active and Sensory Thermopiezoelectric Composite Materials		5. FUNDING NUMBERS WU-708-87-13-00	
6. AUTHOR(S) Ho-Jun Lee			
7. PERFORMING ORGANIZATION NAME(S) AND ADDRESS(ES) National Aeronautics and Space Administration John H. Glenn Research Center at Lewis Field Cleveland, Ohio 44135-3191		8. PERFORMING ORGANIZATION REPORT NUMBER E-12768	
9. SPONSORING/MONITORING AGENCY NAME(S) AND ADDRESS(ES) National Aeronautics and Space Administration Washington, DC 20546-0001		10. SPONSORING/MONITORING AGENCY REPORT NUMBER NASA TM-2001-210892	
11. SUPPLEMENTARY NOTES This report was submitted as a dissertation in partial fulfillment of the requirements for the degree Doctor of Philosophy to Northwestern University, Evanston, Illinois, December 2000. Responsible person, Ho-Jun Lee, organization code 5930, 216-433-3316.			
12a. DISTRIBUTION/AVAILABILITY STATEMENT Unclassified - Unlimited Subject Categories: 24 and 39 Available electronically at http://gltrs.grc.nasa.gov/GLTRS This publication is available from the NASA Center for AeroSpace Information, 301-621-0390.		12b. DISTRIBUTION CODE	
13. ABSTRACT (Maximum 200 words) Analytical formulations are developed to account for the coupled mechanical, electrical, and thermal response of piezoelectric composite materials. The coupled response is captured at the material level through the thermo-piezoelectric constitutive equations and leads to the inherent capability to model both the sensory and active responses of piezoelectric materials. A layerwise laminate theory is incorporated to provide more accurate analysis of the displacements, strains, stresses, electric fields, and thermal fields through-the-thickness. Thermal effects which arise from coefficient of thermal expansion mismatch, pyroelectric effects, and temperature dependent material properties are explicitly accounted for in the formulation. Corresponding finite element formulations are developed for piezoelectric beam, plate, and shell elements to provide a more generalized capability for the analysis of arbitrary piezoelectric composite structures. The accuracy of the current formulation is verified with comparisons from published experimental data and other analytical models. Additional numerical studies are also conducted to demonstrate additional capabilities of the formulation to represent the sensory and active behaviors. A future plan of experimental studies is provided to characterize the high temperature dynamic response of piezoelectric composite materials.			
14. SUBJECT TERMS Composite; Piezoelectric; Temperature; Smart materials; Sensors; Actuators; Finite element method		15. NUMBER OF PAGES 125	
		16. PRICE CODE	
17. SECURITY CLASSIFICATION OF REPORT Unclassified	18. SECURITY CLASSIFICATION OF THIS PAGE Unclassified	19. SECURITY CLASSIFICATION OF ABSTRACT Unclassified	20. LIMITATION OF ABSTRACT

